

# ***Regulation of CD95-induced NF- $\kappa$ B activation***

**Dissertation**

zur Erlangung des akademischen Grades

**doctor rerum naturalium**

**(Dr. rer. nat)**

genehmigt durch die Fakultät für Naturwissenschaften  
der Otto-von-Guericke-Universität Magdeburg

von Master of Science Jörn Holger Buchbinder (geborener Schmidt)

geb. am 04. Februar 1987 in Bremerhaven

Gutachter: Prof. Dr. Inna Lavrik

Prof. Dr. Dirk Brenner

Eingereicht am 19. Juni 2018

Verteidigt am 14. November 2018

## ***Acknowledgement***

I thank my supervisor Prof Dr. Inna Lavrik for giving me the opportunity to do my PhD in the group of translational inflammation research, for interesting scientific discussions and for giving me the possibility to visit scientific conferences.

I would like to thank my cooperation partners for their support, ideas and valuable discussion. In particular I thank Nikita Ivanisenko from the Institute of Cytology and Genetics in Novosibirsk, Russia for his valuable modeling contribution and the good time we spent together. For the mass spectrometry analysis and their patience, I like to thank PD Dr. Thilo Kähne and Yvonne Ducho from the Institute of Experimental Internal Medicine in Magdeburg. In like manner, I like to thank Dr. Robert Flassig, Dennis Pischel, Dr. Kolja Schleich, Michelle Lim, Dr. Gunter Maubach, Prof. Dr. Michael Naumann, Dr. Sissy Just and Prof. Dr. Dirk Schlüter for successfully cooperating with me.

Special thanks are going to Sabine for introducing me into science, helpful discussions, her support and friendship that are lasting longer than our time as office neighbors. I also thank Marc for his support. I like to thank my former colleagues Kira, Claudia, Laura, Max and Johannes for their support and for the good atmosphere in the lab, the office and on the running track. In addition, I like to thank Juliane, Sonya, Miriam, Jenny, Dima, Clara, Max and Florian for supporting my work during their internships and theses.

Last but not least I thank my family and friends for their support during the last years.

## **Abstract**

It is well understood that the death receptor CD95 induces apoptotic cell death but also pro-survival signaling. Defective regulation of CD95 signaling is connected to a number of diseases. While the induction of CD95-induced apoptosis is dependent on caspases, the molecular mechanisms leading to activation of the CD95-mediated pro-survival NF- $\kappa$ B pathway are not yet fully understood. The protein c-FLIP is known to block activation of caspases at the CD95 death inducing signaling complex (DISC) and plays an important role in driving CD95-induced NF- $\kappa$ B activation.

The present study was designed to get new insights into the mechanism of CD95-mediated NF- $\kappa$ B activation. In the course of this study, a new imaging flow cytometry-based method to analyze apoptosis and the NF- $\kappa$ B pathway on single cell level was established. This new method uncovered that both pathways are activated in parallel, which provided further insights into the mechanism of NF- $\kappa$ B activation. It was shown that the DISC protein c-FLIP interacts with a central regulator of the NF- $\kappa$ B pathway, NEMO. Peptides derived from an *in silico* model of the c-FLIP-NEMO interaction were able to reduce CD95-induced NF- $\kappa$ B activation in cells expressing high levels of c-FLIP<sub>L</sub>. In addition, the effect of the CBM complex on CD95-induced NF- $\kappa$ B activation was analyzed. The core components of CBM complex were found to be associated to c-FLIP and NEMO in a mass spectrometry screen. Finally, the autophagy receptor NDP52 was described as a negative regulator of CD95- and TNF-R-induced NF- $\kappa$ B activation. Furthermore, this study showed that NDP52 interacts with NEMO and the DUB A20 and thereby limits NF- $\kappa$ B activation by reducing NEMO ubiquitination.

Taken together, this study uncovered new regulatory mechanisms of CD95-induced NF- $\kappa$ B activity. The identification and further improvement of NEMO-derived peptides that block tumor-promoting CD95-induced NF- $\kappa$ B activation without blocking of CD95-mediated apoptosis has potential for new anti-cancer treatment.

## **Table of content**

Acknowledgement .....	i
Abstract.....	ii
1 Introduction.....	1
1.1 Programmed cell death .....	1
1.1.1 Caspases.....	2
1.1.2 The intrinsic apoptosis pathway.....	5
1.1.3 The extrinsic apoptosis pathway .....	7
1.1.4 The signaling of the prototypic DR CD95 .....	9
1.2 NF- $\kappa$ B signaling.....	14
1.2.1 Canonical NF- $\kappa$ B signaling.....	15
1.2.2 Non-canonical NF- $\kappa$ B signaling .....	17
1.2.3 CBM complex.....	18
1.2.4 DR-induced pro-survival signaling.....	20
1.2.5 v-FLIP reduces NF- $\kappa$ B activation.....	22
1.3 Post-translational modifications in NF- $\kappa$ B and other signaling pathways.....	23
1.3.1 Ubiquitination .....	24
1.4 Autophagy.....	27
1.4.1 The autophagy receptor NDP52.....	28
1.5 Aim of the study .....	30
2 Material and methods.....	31

2.1 Material.....	31
2.1.1 Chemicals and reagents.....	31
2.1.2 Cell culture media and supplements .....	31
2.1.3 Antibodies for immunoblotting.....	31
2.1.4 Secondary antibodies for immunoblotting.....	32
2.1.5 Antibodies for flow cytometry.....	33
2.1.6 Kits.....	33
2.1.7 Buffers .....	33
2.1.8 Plasmids .....	34
2.1.9 Synthetic peptides .....	34
2.1.10 Cell lines .....	35
2.2 Methods .....	35
2.2.1 Cell culture.....	35
2.2.2 Thawing cells.....	36
2.2.3 Freezing cells .....	36
2.2.4 siRNA mediated protein knock down.....	36
2.2.5 Cell stimulation and harvesting for immunoblotting .....	37
2.2.6 Cell lysis .....	37
2.2.7 Determination of protein concentration via Bradford assay .....	38
2.2.8 Immunoblotting.....	38
2.2.9 Immunoprecipitation.....	38

2.2.10 Size exclusion chromatography (gel filtration).....	40
2.2.11 Cell stimulation for imaging flow cytometry.....	41
2.2.12 Staining the cells for imaging flow cytometry.....	41
2.2.13 Imaging flow cytometry data acquisition.....	42
2.2.14 Imaging flow cytometry data analysis.....	42
2.2.15 IL-6 and IL-8 ELISA.....	43
2.2.16 Statistical analysis.....	43
3 Results.....	44
3.1 Stimulation of CD95 results in activation of apoptosis and the NF- $\kappa$ B pathway.....	44
3.2 NEMO and c-FLIP interact independently of CD95 stimulation.....	56
3.3 NEMO-derived peptides influence CD95-induced NF- $\kappa$ B activation.....	58
3.4 Mass spectrometry analysis of c-FLIP and NEMO interacting proteins.....	67
3.5 BCL10 but not MALT1 influences CD95-induced NF- $\kappa$ B activation.....	69
3.6 NDP52 is a negative regulator of DR-induced NF- $\kappa$ B activation.....	74
3.7 NDP52 interacts with NEMO and A20.....	80
4 Discussion.....	85
4.1 Stimulation of CD95 induces NF- $\kappa$ B activity and caspase activation.....	85
4.2 Interaction of c-FLIP and NEMO.....	87
4.3 Effect of caspase inhibition on CD95-induced NF- $\kappa$ B activation.....	90
4.4 MALT1 but not BCL10 influence CD95-induced NF- $\kappa$ B activation.....	91
4.5 The autophagy receptor NDP52 suppresses CD95- and TNF-R-induced NF- $\kappa$ B activation.....	94

4.6 NDP52 interacts with NEMO and A20 and can reduce NEMO ubiquitination.....	95
4.7 Translational implications of this study.....	98
List of abbreviations .....	100
References.....	102
Curriculum vitae .....	118
Publications.....	119
Declaration.....	120

# **1 Introduction**

The balance between cell proliferation and death is important to maintain the homeostasis of multicellular organisms. This balance is regulated *via* pro-death and pro-survival signaling. Its deregulation can result either in the loss of healthy cells or in growth of *e.g.* mutated, tumor cells. Interestingly, stimulation of death receptors (DRs) induces both opposing pathways simultaneously. Different signaling complexes and molecules decide whether the pro-death or the pro-survival pathway outbalances the other one, resulting in death or survival of an individual cell. Getting more understanding of these signaling complexes and molecules could be helpful to find new cures against a number of diseases.

## **1.1 Programmed cell death**

The various forms of programmed cell death (PCD) are essential for the clearance of damaged, infected or obsolete cells in multicellular organisms. PCD is regulated very strictly to ensure that all damaged cells are removed without killing too many useful cells. The most important forms of PCD are apoptosis and necroptosis (Elmore, 2007; Lavrik et al., 2005).

Apoptotic cell death is important for cellular homeostasis (Kerr et al., 1972). It clears damaged or virus infected cells. During embryonic development, it is important for the removal of the cells forming the webbing between fingers and toes, which are evolutionary relics. Deregulation of apoptosis is connected to a number of diseases like cancer, neurodegenerative or autoimmune diseases (Krammer et al., 2007). Apoptosis is characterized by a conserved sequence of morphological changes initiated with nuclear condensation, followed by cell shrinkage, and membrane blebbing which ultimately lead to the dissociation of a cell into apoptotic bodies. The molecular events regulating this process are similarly conserved and include activation of cysteinyl-aspartate specific proteases (caspases), DNA fragmentation and the exposure of phosphatidylserine (PS) to the outer membrane of

an apoptotic cell. Apoptosis is commonly believed to be an immunologically silent cell death form. In addition it was shown that PS serves as “eat me” signals and cytokines are secreted as “find-me” signals, which activate phagocytosis of the dying cells (Cullen et al., 2013).

In contrast to the key apoptotic features necroptosis is characterized by nuclear and cellular swelling, early plasma membrane damage and organelle breakdown (Elmore, 2007). The release of cellular content is accompanied by an inflammatory response. Necroptosis is dependent on the activation of the kinases: receptor interacting serine/threonine protein kinase 1 (RIPK1) and RIPK3 as well as the pseudokinase mixed lineage kinase domain like pseudokinase (MLKL) (Vandenabeele et al., 2010).

### **1.1.1 Caspases**

Caspases (Cysteine-specific aspartate proteases) are the central enzymes, which initiate and promote apoptosis by cleaving their substrates. Caspases recognize specific four amino acids long target sequences ending with an aspartate and cleave their substrates at the carboxy-terminal side of this aspartate residue (Poreba et al., 2013). Caspases are produced as inactive zymogens that are also named proforms or procaspases and are activated by dimerization and subsequent conformational change (Figure 4). Further proteolytic cleavage is required for their stabilization and takes place at specific aspartate residues and results in the release of a small and a large catalytic subunit. Two small and two large catalytic subunits form the active heterotetramer. Caspases can be divided into the three main groups: apoptosis initiator caspases, apoptosis effector or executioner caspases and inflammatory caspases (Figure 1).

The initiator caspases are activated at high molecular weight protein complexes and share a large and a small catalytic domain which form catalytic subunits upon cleavage. Two of these initiator caspases are procaspase-8 and -10. Both can bind *via* their death effector domains (DEDs) to the membrane-bound death inducing signaling complex (DISC), the latter serves as an initiator complex

for apoptosis initiation. Two splice variants of procaspase-8 are known: procaspase-8a and 8b. Procaspase-8a has an additional fragment of two kDa between its second DED and the large catalytic subunit compared to procaspase-8b. Procaspase-10 is expressed in humans but not in mice. The isoforms caspase-10 a, b, d and g positively and negatively regulate DR induced cell death (Horn et al., 2017; Mühlethaler-Mottet et al., 2011). The initiator procaspases-2 and -9 have a caspase activation and recruitment domain (CARD) in their prodomain that is crucial for recruitment to high molecular weight complexes and their subsequent activation. Procaspase-9 is activated in the apoptosome which is important for induction of intrinsic cell death while procaspase-2 is activated in the PIDDosome (Lavrik and Krammer, 2009).

In contrast to the enzymatically inactive executioner procaspases, in the absence of apoptotic stimulus, the initiator procaspases have a low enzymatic activity that is largely enhanced *via* so called proximity-induced activation at high molecular weight complexes. The latter are formed upon apoptosis induction. For instance, two procaspase-8 molecules come in close proximity upon recruitment to the DISC and this close proximity allows them to undergo dimerization and subsequent autocatalytic activation. As a result of activation, initiator caspases activate effector caspase by cleavage of the aspartate residue between the large and small catalytic subunits. This allows formation of the active heterotetramer of executioner caspases. The difference between initiator and effector caspases is structurally reflected in the lack of a large prodomain in the effector caspases-3, -6 and -7 (Figure 1). The activation of effector caspases by initiator caspases multiplies the apoptotic signal and is called caspase cascade.

In contrast to the so far mentioned caspases, the function of the group of inflammatory caspases-1, -4, -5, -11, -12 and -13 is not related to apoptosis (Figure 1). Caspase-1 plays an important role in innate immunity and in processing of pro-inflammatory cytokines. It is activated in the high molecular weight complex “inflammasome” and processes pro-IL-1 $\beta$  and pro-IL-18 into their mature forms IL-

1 $\beta$  and IL-18, and thereby allows their secretion to attract immune cells. The inflammatory caspases-1, -4 and -5 are important for toll-like receptor 3/4 (TLR3/4) signaling in innate immune response as well as the programmed cell death called “pyroptosis” that is not dependent on apoptotic caspases and connected to increased inflammation (Eldridge and Shenoy, 2015). It is known that pyroptosis takes place in pathogen-infected macrophages and leads to cellular burst of the cells. The release of interleukins and pathogens induces an antimicrobial response. In contrast to apoptosis or inflammation, a completely unique function is known for caspase-14. It plays a crucial role in keratinocyte differentiation (Salvesen and Ashkenazi, 2011). Furthermore, some caspases are not expressed in humans, *e.g.* caspase-11 is only present in mouse and is a homolog to the human caspases-4 and -5. Just as caspases-4 and -5 in humans, it is important for innate immune signaling and pyroptosis induction in mice. Another caspase, caspase-12 is very similar to caspase-1 in mouse and is expressed as a precursor form in most human species (Fischer et al., 2002). Its activation and function are not fully understood but it is expressed in the endoplasmic reticulum (ER) and may have functions in ER-stress (Berchtold et al., 2016). In contrast to the first reports, caspase-13 is not expressed in humans and represents a bovine gene (Koenig et al., 2001).

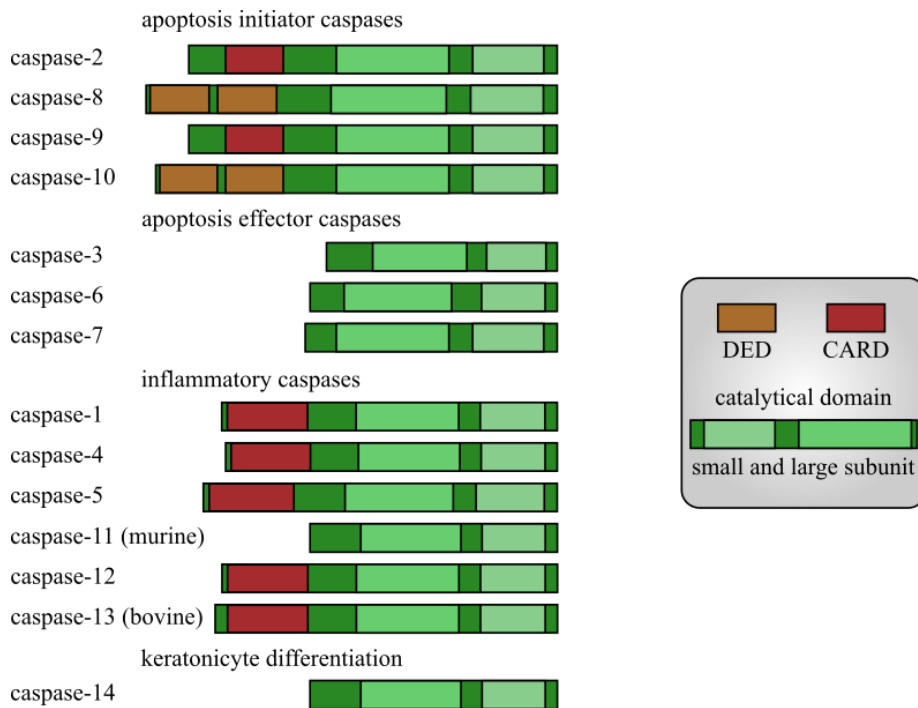


**Figure 1: Main groups of caspases.** The caspases-2, -8, -9 and -10 belong to the group of apoptosis initiator caspases and have a large prodomain, containing CARD or two DEDs, and small and large catalytic domains. They are activated in high molecular weight complexes. The caspases-3, -6 and -7 belong to the group of effector caspases and have a small prodomain and a large and small catalytic domain. Upon activation they cleave apoptotic substrates. The group of inflammatory caspases consists of the caspases-1, -4, -5, -12, the murine caspase-11 and the bovine caspase-13. They are important for secretion of inflammatory cytokines and induction of pyroptosis. Caspase-14 is important for keratinocyte differentiation. DED: death effector domain, CARD: caspase activation and recruitment domain. Figure modified from (Lavrik and Krammer, 2009; Salvesen and Ashkenazi, 2011)

### 1.1.2 The intrinsic apoptosis pathway

Apoptosis can be induced *via* the intrinsic pathway, *e.g.* by DNA damage, reactive oxygen species or growth factor withdrawal or *via* the extrinsic pathway, *e.g.* by stimulation of DRs (Lavrik et al., 2005). Intrinsic apoptosis is regulated *via* formation of pores in the outer mitochondrial membrane and the release of proteins from the intramembrane room into the cytoplasm (Creagh, 2014; Du et al., 2000). The formation of these pores is controlled by the family of B-cell lymphoma 2 (Bcl-2) proteins that have either pro- or anti-apoptotic functions. The family consists of 25 members, *e.g.* with Bcl-2, Bcl-XL, Mcl-1 having anti-apoptotic functions and the so called BH3-only proteins Bid, Bim, Puma,

Noxa and others having pro-apoptotic functions as well as the third group of pro-apoptotic or effector Bcl-2 family members Bak, Bax and Bok. In unstressed cells, the anti-apoptotic Bcl-2 family members prevent the induction of the intrinsic apoptosis pathway by inhibiting Bax and Bak. After apoptotic stimuli like UV- or  $\gamma$ -radiation, or viral infections the delicate balance between pro- and anti-apoptotic Bcl-2 family members is changed after upregulation or activation of the BH3-only members. As a result, the anti-apoptotic members of the Bcl-2 family are inhibited and Bax and Bak are activated, oligomerize and form pores in the outer mitochondrial membrane and thereby allow the release of cytochrome C and SMAC/DIABLO (Figure 2).

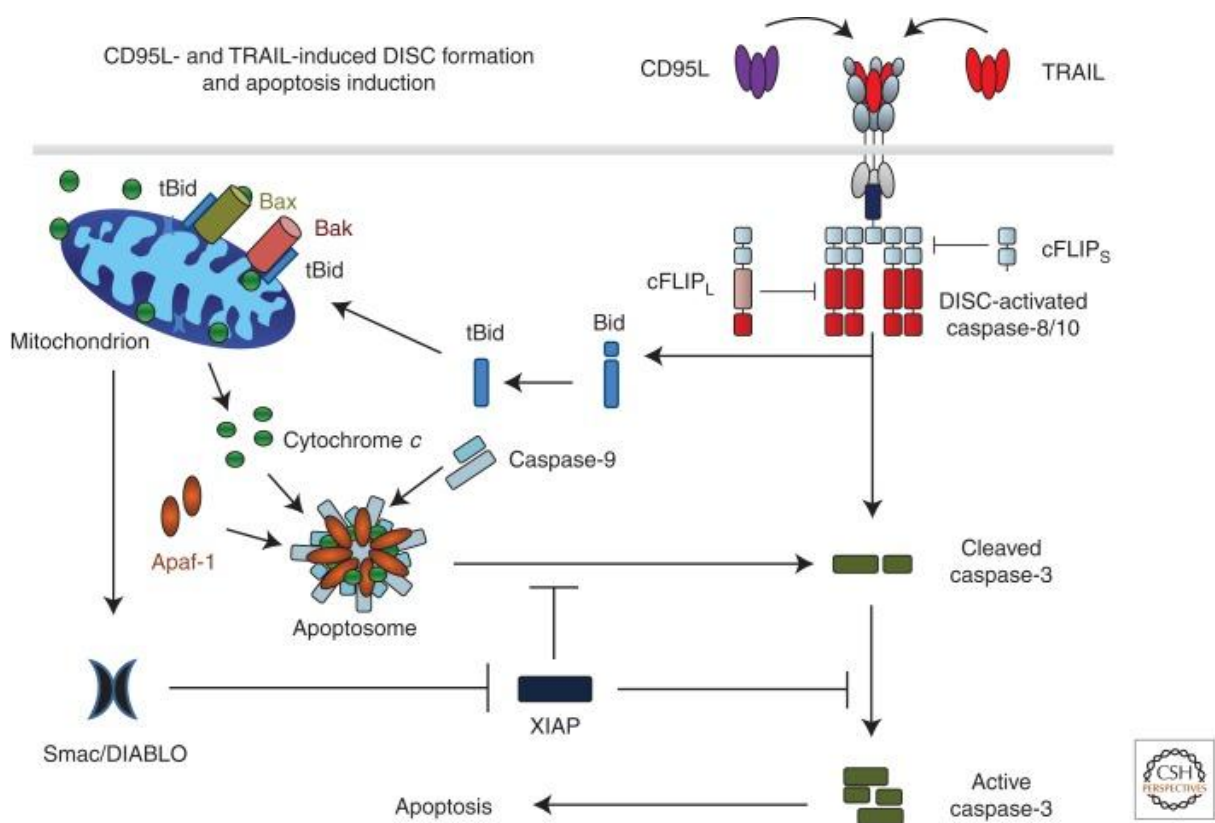


**Figure 2: The intrinsic and extrinsic apoptotic pathway. Stimulation of TRAIL-R or CD95 with their ligands results in DISC formation. The adaptor protein FADD is recruited to the DISC *via* DD-DD interaction. FADD recruits DED containing proteins procaspases-8 and -10 and c-FLIP isoforms to the DISC. Approximately 6 to 10**

**DED containing proteins per FADD molecule are recruited and form DED chains. Procaspases-8 and -10 are activated by dimerization according to the induced proximity model. Short c-FLIP isoforms in these chains block activation of procaspase-8/10 by forming heterodimer, while long c-FLIP isoform can also have activating functions in the heterodimer depending on their concentration in the chains. Active caspase-8 cleaves executioner caspases and Bid. Truncated Bid (tBid) induces Bax and Bak oligomerization and formation of pores in the outer mitochondrial membrane. This allows cytochrome C and SMAC/DIABLO to be released from the mitochondrial intermembrane room into the cytosol. Cytochrome C binds to APAF1, which recruits procaspase-9 into the resulting high molecular weight complex, the apoptosome. Here, procaspase-9 is activated and cleaves executioner caspases, which results in the caspase cascade and apoptotic cell death. The mitochondrial protein SMAC/DIABLO blocks XIAP, the inhibitor of caspase-9 and the executioner caspases-3 and -7. From (Walczak et al., 2013)**

Cytochrome C binds to apoptotic protease activating factor 1 (APAF-1). This interaction induces conformational changes and allows the CARD-domain containing protein APAF-1 to bind ATP and oligomerize in ATP-dependent manner. Oligomerization leads to recruitment of procaspase-9 *via* homotypic interactions of the CARD domains. This high molecular weight complex, called apoptosome or “the wheel of death”, serves as a platform for activation of procaspase-9 *via* the induced proximity model. Activating cleavage of the effector caspases-3, -6, and -7 by caspase-9 induces the caspase cascades which leads to apoptosis (Elmore, 2007). Inhibitor of apoptosis (IAP) proteins suppress the activity of caspases at different levels of the apoptotic pathway (Figure 2), *e.g.* x-chromosome linked IAP (XIAP) blocks the activity of caspases-3 and -7 by binding their enzymatic center (Duckett et al., 1996). After release from the mitochondria, the protein SMAC/DIABLO counteract the effect of XIAPs (Creagh, 2014; Du et al., 2000).

### **1.1.3 The extrinsic apoptosis pathway**

The extrinsic apoptotic pathway is activated by binding of extracellular ligands to their corresponding DRs. DRs are transmembrane receptors. They belong to the tumor necrosis factor (TNF) receptor superfamily and share cysteine rich motifs in their extracellular domain as well as a transmembrane domain and a cytoplasmic death domain (DD) (Guicciardi and Gores, 2009; Lavrik and Krammer, 2012; Lavrik et al., 2005). The best studied DRs are TNF receptor 1 (TNF-R1 known as DR1/CD120a/p55), CD95 (known as FAS/APO-1/DR2), TNF-related apoptosis inducing ligand

receptor 1 (TRAIL-R1, known as DR4) and TRAIL-R2 (known as DR5) (Wajant, 2003). Other human DRs are DR3 (TRAMP) and DR6. These receptors induce programmed cell death and gene activation after stimulation with their ligands TNF $\alpha$ , CD95L (FASL), TNF-related apoptosis inducing ligand (TRAIL), TNF like protein 1A (TL1A) and amyloid precursor protein (APP), respectively (Guicciardi and Gores, 2009; Lavrik et al., 2005; Wajant, 2003).

DR stimulation results in trimerization of the receptor and formation of the DISC (Kischkel et al., 1995; Krammer et al., 2007; Lavrik and Krammer, 2012). First, the adaptor protein Fas-associated death domain protein (FADD) is recruited *via* homotypic DD interactions. FADD recruits the initiator caspases-8 and -10 as well as the protein cellular FLICE (FADD-like IL-1 $\beta$ -converting enzyme) inhibitory protein (c-FLIP) *via* homotypic interactions of the DEDs. Latest studies show that the tandem DED containing proteins caspase-8, caspase-10 and c-FLIP form chain like filament structures at the DISC (Dickens et al., 2012a; Fu et al., 2016; Schleich et al., 2012). Caspase-8 and caspase-10 are activated in the filaments and initiate the caspase cascade by cleaving effector caspases-3, -6 and -7. Extrinsic apoptotic signaling is classified into type-I and type-II cells (Scaffidi, 1998). In type-I cells the amount of active caspase-8 is higher than the required threshold to activate enough effector caspases for induction of the caspase cascade resulting in apoptotic cell death. In contrast to this, type-II cells depend on the amplification of the apoptotic signal by a mitochondrial dependent pathway that is similar to the intrinsic pathway to induce apoptosis (Korsmeyer et al., 2000). Shortly, active caspase-8 cleaves the BH3-only protein Bid into its active form “truncated Bid (tBid)”. Thereupon, tBID induces the Bax and Bak oligomerization and formation of pores in the outer mitochondrial membrane resulting in release of cytochrome C and SMAC/DIABLO (Billen et al., 2008). This results in the formation of the apoptosome and activation of procaspase-9. Activation of procaspases-9 results in activation of executioner caspases and apoptosis similar to the intrinsic pathway (Figure 2).

### 1.1.4 The signaling of the prototypic DR CD95

One of the best studied DRs is CD95. It was discovered as a death inducing receptor *via* agonistic antibody stimulation (Itoh et al., 1991; Trauth et al., 1989). While the first research was focused on understanding CD95 potential to induce apoptosis in tumor cells and to understand the mechanism of cell death induction, its pro-survival mechanisms *via* initiation of anti-apoptotic pathways became focus of the research only recently (Debatin and Krammer, 1995; Guégan and Legembre, 2017). Today it is understood that activation of the pro-survival NF- $\kappa$ B pathway either supports inflammatory silent cell death by inducing cell clearance, but also have a “dark side” by inducing tumor cell growth after apoptosis inducing chemo or radio therapy as a side effect of tissue regeneration (Cullen et al., 2013). While the activation of apoptosis after stimulation of CD95 is well described, the mechanisms of activation of the pro-survival pathways are not fully understood yet (Figure 3).

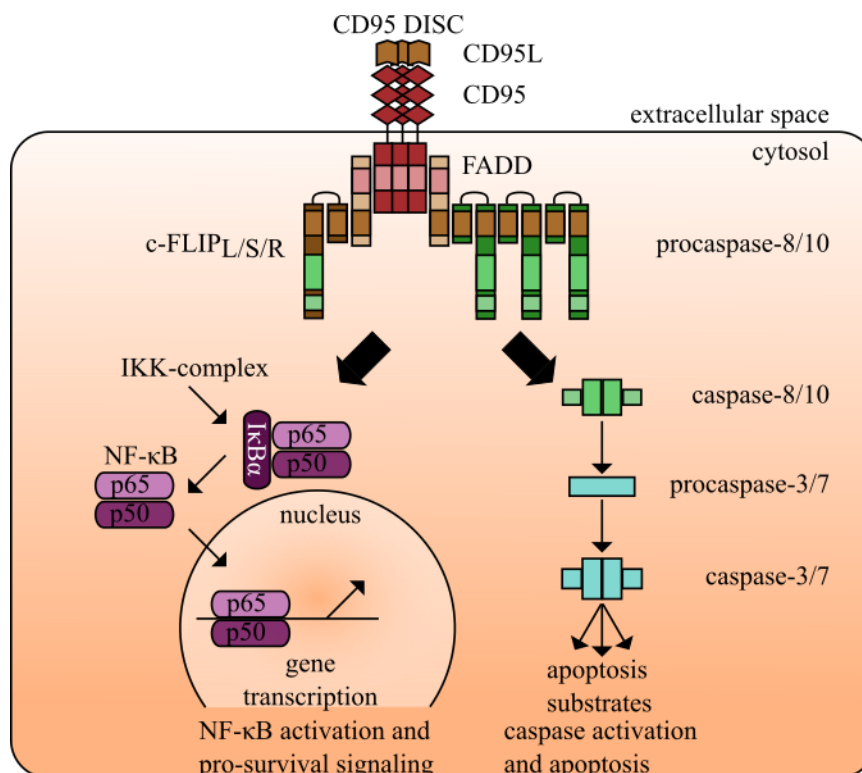


**Figure 3: CD95 signaling pathway. Stimulation of CD95 results in formation of the DISC. Procaspases-8 and -10 are activated at the DISC and activate the executioner caspases-3 and -7 that induce apoptotic cell death.**

**Procaspase-8 also processes c-FLIP<sub>L</sub> to p43-FLIP that can induce the NF-κB pathway via activation of the IKK complex which phosphorylates IκBα. After phosphorylation, IκBα is ubiquitinated and proteasomally degraded. Thereupon, the transcription factors p65 and p50 are able to enter the nucleus and start transcription of NF-κB dependent genes (Details are presented in Chapter 1.2).**

Stimulation of CD95 with its cognate CD95Ligand (CD95L) or antibodies results in receptor trimerization and formation of the DISC. At first, the adaptor protein FADD is recruited to the trimerized receptor *via* homotypic DD interactions (Lavrik and Krammer, 2012). In addition to the DD, FADD also contains a DED which can recruit the DED containing proteins procaspase-8a/b, procaspase-10a/d and different isoforms of c-FLIP (Figure 3) (Lavrik and Krammer, 2012). The DED containing proteins procaspase-8, -10 and c-FLIP form DED chains at the DISC where activation of procaspases-8 and -10 takes place (Dickens et al., 2012a; Schleich et al., 2012). Furthermore, later it was shown that procaspase-8 alone is also able to form filament like structures at the CD95 DISC, and the model of incorporation of c-FLIP and caspase-10 into the filament structure was suggested (Fu et al., 2016). Caspase-10 and c-FLIP are incorporated into the DED chains in a 10-fold lower amount than caspase-8 (Schleich et al., 2016). It is controversially discussed whether c-FLIP is able to block DED chain elongation or not. On the one hand it was shown that c-FLIP<sub>S</sub> is able to block chain formation in an *in vitro* DISC model (Hughes et al., 2016), while on the other hand overexpression of c-FLIP DEDs in HeLa cells did not block chain formation (Schleich et al., 2016). Furthermore, using a computational model of the DISC chains it was suggested that the dissociation/ association rate of caspase-8 molecules is able to restrict the chain length (Schleich et al., 2016). Without restriction of the chain length a few activated receptors would be able to activate all caspase-8 in a cell by forming very long chains, so it is tempting to speculate that a still unknown mechanism for restriction of DISC chains exists.

Activation of procaspase-8a/b (p55/53) at the DISC is induced according to the induced proximity model (Muzio et al., 1998). When two procaspase-8 molecules bind *via* DED-DED interactions they are in close proximity to each other and form homodimers. Thereby inducing a conformational change

that allows activation and cleavage of each other *via* trans- and intramolecular cleavage steps (Figure 4 A). The first cleavage takes place either at D376/D386 (procaspase-8a and 8b) resulting in the cleavage products p43/41 and the small subunit p10 or it takes place at position D210/216 resulting in the cleavage products p26/24 and p30 (Lavrik and Krammer, 2012; Lavrik et al., 2005). The second cleavage step takes place in a way that p43/41 is cleaved at D210/216 into p26/p24 and the large subunit p18 while the cleavage product p30 is cleaved further into subunits p18 and p10 (Figure 4 A). After these cleavage steps the subunits p18 and p10 form the active heterotetramer p18<sub>2</sub>/p10<sub>2</sub> that is released from the DISC (Lavrik et al., 2005). Then the active caspase-8 heterotetramer cleaves the executioner caspases and Bid. When the number of activated executioner caspases reaches a threshold amount, either after direct cleavage by active caspase-8 or after amplification of the signal *via* the mitochondria, the cell undergoes apoptosis (Figure 2).

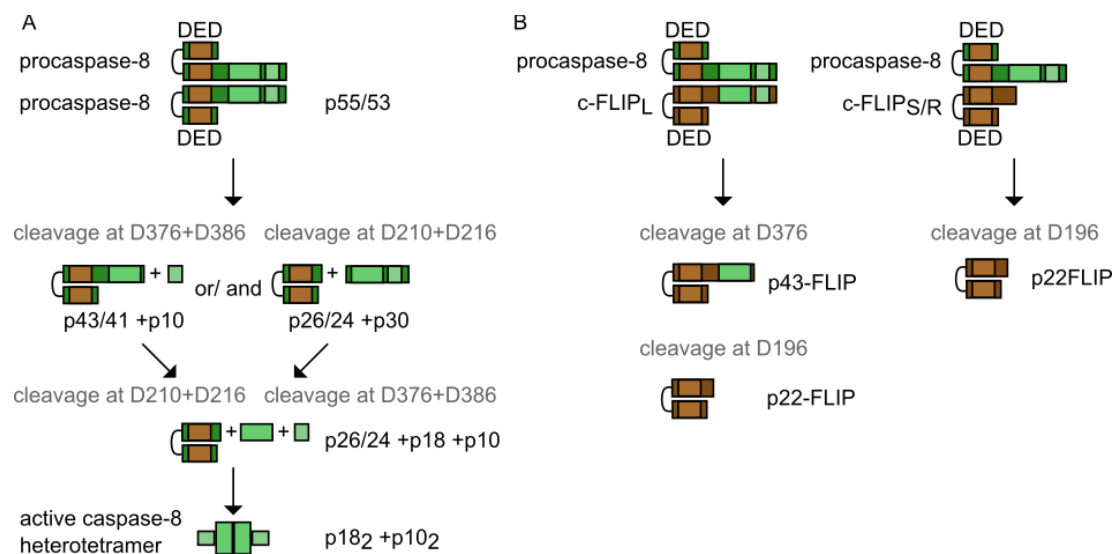


**Figure 4: Cleavage of procaspase-8 and c-FLIP at the DISC.** A) After recruitment of procaspase-8a/b (p55/53) *via* DED-DED interaction two procaspase-8 molecules can form homodimers and undergo trans- and intramolecular cleavage steps. This results in the intermediate cleavage products p43/41+p10 or p26/24+p30. The active heterotetramer consists of two p18 and two p10 subunits. B) When procaspase-8 and c-FLIP<sub>L</sub> form heterodimers at the DISC, procaspase-8 is able to cleave the c-FLIP<sub>L</sub> into p43-FLIP. All isoforms of c-FLIP and p43-FLIP can be cleaved by caspase-8 in the cytosol into p22-FLIP. The cleavage sites are shown in grey. p55/53: p55/53-procaspase-8,

**p43/p41: p43/41-caspase-8, p26/24: p26/24-caspase-8, p30: p30-caspase-8, p18: large catalytic subunit, p10: small catalytic subunit, DED: death effector domain**

In contrast to the pro-apoptotic caspases c-FLIP is an important anti-apoptotic protein. Before the discovery of cellular FLIP (c-FLIP) viral FLIPs (v-FLIPs) were identified as viral proteins containing two DEDs that are able to block CD95-induced apoptosis. It was shown that expression of these proteins was induced by different viruses in cells in the late phases of their infection to block apoptotic cell death (Thome et al., 1997). The blockage of apoptotic cell death allows the virus an increased proliferation. Shortly after discovery of v-FLIPs their cellular homolog c-FLIP was discovered (Irmeler et al., 1997). The gene CFLAR (CASP8 and FADD like apoptosis regulator) encodes the protein c-FLIP (Oztürk et al., 2012). There have been many isoforms on the mRNA level reported so far as well as only three isoforms on the protein level: c-FLIP<sub>Long(L)</sub>, c-FLIP<sub>short(S)</sub> and c-FLIP<sub>Raji(R)</sub> (Golks et al., 2005). The short isoform c-FLIP<sub>S</sub> has a shorter half-life time than c-FLIP<sub>L</sub>. It is marked for proteasomal degradation by ubiquitination of lysines 192 and 195 that are at the C-terminus of its DED2 (Poukkula et al., 2005).

Procaspase-8 is able to cleave c-FLIP in the DED chains at the DISC when c-FLIP-procaspase-8 heterodimers are formed (Figure 4). In contrast to procaspase-8, its homolog c-FLIP does not have enzymatic activity and cannot cleave procaspase-8. However, c-FLIP proteins can be cleaved by procaspase-8 in c-FLIP-procaspase-8 heterodimers. In particular, the long isoform c-FLIP<sub>L</sub> is cleaved by procaspase-8 at the position D376 into p43-FLIP (Golks et al., 2005; Lavrik and Krammer, 2012; Lavrik et al., 2005). Cleavage of all c-FLIP isoforms and p43-FLIP at position D196 that does not take place at the DISC results in formation of p22-FLIP (Oztürk et al., 2012) (Figure 4 B). c-FLIP isoforms and cleavage products influence CD95 signaling in different ways. The short isoforms c-FLIP<sub>R/S</sub> block activation of procaspase-8 at the DISC by forming heterodimers with procaspase-8 and thereby block the formation procaspase-8 homodimers and hence its cleavage. c-FLIP<sub>L</sub> is able to influence CD95 signaling in opposing ways. Similar to the short isoform, it blocks apoptosis at high expression levels

by decreasing the number of procaspase-8 homodimers at the DISC (Figure 5). Intermediate levels of c-FLIP<sub>L</sub> increase procaspase-8 activation resulting in more apoptosis especially at high levels of CD95 stimulation (Figure 5). In particular, c-FLIP<sub>L</sub> is able to stabilize the active center of procaspase-8 in c-FLIP<sub>L</sub>-procaspase-8 heterodimers thereby increasing its catalytic activity (Fricker et al., 2010; Neumann et al., 2010).

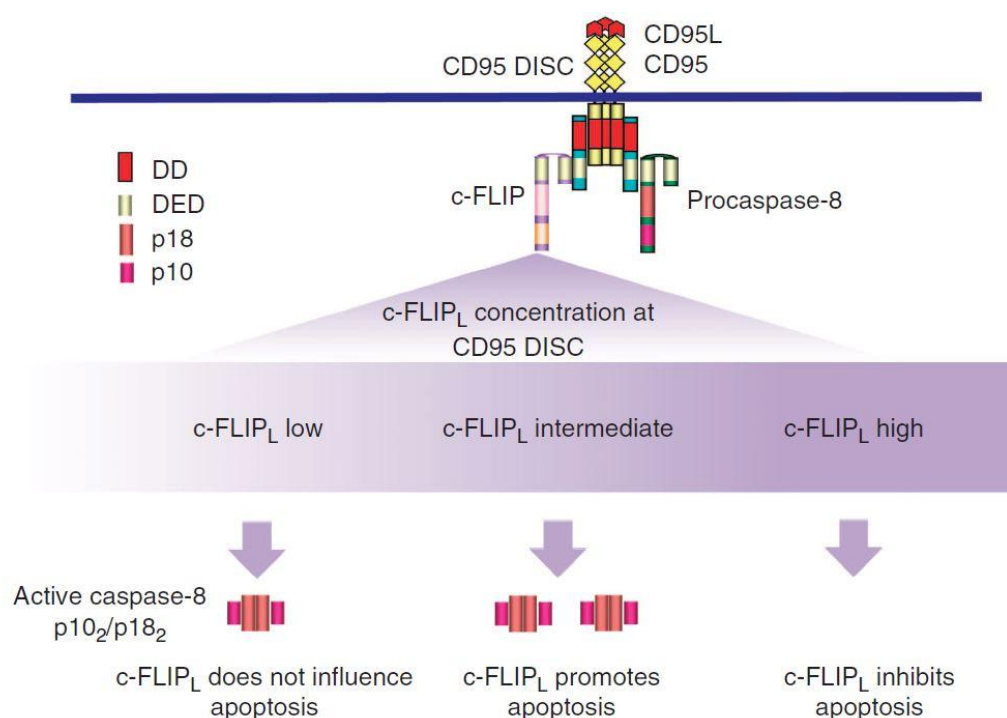


**Figure 5: Effects of c-FLIP<sub>L</sub> concentration on CD95-induced apoptotic signaling. Low levels of c-FLIP<sub>L</sub> do not influence CD95-induced apoptotic signaling. Intermediate levels of c-FLIP<sub>L</sub> promote caspase-8 activation and thereby increase apoptotic signaling after CD95 stimulation, while high levels of c-FLIP<sub>L</sub> block caspase-8 activation and thus CD95-induced apoptosis. From (Lavrik, 2014)**

Caspase-10 is a caspase-8 homolog that is expressed in humans but not in mice. For this reason, extrinsic apoptosis takes place in absence of caspase-10 in murine cells with caspase-8 acting as the only key player, which allows the assumption that caspase-10 is dispensable for extrinsic apoptosis induction. Caspase-10 function in human cells is not fully understood yet. Due to its low expression, it is incorporated in a ten time lower amount than procaspase-8 into the CD95 DISC in human cells and

is activated by cleavage in heterodimers with caspase-8 (Schleich et al., 2016). The activation in procaspase-10 homodimers is possible, but a rather rare event due to the low procaspase-10 levels in the DISC chains. Caspase-10 was recently shown to block caspase-8 activation and increase nuclear factor 'kappa-light-chain-enhancer' of activated B-cells (NF- $\kappa$ B) activation after CD95 stimulation (Horn et al., 2017). Incorporation of procaspase-10 into the DED chains decreases procaspase-8 activation by reducing the number of procaspase-8 homodimers. It is controversially discussed if procaspase-10 is able to bind to FADD or unable to do so (Horn et al., 2017; Mohr et al., 2018). Moreover, other apoptosis independent functions of caspase-10 are discussed, *e.g.* caspase-10 may be connected to autophagic cell death in acute myeloid leukemia cells (Guo et al., 2016).

## **1.2 NF- $\kappa$ B signaling**

The NF- $\kappa$ B signaling pathway is an antagonist of apoptotic signaling and an important pro-survival pathway that is also activated upon DR stimulation. NF- $\kappa$ B is a group of proteins having a function of transcription factors that is expressed ubiquitously in cells throughout the animal kingdom (Gilmore, 2006). It is a major player for controlling inflammatory responses and innate as well adaptive immunity. NF- $\kappa$ B regulates proliferation, cell survival and differentiation not only in the immune system, but also in the epithelium and skeletal system (Hayden and Ghosh, 2012; Zhang et al., 2017). Deregulation of the NF- $\kappa$ B pathway is connected to a number of diseases, *e.g.* chronic inflammation and cancer (Zhang et al., 2017).

The NF- $\kappa$ B family consists of the five DNA binding factors p65 (RelA), RelB, c-Rel, p50 and p52 that all share the rel homology domain. These factors are found in the cytoplasm due to their interactions with inhibitor of kappa B (I $\kappa$ B) proteins. p50 and p52 remain in the cytoplasm due to their localization signals of ankyrin rich repeats in their proforms p100 and p105. Proteolytic cleavage of the proforms results in the release of p50 and p52 that can translocate to the nucleus (Cildir et al.,

2016). Genes that induce cytokine production and cell survival are activated by NF- $\kappa$ B *via* intrinsic or extrinsic factors like genotoxic stress or stimulation of receptors at the cells surface *e.g.* TLR4, TNF-R, CD95, TRAIL-R1/2, and IL1-R (Gilmore, 2006; Hayden and Ghosh, 2008, 2012). NF- $\kappa$ B can be activated by both the so-called canonical or the non-canonical signaling pathway.

### **1.2.1 Canonical NF- $\kappa$ B signaling**

The canonical NF- $\kappa$ B activation takes place within minutes after activation and is regulated *via* the inhibitor of nuclear factor kappa-B kinase (IKK) complex (Figure 6). The IKK complex consists of inhibitor of nuclear factor kappa-B kinase subunit alpha (IKK $\alpha$ ), inhibitor of nuclear factor kappa-B kinase subunit beta (IKK $\beta$ ) and the regulatory subunit NF-kappa-B essential modulator (NEMO (also known as inhibitor of nuclear factor kappa-B kinase subunit gamma (IKK $\gamma$ ))) (Gilmore, 2006; Hayden and Ghosh, 2012). The IKK complex phosphorylates the inhibitor of kappa B (I $\kappa$ B $\alpha$ ), which leads to K48 ubiquitination and hence, proteasomal degradation of I $\kappa$ B $\alpha$  (Figure 6). After I $\kappa$ B $\alpha$  degradation, the nuclear localization signal (NLS) of the NF- $\kappa$ B proteins p65 and p50 are unmasked, hence, they enter the nucleus and start transcription of NF- $\kappa$ B dependent genes, *e.g.* pro-inflammatory cytokines and anti-apoptotic proteins (Harhaj and Dixit, 2011; Hayden and Ghosh, 2012; Jacobs and Harrison, 1998).

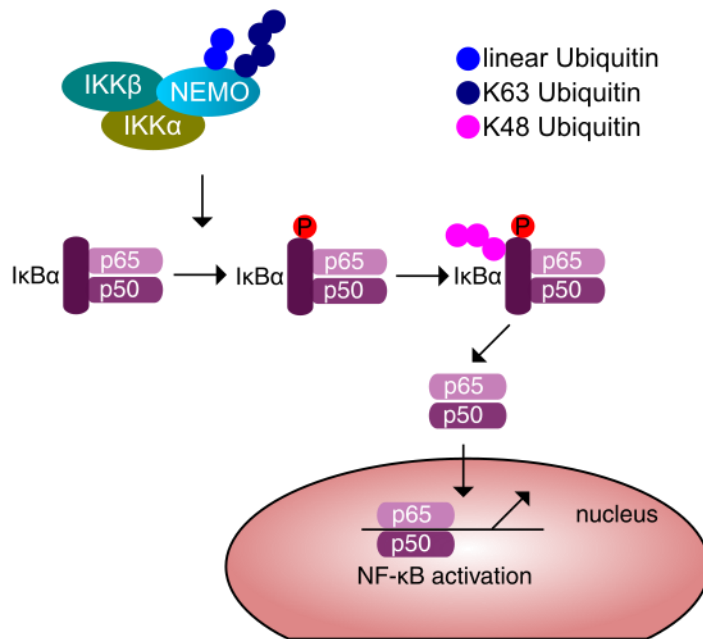


**Figure 6: Canonical NF-κB signaling.** The IKK complex consisting of IKK $\alpha$ , IKK $\beta$  and NEMO (IKK $\gamma$ ) phosphorylates I $\kappa$ B $\alpha$ . Thereupon, I $\kappa$ B $\alpha$  is K48-ubiquitinated and thereby marked for proteasomal degradation. Without bound I $\kappa$ B $\alpha$ , the nuclear localization site of the p65/p50 heterodimer is exposed and the dimer is able to enter the nucleus and start NF-κB dependent gene transcription.

Activation of the regulatory IKK complex subunit NEMO is regulated negatively or positively by interaction with different proteins and post-translational modifications of NEMO (Maubach and Naumann, 2017; Zhang et al., 2017). As an illustration, stimulation of the TNF-R results in formation of the complex I consisting of TNF-R type 1 associated DD protein (TRADD), TNF-R associated factor 2 (TRAF2), TRAF5, cellular inhibitor of apoptosis protein 1/2 (cIAP1/2) and RIPK1. cIAPs can polyubiquitinate itself and RIPK1. The resulting ubiquitin chains allow recruitment of IKK complex *via* NEMO recruitment, attract a complex consisting of TAK1 binding protein 2/3 (TAB2/3) and TGF-beta activated kinase 1 (TAK1) and attract the linear ubiquitin chain assembly complex (LUBAC). After recruitment, TAK1 activates the IKK complex by IKK $\beta$  phosphorylation (Emmerich et al., 2013). LUBAC consists of the adaptor SHANK associated RH domain interactor (SHARPIN) and the

E3 ligases heme-oxidized ERP2 ubiquitin ligase 1 (HOIL-1) and HOIL-1 interacting protein (HOIP). LUBAC can add linear ubiquitin chains to RIPK1 and NEMO and thereby increase recruitment of the IKK complex to NEMO resulting in increased NF- $\kappa$ B activation (Haas et al., 2009; Ikeda et al., 2011; Tokunaga and Iwai, 2012). Another feature of linear ubiquitination of NEMO is an increased NEMO activation by conformational changes and changes of its interaction surface (Hauenstein et al., 2017).

NEMO activity induced by ubiquitination is terminated by deubiquitinating enzymes. The most important deubiquitinases (DUBs) of NEMO are TNF- $\alpha$  interacting protein 3 (TNFAIP3/A20), OTU domain containing deubiquitinase with linear linkage specificity (OTULIN) and Cyldromatosis (CYLD) (Lork et al., 2017). OTULIN specifically acts on linear ubiquitin chains, thereby blocking RIPK1 and NEMO interaction and IKK complex activation by TAK1 (Keusekotten et al., 2013). CYLD binds to NEMO or LUBAC and acts on K63 and linear ubiquitin chains and thereby reducing IKK activation (Kovalenko et al., 2003). A20 specifically deubiquitinates K63 ubiquitin chains or directly binds to NEMO and prevents RIPK1 recruitment (Lork et al., 2017; Wertz et al., 2004).

### **1.2.2 Non-canonical NF- $\kappa$ B signaling**

The non-canonical NF- $\kappa$ B pathway is activated by lymphotoxin  $\beta$ -receptor, receptor activator of nuclear factor kappa-B ligand (RANKL) or B-cell activating factor (BAFF). It is important for cell differentiation and cell development. While the IKK complex is the central activator of canonical NF- $\kappa$ B activation, the NF- $\kappa$ B-inducing kinase (NIK) is the central activator of non-canonical NF- $\kappa$ B. Under non-activated conditions, NIK is constantly K48 ubiquitinated by a complex of TNF receptor-associated factor 3 (TRAF3), TRAF2, and cIAP1/2 and thereby marked for proteasomal degradation (Cildir et al., 2016). After activation, TRAF3, TRAF2, and cIAP1/2 are bound to receptors and NIK is able to activate IKK $\alpha$  by phosphorylation. IKK $\alpha$  phosphorylates the cytoplasmic p100/RelB complex that is thereby K48 ubiquitinated. The C-terminal ankyrin repeat rich domain of p100 is specifically

degraded by proteasome and the p52/RelB complex is able to enter the nucleus and start gene transcription (Cildir et al., 2016; Hayden and Ghosh, 2008, 2012).

Influencing of the NF- $\kappa$ B pathway to cure diseases has to be very specific. Decreasing NF- $\kappa$ B activity reduces growth of tumor cells on the one hand, but also decreases activation of anti-tumor immune cells on the other hand. Additionally, the NF- $\kappa$ B pathway is important for many processes in different cells and tissues and non-specific inhibitors or activators of NF- $\kappa$ B would influence all of these processes causing unwanted side effects (Cildir et al., 2016; Hayden and Ghosh, 2012; Maubach and Naumann, 2017; Zhang et al., 2017). Cell specific inhibitors or activators of the NF- $\kappa$ B pathway could be able to solve this dilemma and would help to decrease side effects.

### **1.2.3 CBM complex**

The CBM complex is important to link B-cell receptor (BCR) and T-cell receptor (TCR) stimulation to NF- $\kappa$ B activation in lymphocytes (Meininger and Krappmann, 2016; Turvey et al., 2014). As an illustration, its NF- $\kappa$ B activating function is important for adaptive immune response (Turvey et al., 2014). This important high molecular weight protein complex consists of the caspase recruitment domain family member 11 (CARD11, also known as CARMA1), B-cell chronic lymphocytic leukemia/lymphoma 10 (BCL10) and mucosa associated lymphoid tissue lymphoma translocation 1 (MALT1).

The protein CARD11 recruits BCL10 *via* homotypic interactions of their CARD domains (Figure 7). Another important function of CARD11 is that it serves as a link for the recruitment of CBM complex to the membrane. In particular, CARD11 is activated by phosphorylation by protein kinase c (PKC). The phosphorylation of CARD11 changes its autoinhibitory structure and allows interaction with BCL10 (Meininger and Krappmann, 2016; Qiao et al., 2013; Turvey et al., 2014). This interaction allows formation of the CBM complex because BCL10 links CARD11 to MALT1 and they

form filament like structures (Turvey et al., 2014; Wang et al., 2007). MALT1 is connected to the CBM complex *via* its two N-terminal immunoglobulin like domains and *via* its DD (Figure 7).

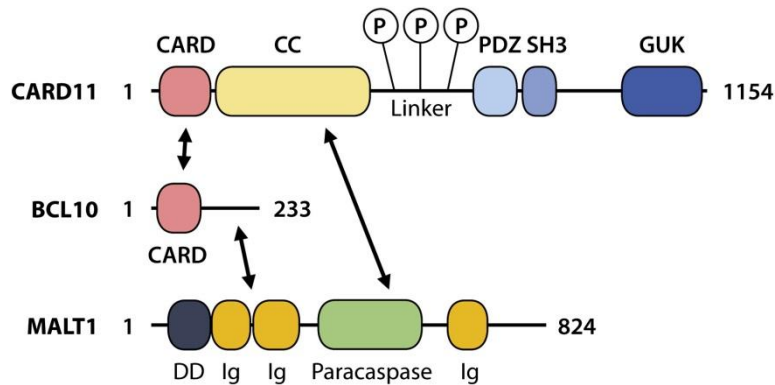


**Figure 7: Schematic overview of the domain structure of the CARD11, BCL10, MALT1 (CBM) signaling complex (Turvey et al., 2014). coiled coil region (CC), immunoglobulin-like domain (Ig).**

After activation, BCL10 and MALT1 are K63 and linear ubiquitinated. TRAF6 ubiquitinates BCL10 and MALT1 with K63-linked chains (Sebban-Benin et al., 2007). This allows recruitment of NEMO as well as the ubiquitin binding adaptors TAB2 and TAB3 connected to the kinase TAK1. TAK1 induces IKK $\alpha$  and IKK $\beta$  phosphorylation (Meininger and Krappmann, 2016; Turvey et al., 2014). Parts of the LUBAC complex were found incorporated into the CBM complex linking linear ubiquitin chains to NEMO thereby activating the NF- $\kappa$ B pathway (Dubois et al., 2014; Yang et al., 2014). MALT1 paracaspase domain has a proteolytic activity and cleaves MALT1 itself, BCL10, RelB, A20, CYLD and others. By cleavage of the inhibitors of canonical NF- $\kappa$ B pathway RelB, A20 and CYLD, it blocks negative feedback mechanisms and increases NF- $\kappa$ B activation (Lork et al., 2017; Turvey et al., 2014). MALT1 cleaves the LUBAC component HOIL1 thereby reducing HOIP levels and LUBAC activity and terminates NF- $\kappa$ B activity (Elton et al., 2016; Klein et al., 2015). It was suggested that these opposite functions allows MALT1 to initiate NF- $\kappa$ B signaling by activation of IKK and LUBAC, enhance it by cleavage of negative regulators and later terminate it by the cleavage of HOIL1 (Hailfinger et al., 2016).

#### **1.2.4 DR-induced pro-survival signaling**

Stimulation of DR not only results in cell death, but also in activation of pro-inflammatory, anti-apoptotic pathways such as the NF- $\kappa$ B pathway (Lavrik et al., 2005; Vanden Berghe et al., 2015). While stimulation of CD95, TRAIL-R1 and -R2 mainly induces cell death, stimulation of TNF-R primarily results in cytokine and chemokine production (Lavrik et al., 2005; Walczak et al., 2013). TNF-R stimulation-induced cell death mostly takes place upon inhibition of NF- $\kappa$ B signaling. Stimulation of DRs in presence of caspase inhibitors may result in an alternative cell death – regulated necrosis or necroptosis. These different signaling outcomes of CD95/TRAIL-R1/2 *versus* TNF-R are reflected by different signaling complexes which have similar components, but differ in their stoichiometry and posttranslational modifications (Vanden Berghe et al., 2015). Stimulation of CD95 or TRAIL-R results in the formation of the DISC including the receptors that mainly induces cell death, and in a formation of the cytosolic complex II that induces both pro-inflammatory and cell death pathways (Dickens et al., 2012b; Lavrik et al., 2008; Wajant, 2003). In contrast to this, stimulation of the TNF-R results in formation of the complex I including the TNF-R that activates pro-inflammatory pathways, *e.g.* NF- $\kappa$ B and JNK, and a cytosolic complex II that initiates cell death (Micheau and Tschopp, 2003). While stimulation of TNF-R is important for the activation of immune cells (Haas et al., 2009; Walczak et al., 2013), CD95 plays a role in killing cancer or virus infected cells by cytotoxic killer and natural killer cells (Peter et al., 2015). Post-translational modification of proteins, *e.g.* acetylation, ubiquitination, phosphorylation or sumoylation are important regulators of complex I/II function thereby controlling downstream signaling events (Please, see chapter 1.3 Post-translational modifications in NF- $\kappa$ B and other signaling pathways for more details on PTM control) (Asaoka et al., 2011; Harhaj and Dixit, 2011; Keusekotten et al., 2013; Tokunaga and Iwai, 2012; Wertz et al., 2004). It is described that the loss of linear ubiquitination of TNF-R-induced complex I reduces TNF-R-induced NF- $\kappa$ B activation and the stability of complex I, thereby enhancing the formation of complex II resulting in increased TNF-R-induced cell death (Walczak et al., 2012)

The activation of the pro-inflammatory, anti-apoptotic NF- $\kappa$ B pathway after CD95 stimulation has important functions. First, it induces the expression of anti-apoptotic proteins and thereby influences further signaling outcome, *e.g.* blocking of apoptotic cell death by increased expression of the anti-apoptotic proteins such as cIAP1, cIAP2 and others (Geserick et al., 2009; Jönsson et al., 2003). Secondly, it induces secretion of cytokines that serve as “find me” and “eat me” signals thereby recruiting phagocytes and helping to clear the apoptotic dying cell *in vivo* (Cullen et al., 2013). It was shown that the secretion of these cytokines after CD95 stimulation is NF- $\kappa$ B dependent and that the proteins RIPK1, cIAP1 and cIAP2 as well as the known DISC proteins FADD and caspase-8 are necessary for increased cytokine secretion (Cullen et al., 2013; Geserick et al., 2009).

For the TRAILR1/2 that induces signaling pathways similar to CD95, a role of caspase-8 in activation of NF- $\kappa$ B independent of caspase-8 enzymatic activity was recently reported (Henry and Martin, 2017). Here, caspase-8 attracts TRAF2 and RIPK1 thereby allowing recruitment of cIAP1/2 *via* TRAF2. cIAP1/2 ubiquitinate RIPK1 allowing formation of a cytosolic platform called FADDosome consisting of FADD, caspase-8 and RIPK1. Thereby, RIPK1 is ubiquitinated and then recruits the TAK1/TAB1/TAB2/3 complex followed by the IKK complex that is then activated by TAK1 dependent phosphorylation of IKK $\alpha$  (Henry and Martin, 2017). It is not described yet, if this mechanism is also important for CD95 signaling.

In addition to its important functions in mediating apoptosis induction, c-FLIP is also important for pro-inflammatory signaling induction. The effects of the different c-FLIP isoforms on CD95-induced NF- $\kappa$ B activation were discussed controversially for a long time because most of the corresponding studies were performed using overexpression of c-FLIP. In particular, high overexpression levels of c-FLIP might significantly change signal transduction at the level of the DISC by replacing procaspase-8 homodimers with c-FLIP-procaspase-8 heterodimers and thereby blocking the signal transduction by preventing procaspase-8 activation. The cleavage of c-FLIP<sub>L</sub> is

important for activation of the pro-inflammatory NF- $\kappa$ B pathway (Imamura et al., 2004; Kreuz et al., 2004; Neumann et al., 2010). It was shown that the cleavage product p43-FLIP, but not non-cleavable c-FLIP<sub>L</sub> mutants activate the NF- $\kappa$ B pathway after CD95 stimulation (Golks et al., 2006; Koenig et al., 2014; Neumann et al., 2010). The mechanism of NF- $\kappa$ B activation by c-FLIP is not fully deciphered, yet. The cleavage product p22-FLIP strongly activates the NF- $\kappa$ B pathway by direct interaction with the IKK subunit NEMO and activation of the IKK complex (Golks et al., 2006). It is not fully understood how p43-FLIP induces NF- $\kappa$ B activation. It was suggested that p43-FLIP is able to bind directly to the IKK complex subunit NEMO and thereby activate the NF- $\kappa$ B pathway. In an alternative assumption, p43-FLIP recruits TRAF2 and thereby activates NF- $\kappa$ B activation (Cullen et al., 2013; Karl et al., 2014; Kataoka and Tschopp, 2004; Neumann et al., 2010).

### ***1.2.5 v-FLIP reduces NF- $\kappa$ B activation***

Some viruses activate the NF- $\kappa$ B signaling pathway to block cell death of the infected cells by expression of anti-apoptotic NF- $\kappa$ B target proteins. They express viral c-FLIP homologues called v-FLIPs that block cell death induction by inhibition of the DISC or directly bind to NEMO thereby activating the NF- $\kappa$ B pathway (Baratchian et al., 2016; Briggs et al., 2017; Schleich et al., 2016; Tolani et al., 2014; Yang et al., 2005). The advantage of blocking apoptotic cell death for the virus is an increased virus production of infected cell. For the ks-v-FLIP (expressed by the Kaposi's sarcoma herpes virus (KSHV)) a crystal structure of its interaction with a part of the NEMO protein is reported. This interaction of ks-v-FLIP and the central region of NEMO (amino acids 150–272) might induce constitutive NF- $\kappa$ B activation by NEMO activation (Bagn ris et al., 2008; Baratchian et al., 2016).

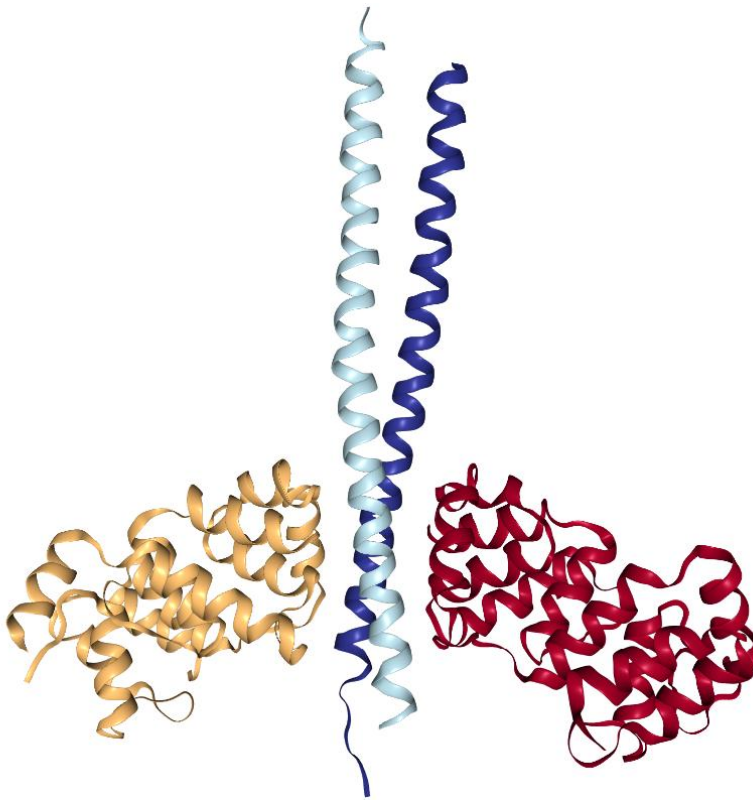


**Figure 8:** Crystal structure of v-FLIP/NEMO (PDB 3CL3). The two ks-v-FLIP (Kaposi's sarcoma herpes virus (KSHV)) domains (yellow and red) interacting with the NEMO dimer (bright and dark blue) are shown (Bagn ris et al., 2008). The structure is derived from the NEMO part 193 – 252 and the ks-v-FLIP amino acids 2 – 174. The ks-v-FLIP sequence includes its tandem DEDs (DED1: amino acids 5 - 8, DED2: amino acids 94 – 168). From the protein data bank (Berman, 2000).

### ***1.3 Post-translational modifications in NF- $\kappa$ B and other signaling pathways***

Post-translational modifications (PTMs) are not only necessary for the activation of the NF- $\kappa$ B signaling pathway but also are important for the regulation of many other protein activities. They include cleavage of the protein, attachment of inorganic and organic molecules, addition of small proteins, and binding of proteins to bigger protein complexes. The most common PTMs are phosphorylation, acetylation, glycosylation, amidation, hydroxylation, methylation, and ubiquitination

(Khoury et al., 2011). Among other processes, PTMs influence the activity, localization, stability, or degradation of a protein. In the present study, the attention was especially focused to ubiquitination.

### **1.3.1 Ubiquitination**

One of the important PTMs is the addition of ubiquitin to a target protein. This process is called ubiquitination or ubiquitylation. Ubiquitin is a small protein with the molecular weight of 8.5 kDa that consists of 76 amino acids (Goldstein et al., 1975). The name is derived from its ubiquitous expression in eukaryotic cells and shows a high degree of conservation in different species. Ubiquitin is linked to lysine (K) residues of substrate proteins or other ubiquitin molecules to form chains in a multi-step process. First, an E1 enzyme activates ubiquitin in an ATP dependent mechanism. This results in a thioester binding between the E1 enzyme and the C-terminus of ubiquitin. Second, the active ubiquitin is transferred from the E1 enzyme to the active cysteine of an ubiquitin conjugating E2 enzyme. Third, an E3 ubiquitin ligase forms an isopeptide bond between the C-terminal glycine of ubiquitin and a lysine of the target protein (Hershko et al., 1983; Zinngrebe et al., 2014). While only two E1 enzymes are encoded in the human genome, at least 38 E2 enzymes and more than 600 E3 enzymes exist (Ye and Rape, 2009). The variety of E3 enzymes allows high specificity of the ubiquitination process in modifying the target proteins.

Proteins are ubiquitinated with one ubiquitin (monoubiquitination) or with chains of ubiquitin linked *via* one of the seven lysine (K6, K11, K27, K29, K33, K48, K63) residues of ubiquitin or *via* its N-terminus (M1, linear, Figure 9). This linkage results in chains of mixed linkage as well as chains consisting only of one linkage type. Also, linkage of more than one ubiquitin to another ubiquitin can form branched structures (Husnjak and Dikic, 2012). For the study on NF- $\kappa$ B activation, the effects of K48, K63 and linear ubiquitin chains are most important.

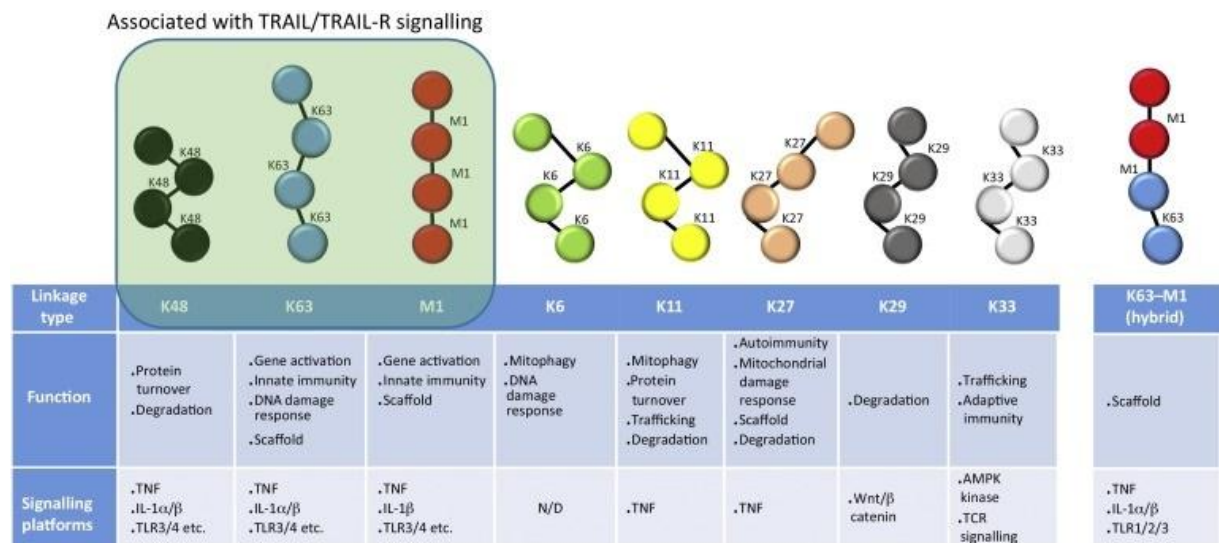


**Figure 9: Ubiquitin chain types, its functions and signaling platforms.** Ubiquitin chains are formed from ubiquitin monomers *via* isopeptide or peptide (linear) bonds. The linkage is possible *via* one of seven lysine (K6, K11, K27, K29, K33, K48, K63) residues of ubiquitin or *via* its N-terminus (M1, linear). K48, K63 and linear chains are associated to TRAIL-R signaling and are most important in this study of CD95-induced NF- $\kappa$ B signaling. Below the chain type their main functions and signaling platforms are shown. From (Lafont et al., 2018)

The variety of polyubiquitin chain linkages allows regulation of a high number of specific cellular functions (Figure 9). The best studied ubiquitin chains are linked *via* K48 and mark target proteins for proteasomal degradation, this was also the first described function of ubiquitin chains (Chau et al., 1989). The proteasome is a multiprotein complex that consists of several proteases and is found in all eukaryotes and archaea and in some bacteria. It is important for breakdown of damaged proteins and thereby additionally regulates several signal pathways by changing protein levels. For example, in the canonical NF- $\kappa$ B signaling pathway the inhibitor I $\kappa$ B $\alpha$  is K48 ubiquitinated after phosphorylation and thereby marked for proteasomal degradation. After degradation, the transcription factors p50 and p65 are not hold in the cytosol any longer and are able translocate to the nucleus (Zinngrube et al., 2014). A different form of ubiquitin linkage, the K63 linked ubiquitin chains support the assembly of protein complexes and are linked to signaling events in DNA damage and cytokine production (Zinngrube et al., 2014). K63 chains linked to NEMO are important for recruitment of the TAB2/3-TAK1 complex and thereby activate the IKK complex (Adhikari et al., 2007). Notably, it was discovered that mixed

K63-linear ubiquitin chains are important for pro-inflammatory IL-1 signaling. In this case, the K63 polyubiquitination was shown to be a prerequisite for attraction of HOIP and linear ubiquitination (Emmerich et al., 2013). Linear ubiquitin chains are ligated to target proteins exclusively by the LUBAC protein complex and support assembly of protein complexes (Haas et al., 2009; Tokunaga et al., 2009). As an illustration of these effects, it was shown that deletion of LUBAC or blockade of linear ubiquitin recognition strongly reduced NF- $\kappa$ B activation after TNF-R stimulation or genotoxic stress (Haas et al., 2009; Niu et al., 2011; Rahighi et al., 2009).

Ubiquitination can be reversed by DUBs. Deubiquitination is important for reversing functions of ubiquitination, thereby DUBs regulate many signaling pathways. Around 100 DUBs are known and they recognize specific ubiquitin linkage types. DUBs can be divided into five families: ubiquitin c-terminal hydrolases (UCHs), ovarian tumor proteases (OTUs), ubiquitin specific proteases (USPs), josephins and JAB1/MPN/MOV34 metalloenzymes, with the first four groups being cysteine proteases and the last group being zinc metalloproteases (Komander et al., 2009). Noteworthy, OTULIN is the only known DUB for linear ubiquitin linkage chains (Fiil et al., 2013; Keusekotten et al., 2013; Rivkin et al., 2013). The activity of DUBs is needed for three major functions: Firstly, ubiquitinated proteins are deubiquitinated and are thereby for example rescued from proteasomal degradation. Secondly, DUB activity modifies protein ubiquitination by removing of a specific linkage type which is then replaced by different specific ubiquitin chain. Thirdly, DUB activity is needed for precursor processing and cleavage of polyubiquitin chains and thereby making them available for further usage by the ubiquitin ligation systems (Gupta et al., 2018; Komander et al., 2009; McClurg and Robson, 2015).

## 1.4 Autophagy

The PTM ubiquitination does not only play an important role in NF- $\kappa$ B activation but also in the induction of autophagy. Autophagy is a regulated process that degrades unnecessary or dysfunctional cellular components thereby maintaining cellular homeostasis. Autophagy also supports cells to survive starving conditions by digesting cellular components. These cellular components are bulk protein aggregates, dysfunctional organelles or invading pathogens (Kroemer et al., 2010; Levine et al., 2011). Different autophagy pathways are known and they are mainly regulated by specific proteins called autophagy related (ATG) proteins, that were found first in yeasts (Tsukada and Ohsumi, 1993).

Different forms of autophagy exist and they are named by its target. Macroautophagy is the most prominent autophagy process in cells and leads to degradation of organelles and proteins. The first step in macroautophagy is the formation of the double-layered membrane structure called phagophore around the target of degradation. The formation of the phagophore is dependent on specific autophagy receptors that recognize their target and bridge it to Atg8/LC3 proteins (LC3 in mammals) which finally results in the formation of the double membrane layered vesicle called autophagosome (Heller et al., 1975; Randow and Youle, 2014). The autophagosome transports its content to lysosomes and fuses to the lysosomes outer membrane. This process results in degradation of the autophagosomes inner membrane and its content *via* lysosomal lysis. In contrast to this, during microautophagy the cytosolic material that should be degraded is directly engulfed into the lysosome. Microautophagy is often activated under starvation conditions to ensure cell survival *via* providing of cellular components, especially amino acids, for basic cellular processes. Also during chaperone-mediated autophagy, chaperone targeted proteins are directly transported through the lysosomal membrane. This allows selective degradation of single proteins and hence, regulation of protein levels and signaling pathways. Also, the selective degradation of whole organelles *e.g.* mitochondria by autophagy can take place, which is called mitophagy. Healthy mitochondria constantly import and degrade the protein PTEN-induced putative kinase 1 (PINK1). If a mitochondrion is damaged, PINK1 accumulates

at the outer mitochondrial membrane. Then the E3 ubiquitin ligase parkin binds to PINK1 and ubiquitinates the damaged mitochondrion. This ubiquitination marks the mitochondrion for interaction with the autophagy receptors p62 and NBR1 that recruit the phagophore *via* LC3 binding and thereby starts its autophagic break down (Randow and Youle, 2014). Another similar autophagic process is xenophagy, and here invading bacteria or viruses are ubiquitinated by the cellular innate immune system and thereby marked for autophagic degradation (Corrocher et al., 1975; Xie et al., 2015).

#### **1.4.1 The autophagy receptor NDP52**

An autophagy receptor that is involved in virus-host interactions is the nuclear dot protein 52 (NDP52, also known as calcium binding and coiled-coil domain 2 (CALCOCO2)) and was first described as a nuclear protein (Korioth et al., 1995). Later it was shown that it is mainly not nuclear, but localized in the cytosol and involved in degradation of invading pathogens by autophagy (xenophagy) (Mostowy et al., 2011; Thurston et al., 2009; van Wijk et al., 2017). It is able to bind polyubiquitin and galectin 8, which marks pathogen damaged vesicles, and bind to LC3 thereby inducing autophagosome formation (Thurston et al., 2009, 2012; Verlhac et al., 2015). This mechanism is important to restrict cellular infection with bacteria, *e.g. Salmonella, Listeria* and *Shigella* (Thurston et al., 2012).

NDP52 is 52 kDa large and has several domains that are important for its functions linked to autophagy of pathogens and ubiquitinated targets. N-terminal, it has a SKICH-domain that binds to the ubiquitin binding proteins nap1 and sintbad. The ubiquitin-binding function of Nap1 and sintbad was shown to be important for inhibiting bacterial growth in cytosolic vesicles by ubiquitination of these vesicles (Thurston et al., 2009). The central LC3 interacting (LIR) domain of NDP52 interacts with LC3C (Verlhac et al., 2015) thereby inducing autophagosome formation and degradation of the bacteria containing vesicles. The middle region of NDP52 is predicted to form a coiled coil domain (white, Figure 10). This coiled coil domain is important to form NDP52 dimers and interacts with the

E3 ubiquitin ligase leucine rich repeat and sterile  $\alpha$  motif containing 1 (LRSAM1) during xenophagy (Huett et al., 2012; Kim et al., 2013). It was shown that NDP52 is able to specifically degrade TLR pathway components thereby increasing TLR-induced NF- $\kappa$ B activation (Inomata et al., 2012). Interestingly, whole exome sequencing showed that the missense mutation V248A in the coiled coil domain of NDP52 is linked to Crohn's disease (CD) (Ellinghaus et al., 2013). CD is an inflammatory bowel disease that is caused by defective xenophagy. The V248A mutation reduces NDP52 ability to limit TLR3-induced NF- $\kappa$ B activation and thereby give rise to bowel inflammation (Ellinghaus et al., 2013). The galectin 8 interacting region (GIR) of NDP52 specifically interacts with the sugar receptor galectin 8 which is important to mark pathogen damaged vesicles (Thurston et al., 2012). NDP52 second ZF (zinc finger) domain (dark red aa420-446, Figure 10) is able to bind to K63, K48, and M1-linked ubiquitin while the first ZF (light red, Figure 10) has no ubiquitin binding activity (Xie et al., 2015).

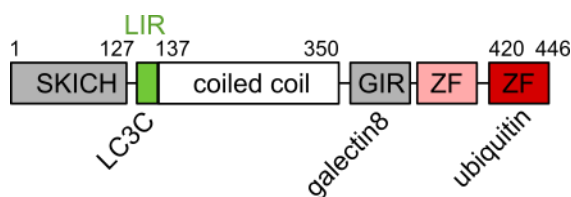


**Figure 10: NDP52 domain structure.** The top shows NDP52 with important domains (not scaled). Below, selected interaction partners are shown. SKICH: SKIP carboxyl homology, LIR (green): LC3 interacting region, GIR: galectin interacting region, ZF (red): zinc finger domain

## **1.5 Aim of the study**

While it is well described how stimulation of CD95 induces cell death by activation of the caspase cascade, it is not fully understood how the receptor activates the NF- $\kappa$ B pathway (Lavrik and Krammer, 2012). Several key points of CD95-mediated NF- $\kappa$ B control were addressed in this study. Of special interest in this study has been deciphering how these opposing pathways are induced in parallel in one single cell (Peter et al., 2015). On the molecular level, different proteins are described to be important for CD95-induced NF- $\kappa$ B activation, *e.g.* caspase-8, FADD, c-FLIP, TRAF2, NEMO (Golks et al., 2006; Kataoka and Tschopp, 2004; Neumann et al., 2010). The main focus of this study has been to analyze the role of c-FLIP and NEMO in CD95-induced NF- $\kappa$ B activity. Furthermore, as yet unidentified interaction partners of c-FLIP and NEMO play the key role in CD95-mediated NF- $\kappa$ B control, the major focus of this work was directed towards identification of the new interactome of these proteins.

For deciphering the life/death decision in single cells new methods that overcome the limits of bulk population analysis by immunoblotting and the limit in the number of analyzed cells in microscopy had to be developed. Understanding the signaling pathway at molecular and single cell levels will enable to specifically control cellular responses and thereby cure diseases that are a result of imbalanced CD95 signaling. For example, blocking CD95-induced NF- $\kappa$ B activation might help to kill cancer cells that are using this pathway as a pro-survival mechanism to escape CD95-induced apoptosis (Peter et al., 2015). Of special interest was to identify the role of the c-FLIP-NEMO interaction for activating the NF- $\kappa$ B pathway. Another major focus was the analysis if this interaction is direct or indirect and to find as above mentioned new interactions partners of c-FLIP and NEMO to better understand the CD95-induced NF- $\kappa$ B activation. This will allow the development of new specific inhibitors of CD95-induced pro-survival signaling and thereby pave the way towards new efficient anti-cancer therapies.

## 2 Material and methods

### 2.1 Material

#### 2.1.1 Chemicals and reagents

All chemicals were ordered from Carl Roth (Karlsruhe, Germany), Sigma Aldrich (Taufkirchen, Germany) or PanReac Applichem (Darmstadt, Germany) if not stated otherwise.

Reagent	Manufacturer
7AAD (7-Aminoactinomycin D)	BioLegend (San Diego, USA)
Precision Plus Protein Marker	Biorad (Hercules, USA)
Protein A Sepharose	GE Healthcare (Freiburg, Germany)
Z-Val-Ala-DL-Asp-fluoromethylketone (zVAD)	Bachem (Weil am Rhein, Germany)

#### 2.1.2 Cell culture media and supplements

Media/ reagent	Manufacturer
DMEM/ HamsF12 (1:1)	Biochrom AG (Berlin, Germany)
RPMI1640	Life (Darmstadt, Germany)
Fetal calf serum (FCS)	Biochrom AG (Berlin, Germany)
Penicillin/ Streptomycin (Pen/Strep)	Biochrom AG (Berlin, Germany)
Puromycin	Invivogen (Toulouse, France)
Trypsin EDTA (0.05%)	ThermoFisher (Schwerte, Germany)

#### 2.1.3 Antibodies for immunoblotting

Antigen	Company	Dilution	Species
A20 (clone A12)	SantaCruz (Dallas, USA)	1:500	mouse
Actin (A2103)	Sigma (Taufkirchen, Germany)	1:4,000	rabbit
BCL10	CellSignalingTechnology (Danvers, USA)	1:2,000	rabbit
Calcoco2/NDP52 (12229)	ProteinTech (Rosemont, USA)	1:4,000	rabbit
Carma1/CARD11 (166910)	SantaCruz (Dallas, USA)	1:200	mouse
Caspase-8 (clone C15)	Gift of Peter Krammer, DKFZ (Heidelberg, Germany)	1:10	mouse IgG2b
CD95 (715)	SantaCruz, (Dallas, USA)	1:2,000	rabbit
c-FLIP (clone NF-6)	Gift of Peter Krammer, DKFZ (Heidelberg, Germany)	1:500	mouse IgG1
FADD (clone 1C4)	Gift of Peter Krammer, DKFZ (Heidelberg, Germany)	1:500	mouse IgG1

<b>Antigen</b>	<b>Company</b>	<b>Dilution</b>	<b>Species</b>
FLAG	Sigma (Taufkirchen, Germany)	1:2,000	mouse IgG1
GAPDH (48166)	SantaCruz, (Dallas, USA)	1:2,000	goat
HA (3724)	CellSignalingTechnology (Danvers, USA)	1:1,000	mouse IgG1
I $\kappa$ B $\alpha$ (4812)	CellSignalingTechnology (Danvers, USA)	1:2,000	rabbit
IKK $\gamma$ /NEMO (FL-419)	SantaCruz, (Dallas, USA)	1:400	rabbit
IKK $\gamma$ /NEMO (DA10-12)	CellSignalingTechnology (Danvers, USA)	1:2,000	mouse IgG1
MALT1 (130494)	SantaCruz, (Dallas, USA)	1:200	mouse IgG1
Phospho-I $\kappa$ B $\alpha$ (2859)	CellSignalingTechnology (Danvers, USA)	1:1,000	rabbit
Phospho-I $\kappa$ B $\alpha$ (Ser32/36, 9246)	CellSignalingTechnology (Danvers, USA)	1:2,000	mouse IgG1
RIP1 XP (3493)	CellSignalingTechnology (Danvers, USA)	1:2,000	rabbit
TRAF2 (4724)	CellSignalingTechnology (Danvers, USA)	1:1,000	rabbit
UBC9 (sc271057)	SantaCruz, (Dallas, USA)	1:400	mouse IgG1
Ubiquitin (3936)	CellSignalingTechnology (Danvers, USA)	1:2,000	mouse IgG1
Ubiquitin K48 (12805)	CellSignalingTechnology (Danvers, USA)	1:2,000	rabbit
Ubiquitin K63 (12930)	CellSignalingTechnology (Danvers, USA)	1:2,000	rabbit

### **2.1.4 Secondary antibodies for immunoblotting**

<b>Antigen</b>	<b>Company</b>	<b>Dilution</b>	<b>Species</b>
Mouse IgG1	SantaCruz (Dallas, USA)	1:5,000	goat
Mouse IgG 2a	SantaCruz (Dallas, USA)	1:5,000	goat
Mouse IgG 2b	SantaCruz (Dallas, USA)	1:5,000	goat
Total mouse IgG	SantaCruz (Dallas, USA)	1:5,000	goat
Rabbit IgG	SantaCruz (Dallas, USA)	1:10,000	goat
Goat IgG	SantaCruz (Dallas, USA)	1:10,000	rabbit
Non-denaturated mouse IgG (easyblot mouse)	GeneTex (Irvine, USA)	1:1,000	Not specified
Non-denaturated rabbit IgG (easyblot rabbit)	GeneTex (Irvine, USA)	1:2,000	mouse

### 2.1.5 Antibodies for flow cytometry

Antigen	Conjugated dye	Manufacturer	Usage per 5*10 <sup>5</sup> cells in 50 µl
Cleaved caspase-3 (Asp175)	AlexaFluor488	CellSignalingTechnology (Danvers, USA)	1 µl
Cleaved caspase-3 (Asp175)	AlexaFluor647	CellSignalingTechnology (Danvers, USA)	1 µl
NF-κB p65	PE	CellSignalingTechnology (Danvers, USA)	0.5 µl

### 2.1.6 Kits

Name of the kit	Manufacturer
Pierce co-IP-kit	FisherScientific (Schwerte, Germany)
Human IL-6 Elisa MAX standard	BioLegend (San Diego, USA)
Human IL-8 Elisa MAX standard	BioLegend (San Diego, USA)

### 2.1.7 Buffers

Lysis buffer	
20 mM	TrisHCl pH7.4
137 mM	NaCl
2 mM	EDTA
10 %	Glycerol
1 %	Triton X-100
According to manufacturer 1x	Complete protease inhibitor (Roche, Mannheim, Germany)

PBS (2 l, 20x concentrated)	
320 g	NaCl
8 g	KCl
56.8 g	Na <sub>2</sub> HPO <sub>4</sub> without H <sub>2</sub> O
8 g	KH <sub>2</sub> PO <sub>4</sub>
Add to 2 l	Deionized H <sub>2</sub> O

**PBS-T (0.1 %):** add 1 ml TWEEN20 to 1 l PBS

**Blocking buffer:** add 50 g non-fat dried milk powder to 1 l of PBS-T

<b>Electrophoresis buffer (2 l, 10x concentrated)</b>	
60.6 g	Tris
288 g	Glycin
20 g	SDS
Add to 2 l	Deionized H <sub>2</sub> O

### 2.1.8 Plasmids

Name	Background	Reference
c-FLIP <sub>L</sub>	pcDNA3	(Golks et al., 2006)
NDP52 WT	NDP52 WT cloned into pIRESpuro3, EcoR1/Nhe1	(Öztürk, 2014)

### 2.1.9 Synthetic peptides

Peptides were synthesized by LifeTein LLC (Summerset, NJ, USA) and had at least 95 % purity. The N-terminus was acetylated and the C-terminus was amidated for extended stability. LifeTein has performed quality control *via* mass spectrometry and liquid chromatography analysis.

Name	Peptide sequence	MW	Domains
tat-Nemo-FITC	GRKKRRQRRRPQLAQLQVAYHQLFQEYDNHI	4436,09	tat +Nemo 227-245
tat-scr-Nemo-FITC	GRKKRRQRRRPQAVNLEQYQQLDAFILHHYQ	4436,09	tat +scrNemo
tat-Nemo	GRKKRRQRRRPQLAQLQVAYHQLFQEYDNHI	3975,57	tat +Nemo 227-245
tat-scr-Nemo	GRKKRRQRRRPQAVNLEQYQQLDAFILHHYQ	3975,57	tat +scrNemo
Nemo-tat	LAQLQVAYHQLFQEYDNHIGRKKRRQRRRPQ	3975,57	Nemo 227-245 +tat
Scr-Nemo-tat	AVNLEQYQQLDAFILHHYQGRKKRRQRRRPQ	3975,57	scrNemo 227-245 +tat
Nemo-R9	LAQLQVAYHQLFQEYDNHIKSSRRRRRRRRR	4079,69	Nemo 227-248 +R9
Scr-Nemo-R9	EQAQSYIVAHYDLFNLHKQSLRRRRRRRRR	4079,69	scrNemo 227-248 +R9
FNIIP	LAQLQVAYHQLFQEYDNHIKSS	2673,94	Nemo 227-248

Name	Peptide sequence	MW	Domains
scrFNIIP	EQAQQSYIVAHYDLFNLHKQSL	2673,94	scrNemo 227-248
superFNIIP	LAQLQVAYHQLFQEYYNHKSSRRRRRRRRR	4127,69	opt.Nemo 227-248 +R9
nosuperFNIIP	LAQLQVAYHQLAQEYANHIKSSRRRRRRRRR	3959,49	neg.con. Nemo 227-248 +R9

### 2.1.10 Cell lines

Cell line	Properties	Media	Origin
HeLa cells overexpressing CD95 (HeLa-CD95)	Cervix carcinoma cells stably expressing CD95	DMEM/HamsF12 (1:1), 10% FCS, 1% Pen/Strep, 10 ng/ml Puromycin	(Neumann et al., 2010)
HeLa-CD95 c-FLIP <sub>L</sub> overexpressing (LW3)	HeLa-CD95 with additional expression of c-FLIP <sub>L</sub>	DMEM/HamsF12 (1:1), 10% FCS, 1% Pen/Strep, 10 ng/ml Puromycin	(Busse, 2017; Espe, 2017)
Jurkat (DSMZ: ACC 282)	T-cell leukemia	RPMI1640, 10% FCS, 1% Pen/Strep	(DSMZ: ACC 282)
HeLa FRL	HeLa-CD95 with overexpression of c-FLIP <sub>Long</sub> and c-FLIP <sub>Raji</sub>	DMEM/HamsF12 (1:1), 10% FCS, 1% Pen/Strep, 10 ng/ml Puromycin	(Fricker et al., 2010)

## 2.2 Methods

### 2.2.1 Cell culture

Cells were cultivated at 37°C, 95% humidity and 5% CO<sub>2</sub>. Cells were sub-cultivated under sterile conditions in a sterile work bench. Adherent cells were split by trypsin detachment every two to three days and not grown to a concentration higher than 2\*10<sup>7</sup> cells per 175cm<sup>2</sup> growing area. Suspension cells were divided every two to three days into fresh media and not grown to more than 5\*10<sup>5</sup> cells per ml.

### **2.2.2 Thawing cells**

Media was prepared, added to cell culture flask and incubated at 37°C, 95% humidity and 5% CO<sub>2</sub> for 30 minutes. Cells were thawed in 37°C water bath for 90 to 120 seconds and immediately transferred to the prepared flask. After 24 hours media was removed and fresh media was given to the cells.

### **2.2.3 Freezing cells**

Adherent cells were detached with trypsin and washed with PBS. Suspension cells were washed with PBS.  $5 \times 10^6$  cells were suspended in 900  $\mu$ l FCS and 100  $\mu$ l DMSO. Cells were frozen in “Mr. Frosty TM” freezing container at -80°C and transferred to -150°C after two days.

### **2.2.4 siRNA mediated protein knock down**

Reduction of protein levels (knock down) was performed by transfecting small interfering RNA (siRNA) with DharmaFECT1 transfection reagent according to the manufactures protocol (Dharmacon, Lafayette, USA). Shortly,  $1.25 \times 10^5$  cells per 6-well plate were seeded in antibiotic free media. On the next day, the media was replaced with 1.6 ml fresh antibiotic free media. 10  $\mu$ l of 5  $\mu$ M siRNA were mixed with 190  $\mu$ l OptiMEM (FisherScientific, Schwerte, Germany) while 5  $\mu$ l of DharmaFECT1 were mixed with 195  $\mu$ l OptiMEM in a second tube. After 10 minutes at room temperature, both tubes were mixed and incubated another 20 minutes at room temperature. 400  $\mu$ l of this transfection mix were dropwise added to the cells. After 24 hours, media was replaced with new antibiotic free media. After 48 hours cells were stimulated as described below. For IL-6 and IL-8 ELISA, cells were trypsinated after 24 hours and seeded into 96 well plate and 6 well plates.

Dual knock down and re-expression of NDP52 was performed with DharmaFECTDuo transfection reagent (Dharmacon, Lafayette, USA) according to the manufactures’ protocol. Therefore, 4  $\mu$ l of 5  $\mu$ M siRNA targeting NDP52 and 1  $\mu$ g vector for re-expression of NDP52 per well in a 6-well plate were transfected in parallel into the cells.

<b>Target protein</b>	<b>Product name</b>	<b>Manufacturer</b>
NDP52/ Calcoco2	ON-TARGET plus Human NDP52/CALCOCO2 siRNA pool	Dharmacon (Lafayette, USA)
BCL10	Hs_BCL10_4 FlexiTube siRNA and Hs_BCL10_7 FlexiTube siRNA (1:1 mix)	Qiagen (Hilden, Germany)
MALT1	Hs_MALT1_1 FlexiTube siRNA and Hs_MALT1_6 FlexiTube siRNA (1:1 mix)	Qiagen (Hilden, Germany)

### ***2.2.5 Cell stimulation and harvesting for immunoblotting***

For stimulation of adherent cells  $5 \times 10^5$  cells per well were seeded in a 6-well plate. On the next day, medium was removed and 0.5 ml fresh medium including stimulation reagents was added. After stimulation, ice-cold PBS was added to the media and cells were scratched off with cell scrapers, media and cells were transferred to a reaction tube, and spun down at 500xg and 4°C for 5 minutes. After removing the supernatant, cells were washed one more time with 1 ml of PBS and spun down at 500xg and 4°C for 5 minutes. Supernatant was aspirated and cell pellet was directly subjected to cell lysis or stored at -20°C for short term storage and at -80°C for long term storage.

Suspension cells were counted on the day of stimulation and  $1 \times 10^6$  cells were stimulated in a well of a 24 well plate in 1 ml of fresh medium. After stimulation cells were mixed with ice-cold PBS and spun down at 500xg and 4°C for 5 minutes. Cells were washed one more time with 1 ml of PBS and spun down at 500xg and 4°C for 5 minutes. Supernatant was aspirated and the cell pellet was directly subjected to cell lysis or stored at -20°C.

### ***2.2.6 Cell lysis***

For the cell lysis, the cell pellet was suspended in lysis buffer (20 mM Tris HCl, pH 7.4, 137 mM NaCl, 2 mM EDTA, 10% glycerol, 1% Triton X-100, 1x protease inhibitor mix (Roche, Mannheim, Germany)) and incubated for 30 minutes on ice. After centrifugation for 15 minutes at 4°C and 14,600xg, the supernatant was transferred to new tubes and the pellet consisting of cell debris was discarded. For immunoblotting, protein concentrations were determined with Bradford assay.

### **2.2.7 Determination of protein concentration via Bradford assay**

Bradford reagent was prepared by mixing 10 ml of BioRad Bradford protein assay reagent (Biorad, Hercules, USA) with 40 ml of MilliQ water. 2 µl of the cell lysate was pipetted into a cuvette. Then, 1 ml of Bradford reagent was added to the cuvettes. After short vortexing and 5 minutes incubation time, the absorbance at 595 nm was measured with a photo spectrometer (Biorad, Hercules, USA). BSA standard (Biorad, Hercules, USA) was used for establishing standard curve.

### **2.2.8 Immunoblotting**

25 µg total protein lysate was heated at 95°C in Laemmli buffer for 5 minutes. Samples were loaded on pre-cast SDS mini-PROTEAN TGX stain-free™ (mini) or Criterion TGX™ (midi) gels (all Biorad, Hercules, USA). Proteins were separated using Biorad TetraCell at constant voltage of 120 V. Transfer to nitrocellulose membrane (Trans-Blot Turbo RTA Mini Nitrocellulose Transfer Kit) was performed in TransBlot Turbo system according to the manufacturer's instructions (Biorad, Hercules, USA) with 25 V, 2.5 A for 7 minutes. After blotting membranes were washed in PBS-T once (PBS with 0,05% Tween), blocked for one hour in 5% non-fat dried milk in PBS-T, washed 3 times with PBS-T and incubated over night with primary antibodies.

On the next day, membranes were washed three to four times with PBS-T and incubated for one hour at room temperature with HRP labeled isotype specific secondary antibodies (SantaCruz, Dallas, USA) in 5% non-fat dried milk in PBS-T. After washing the membranes three times with PBS-T, 1 ml of the HRP substrate "Luminata forte" (strong substrate) or "crescendo" (middle strong substrate, MerckMillipore, Darmstadt, Germany) per membrane was added. Detection was performed with ChemiDoc imaging system (Biorad, Hercules, USA).

### **2.2.9 Immunoprecipitation**

First, protein A sepharose beads were prepared for immunoprecipitations (IPs). Therefore, 0.5 g protein A sepharose beads were put into a 50 ml reaction tube. The tube was filled with MilliQ water

and inverted till the beads were completely solved (no vortexing). For washing, beads were spun down for 10 minutes at 500xg and supernatant was discarded. After three more washing steps with 50 ml MilliQ water, one third of the beads volume lysis buffer was added and beads were stored at 4°C.

For standard IP,  $1 \times 10^7$  cells were stimulated, harvested and lysed in 1 ml lysis buffer. 900 µl of the lysate was used for IP. 10 µl protein A sepharose beads and required concentration of antibodies (0.5-5 µg) were added to lysate and incubated end over end mixing at 4°C from 2 hours to over-night. Over-night incubation was used for IP of the DISC and complex. After this incubation, the beads were washed four times by adding 1 ml of cold PBS and spinning down of the beads for 5 minutes at 500xg and 4°C. After the last wash, the remaining PBS was aspirated with a 50 µl Hamilton pipette. Special care was taken to clean the Hamilton pipette between the washing steps. Beads were stored at -20°C or directly boiled in 30 to 60 µl 1x Laemmli buffer for 5 minutes.

For analyzing of protein modifications, denaturing IPs were performed. Cells were lysed as described before, but instead of 1 ml standard lysis buffer, a small volume of 100 µl lysis buffer supplemented with 10 mM N-ethylmaleimide (NEM) was used. After transfer of the lysates to new tubes, SDS was added to a final concentration of 1% and the lysates were boiled at 95°C for 5 minutes. After boiling, 900 µl of standard lysis buffer was added to dilute the SDS to a final concentration of 0.1%. The following IP was performed as described above.

For analysis of proteins that have a similar size as the light or heavy chain of the antibodies used for IP (approximately 25 kDa or 50 kDa, respectively), IPs were performed with antibodies covalently coupled to beads. For covalent antibody coupling, the Pierce CO-IP kit (FisherScientific, Schwerte, Germany) was used according to the manufacturer's instruction. Shortly, antibodies were coupled to the beads, incubated with the lysates for 2 h or overnight and washed four times with 200 µl PBS. Bound proteins were eluted with the CO-IP kit's elution buffer without eluting the coupled antibodies. Eluates were mixed with Laemmli buffer and subjected to immunoblotting.

### **2.2.10 Size exclusion chromatography (gel filtration)**

Size exclusion chromatography (gel filtration) was performed with a Superose 6 10/300 column that was connected to the Äkta pure 25 L chromatography system (both GE Healthcare, Freiburg, Germany) and was washed with at least two column volumes (CV) of lysis buffer overnight. On the day of the experiment, HeLa-CD95 cells were stimulated with 50 ng/ml CD95L for 15 minutes, harvested, and lysed. After protein concentration determination, lysates were diluted with lysis buffer to a final protein concentration of 10 mg/ml. 500 µl of this lysate was filled into a 250 µl sample loop with a syringe to ensure that the sample loop is completely filled with lysate. During the gel filtration run, first the column was equilibrated with 0.4 CV lysis buffer. After equilibration, the sample was loaded with 500 µl lysis buffer from the sample loop onto the column. After another 0.25 CV, the fractionation was started. 26 fractions with 500 µl sample volume were collected in reaction tubes preloaded with 20 µl protease inhibitor. These fractions were analyzed by immunoblot or pooled for IPs as described below. All gel filtration steps were performed at 4°C and with a pump speed of 0.2 ml/min.

For DISC IPs the fractions 2 to 6, 7 to 10, 11 to 14, 15 to 18, 19 to 22 and 23 to 27 were pooled together. Next, 2 µg of  $\alpha$ -APO-1 antibody with 10 µl of protein A sepharose beads were added and incubated at 4°C overnight at end over end mixing. Beads were washed three times with 1 ml lysis buffer and once with 1 ml PBS and boiled in Laemmli buffer for immunoblot analysis. IP supernatant was incubated with 10 µl of protein A sepharose beads to remove remaining  $\alpha$ -APO-1 antibody. After 2 hours end over end mixing at 4°C, the supernatant of the protein A sepharose beads was subjected to caspase-8, c-FLIP or FADD IP. Therefore, it was mixed with 10 µl of protein A sepharose beads and 10 µg of caspase-8 antibody, 2 µg of c-FLIP antibody (clone NF-6) or 2 µg of FADD antibody. After 2 hours end over end mixing at 4°C the beads were washed three times with 1 ml lysis buffer and once with 1 ml PBS. Finally, the beads were boiled in Laemmli buffer for 5 minutes at 95°C and subjected to immunoblot analysis.

### **2.2.11 Cell stimulation for imaging flow cytometry**

2.5\*10<sup>5</sup> HeLa cells per well in a 6-well plate were seeded. On the next day, medium was removed and cells were stimulated or left untreated in 0.5 ml fresh medium. After stimulation, medium was removed and collected in a reaction tube. Cells were washed once with PBS to remove leftovers of medium and PBS was transferred to the collection tube. Trypsin was added to the cells to induce detachment and cells were incubated for 5 minutes at 37°C. After the incubation, detachment was checked *via* microscopic inspection and cells were transferred to the collection tube. As apoptosis is accompanied by detachment, it is important to harvest adherent cells that are healthy or in early phase of apoptosis as well as detached dead cells swimming in the medium. After centrifugation for 5 minutes at 500xg and 4°C supernatant was removed and cell pellet were washed with 1 ml PBS in 1.5 ml tubes for further fixation.

### **2.2.12 Staining the cells for imaging flow cytometry**

After stimulation, cells were transferred into reaction tubes, spun down at 500xg at 4°C for five minutes and supernatant was aspirated. Cells were suspended in 250 µl of PBS and 250 µl of 6% formaldehyde in PBS was added. Cells were incubated for 10 minutes at room temperature. After spinning down and aspiration of the supernatant, 100 µl of ice-cold 90% methanol (in water) was added to the cells and cells were incubated for 30 minutes on ice. At this stage of the experiment, it is possible to transfer cells to -20°C for long time storage.

For staining, cells were spun down at 500xg and 4°C for 5 minutes and supernatant was aspirated. Cells were washed twice with 500 µl of incubation buffer (5 g/l serum albumin fraction V in PBS). Next, cells were suspended in 50 µl of incubation buffer and stained with antibodies (see 2.1.5) coupled to fluorescent dyes for 1h on-ice in the dark. Cells were spun down, supernatant was aspirated and cells were washed one more time with incubation buffer. Cells were resuspended in 30 µl PBS and

at least 5 minutes before measurements, 3  $\mu$ l 7AAD (50  $\mu$ g/ml, BioLegend, San Diego, USA) was added to ensure similar incubation times during the measurement.

### **2.2.13 Imaging flow cytometry data acquisition**

Cells were analyzed with Amnis FlowSight. Images of 10,000 cells in the required fluorescence channels (FITC: channel 2 (wave length 505-560 nm), PE: channel 3 (560-595 nm), 7AAD: channel 5 (642-745 nm), AlexaFluor647: channel 11 (642-745 nm)) as well as in two bright field channels (channel 1 (435-505 nm) and 9 (560-595 nm)) and the dark field channel (channel 6) were acquired. Therefore, a single cell selection in the area of a mask in the bright field channel 1 (M1) *versus* aspect ratio M1 blot was used. Depending on the fluorescent dyes used in the experiment, cells were excited with the corresponding 405 nm, 488 nm, 561nm and/or 642 nm lasers. Samples serving as positive controls were used to adjust the laser to the optimal power and special care was taken that the maximal pixel intensities were not exceeding the maximal measuring range. For compensation of the spectral overlaps, single dye stained cells were acquired in presence of switched off bright field LEDs and dark field laser.

### **2.2.14 Imaging flow cytometry data analysis**

Data analysis was performed with the IDEAS software versions 6.0 to 6.2. Automated compensation was calculated with single dye stained samples. For the analysis, images of focused cells were selected by using the gradient RMS feature of the bright field channel, which describes the sharpness of the images. As a second step, single cells were selected by the parameters area and aspect ratio of the bright field mask. The aspect ratio describes the ratio between the longest and the shortest axis of a mask covering the cells, while the area simply describes the area of the bright field mask. Cell doublets have a smaller/decreased aspect ratio compared to single cells, while clumps of cells have a similar aspect ratio, but an increased cell area. By using these two characteristics, single cells can be easily identified.

For analyzing the p65 translocation, only cells with a double staining for p65 and nuclear 7AAD were selected. The translocation of p65 was analyzed by comparing the similarity of the p65 and the nuclear 7AAD signals. The similarity of these two signals was analyzed within a mask in the 7AAD images called “morphology” that represents the nucleus and is smaller than the standard mask. If p65 is mainly in the cytosol the similarity of the two signals is low and a low similarity score is calculated. After p65 translocation to the nucleus a higher similarity score can be observed. The activation of caspase-3 was analyzed using the intensity of the staining for active caspase-3 (Schmidt et al., 2015).

### **2.2.15 IL-6 and IL-8 ELISA**

For ELISA analysis,  $1.2 \times 10^3$  cells per well were seeded in transparent flat bottom 96 well plates. On the following day, media was removed, 75  $\mu$ l fresh medium was added and cells were pre-incubated with 50  $\mu$ M caspase inhibitor zVAD for 30 minutes. Afterwards, cells were stimulated with CD95L or TNF $\alpha$  in a total volume of 150  $\mu$ l. After 24 hours of stimulation, the IL-6 and IL-8 levels in the supernatant were measured with IL-6 and IL-8 ELISA kit (BioLegend, San Diego, USA) according to the manufacturer’s instructions.

### **2.2.16 Statistical analysis**

For data processing, storage and statistical analysis of data, the software programs Excel (Microsoft Cooperation, Redmond, USA) and Prism 7 (Graph Pad Software, La Jolla, USA) were used. Number of repeats and used statistical tests are described in each figure legend in the chapter “results”.

## **3 Results**

### **3.1 Stimulation of CD95 results in activation of apoptosis and the NF- $\kappa$ B pathway**

It is well known, that CD95L stimulation leads to induction of apoptosis and the NF- $\kappa$ B pathway (Cullen et al., 2013; Fricker et al., 2010; Lavrik and Krammer, 2012). To analyze whether in our system CD95 stimulation also leads to the same signaling outcome, the cervix carcinoma HeLa cells with CD95 overexpression (HeLa-CD95 (Neumann et al., 2010)) were stimulated with CD95L in the presence or absence of the pan-caspase inhibitor carbobenzoxy-valyl-alanyl-aspartyl-(O-methyl)-fluoromethylketone (zVAD) to selectively inhibit apoptosis (Neumann et al., 2010).

Stimulation with 250 ng/ml CD95L resulted in activation of the apoptotic and the NF- $\kappa$ B pathways. Apoptosis induction was detected *via* the signals of cleavage products of procaspase-8a/b (p55/53) - p43/41, p30 and p18 - appearing 40 minutes after stimulation (Figure 11). The detection of the p18 cleavage product indicates full activation of caspase-8 and formation of the heterotetramer p10<sub>2</sub>/p18<sub>2</sub>, which activates the apoptotic pathway by cleavage of effector caspases-3/-7 and Bid (Lavrik and Krammer, 2009). The cleavage products p19 and p17 of procaspase-3 (p35) were detected after 40 to 60 minutes of stimulation *via* immunoblot analysis (Figure 11). Cleavage of c-FLIP<sub>L</sub> into p43-FLIP was monitored 20 to 40 minutes after stimulation (Figure 11). NF- $\kappa$ B activation was determined by analyzing the phosphorylation and degradation of I $\kappa$ B $\alpha$  (Figure 11). Phosphorylation of I $\kappa$ B $\alpha$  results in its K48 ubiquitination and proteasomal degradation (Hayden and Ghosh, 2008), thereby allowing translocation of the NF- $\kappa$ B subunits p50 and p65 to the nucleus. This change of I $\kappa$ B $\alpha$  phosphorylation status and the reduction of the I $\kappa$ B $\alpha$  levels were detected after 40 minutes of CD95L stimulation (Figure 11).

Addition of zVAD prior to stimulation with CD95L inhibited caspase activation (Figure 11), whereas I $\kappa$ B $\alpha$  degradation was not affected (Figure 11). Interestingly, the signal of phosphorylated

I $\kappa$ B $\alpha$  sustained upon the addition of zVAD for a longer period of time (Figure 11). The inhibition of caspases resulted in a lack of appearance of both, procaspase-8 cleavage products (p43/p41 and p18) and procaspase-3 cleavage products (p19 and p17, Figure 11). The cleavage of c-FLIP<sub>L</sub> to p43-FLIP was not affected by addition of the caspase inhibitor zVAD but p43-FLIP degradation was slower (Figure 11). These results allow suggesting that apoptosis and NF- $\kappa$ B pathway are activated in parallel after CD95 stimulation. These observations give raise to the question whether the activation of both pathways occurs in the same or in different cells.

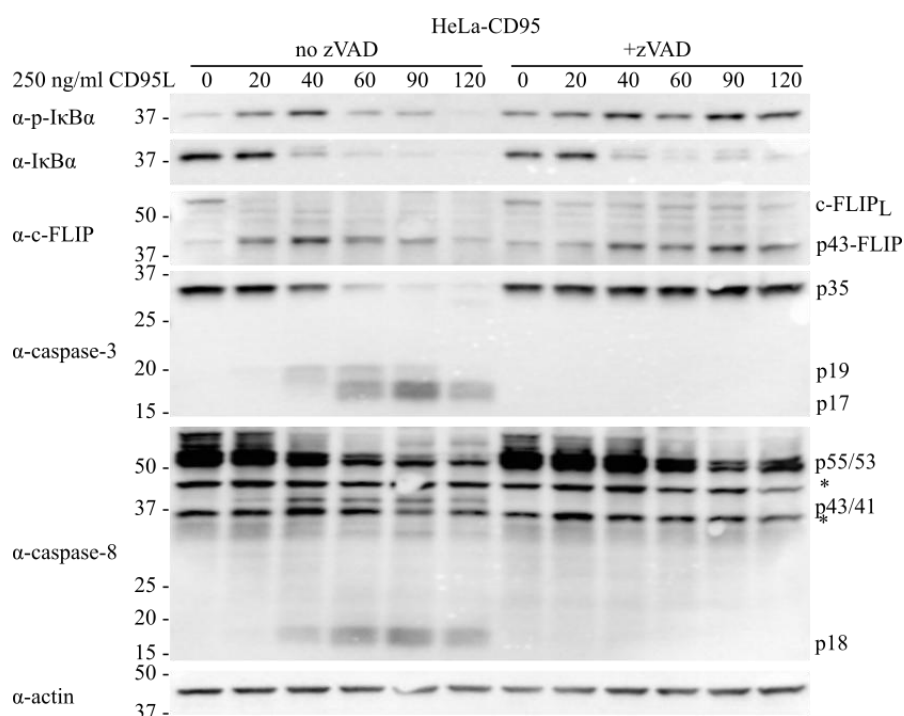


**Figure 11: CD95 stimulation activates NF- $\kappa$ B and caspase cleavage.** HeLa-CD95 cells were pre-incubated in absence or presence of 50  $\mu$ M zVAD for 30 minutes and stimulated with 250 ng/ml CD95L for indicated time periods, lysed and analyzed by immunoblotting with indicated antibodies. Presented is one representative result out of three independent experiments. Actin was used as a loading control. SFL: SuperFasL, \* non specific band

Several ligands and antibodies can trigger CD95-mediated signaling. In this study mainly the supernatant of HEK293T cells producing trimerized CD95L was used for stimulation of CD95 (Neumann et al., 2010). In addition, commercially purified CD95L and agonistic  $\alpha$ -CD95 ( $\alpha$ -APO-1)

antibody were used for CD95 stimulation. To analyze the effects of different ligands and ensure that no other components of the HEK293T cell supernatant than the trimerized CD95L are responsible for the observed effects on CD95 signaling, the effects of the supernatant (CD95L), commercially available purified ligand (SFL) and  $\alpha$ -APO-1 antibody were compared in HeLa-CD95 cells. Cells were stimulated with these reagents for up to 120 minutes and lysates were analyzed with immunoblotting for I $\kappa$ B $\alpha$  phosphorylation and degradation as well as procaspase-8a/b proteolytic processing. Stimulation with 250 and 500 ng/ml of CD95L resulted in phosphorylation and degradation of I $\kappa$ B $\alpha$  beginning after 20 minutes of stimulation (Figure 12 A). The cleavage products p43/41 of procaspase-8a/b appeared after 10 minutes of CD95L stimulation and p18 appeared after 20 minutes of CD95L stimulation (Figure 12 A). Procaspase-8a/b (p55/53) cleavage was a little stronger with 500 ng/ml CD95L stimulation, while kinetics of I $\kappa$ B $\alpha$  phosphorylation and degradation were not affected by the increase of CD95L concentration (Figure 12 A). Similar to the CD95L-containing supernatant, stimulation with 800 ng/ml of the commercial purified SuperFasLigand (SFL) resulted in phosphorylation and degradation of I $\kappa$ B $\alpha$  after 20 minutes of stimulation and appearance of the procaspase-8a/b cleavage products p43/41 after 20 minutes and p18 after 40 minutes (Figure 12 B). In addition, stimulation of the cells with the agonistic  $\alpha$ -APO-1 antibody (500 ng/ml) resulted in similar kinetics of I $\kappa$ B $\alpha$  phosphorylation and degradation after 20 minutes of stimulation and appearance of the procaspase-8a/b cleavage products p43/41 after 20 minutes, while p18 appeared a little later after 40 to 60 minutes as detected by immunoblot analysis (Figure 12 C).

Taken together, these results indicate that CD95L from different sources as well as agonistic  $\alpha$ -APO-1 antibody evoke similar kinetics of I $\kappa$ B $\alpha$  phosphorylation and degradation as well as procaspase-8a/b cleavage and both can be used equivalently and interchangeably in this study.

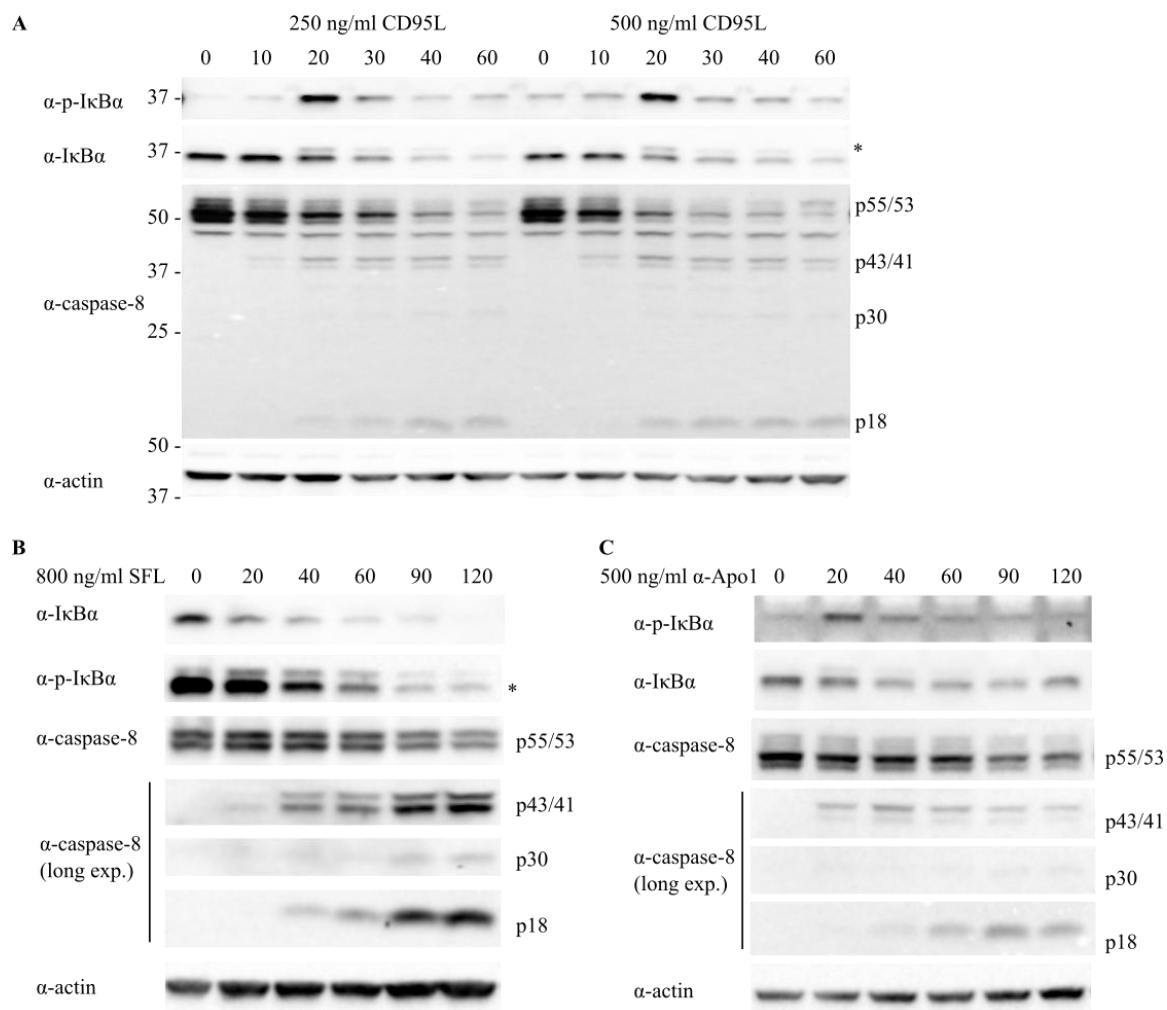


**Figure 12: Effect of different CD95 stimulation reagents on activation of NF-κB activation and apoptosis induction.** A) HeLa-CD95 cells were stimulated with 250 or 500 ng/ml CD95L, respectively, for indicated periods of time, lysed and analyzed with immunoblotting with the indicated antibodies. B) Cells were stimulated with 800 ng/ml SuperFasLigand (SFL) for the indicated time periods and analyzed like in A. C) Cells were stimulated with 500 ng/ml α-APO-1 antibody for the indicated time periods and analyzed as in B. Actin was used as loading control. Presented is one representative result out of three independent experiments. \* non-specific band

Immunoblotting allows to follow the activation of apoptotic and NF-κB pathway in a bulk population of cells, but does not allow to draw any conclusions about the signal transduction events occurring on the single cell level. The immunoblotting results represent the mixed signal of all lysed cells from one sample. Thus, distinguishing if both pathways are activated in the same cell or if NF-κB is activated in one part of the cell population, while the other part activates apoptosis pathway cannot

be determined *via* immunoblotting. However, the use of imaging flow cytometry allows determining activation of both pathways in parallel in single cells. Imaging flow cytometry is a combination of flow cytometry and microscopy and acquires large numbers of cell pictures in a short time in up to 12 different fluorescence channels. Hence, in this work it was decided to develop an image flow cytometry-based approach that allows distinguishing activation of apoptotic and NF- $\kappa$ B pathways in single cells.

To analyze the activation of the apoptotic and NF- $\kappa$ B pathways, HeLa-CD95 cells were stimulated, harvested, fixed, permeabilized and stained with antibodies against the NF- $\kappa$ B subunit p65 and cleaved caspase-3 (cleavage site Asp175). Additionally, the nucleus was stained with the DNA dye 7AAD. The combination of 7AAD and p65 staining allows following the translocation of p65 into the nucleus as a key feature of NF- $\kappa$ B activation (Figure 6). The staining for the cleaved executioner caspase-3 indicates the activation of the apoptotic pathway. HeLa-CD95 cells stimulated with 250 ng/ml CD95L for 60 minutes can be gated in four different populations based on the intensity of staining for active caspase-3 and the similarity (sim.) of the nuclear 7AAD and the p65 signal. Cells in the first population have no active caspase-3 and no nuclear p65 translocation (Figure 13 A). Cells in the second population have no active caspase-3 but p65 translocation to the nucleus (Figure 13 B). The cells in the first two populations, that do not have active caspase-3, possess the morphology of viable cells as can be concluded from images in the bright field. Cells in the first and third populations that do not have p65 translocation are characterized by a “ring-shaped” green signal for p65 in the cytoplasm and an overlay of this signal with the red 7AAD signal from the nucleus shows clear separation of the signals (Figure 13 A, C). After translocation of p65 into the nucleus, the p65 signal is equally distributed all over the cell and the overlay of the green p65 and red nuclear 7AAD signals shows a yellow nucleus (Figure 13 B, D). The third population comprises the cells that have active caspase-3 but no nuclear p65 (Figure 13 C) and the cells in the fourth population have active caspase-3 and nuclear p65 (Figure 13 D). Cells in the third and fourth populations show apoptotic morphological

changes. These apoptotic changes include membrane blebbing that is visible in the bright field channel and fragmentation of the nucleus that is visible in the 7AAD signal of the nucleus (Figure 13 C, D). The data demonstrate the applicability of imaging flow cytometry for the detection of apoptosis and NF- $\kappa$ B activation on the single cell level.

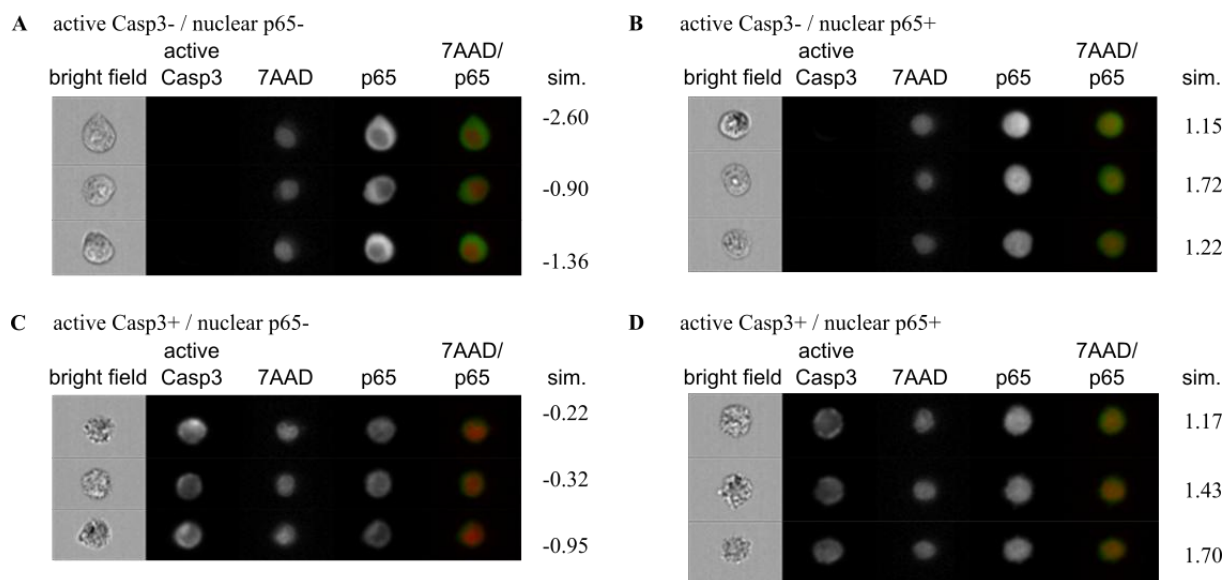


**Figure 13: Imaging flow cytometry allows following cleavage of caspase-3 and p65 translocation to the nucleus.** HeLa-CD95 cells were stimulated with 250 ng/ml CD95L for 60 minutes, harvested, fixed, permeabilized and stained with antibodies against p65 and caspase-3 cleaved at Asp175. The nucleus was stained with 7AAD. Cells were gated for caspase-3 (Casp-3) and p65 translocation to the nucleus (nuclear p65). Casp3: caspase-3, sim.: similarity score (7AAD/p65), - negative, + positive

In contrast to standard flow cytometry that is based mainly on signal intensities, imaging flow cytometry analysis in addition uses image derived features. Furthermore, image analysis is one of the first steps in the data analysis in imaging flow cytometry. After the image acquisition, images which are not suitable for further processing have to be excluded from further analysis. This exclusion includes non-focused images (Figure 14 A), images not showing single cells (Figure 14 B) and cells that were not successfully stained for 7AAD and p65 (Figure 14 C). Calculating feature values from the acquired images makes advantage of the high numbers of cell images derived from imaging flow cytometry. NF- $\kappa$ B activation was quantified *via* determining the p65 translocation into the nucleus by

calculating a feature called similarity of the nuclear 7AAD and the p65 signals. This feature is calculated by estimating the degree of similarity of the pixel values of the 7AAD and p65 signals. For example, a low similarity describes a low correlation of the signals and hence mainly cytosolic p65 and a low p65 translocation to the nucleus indicating no NF- $\kappa$ B activation. Stimulation of HeLa-CD95 cells with 250 ng/ml CD95L was monitored *via* clear changes in the similarity (7AAD/p65) *versus* intensity of active caspase-3 blot (Figure 14 D, E). Without stimulation, most cells had no active caspase-3 and had no p65 in the nucleus (Figure 14 D). After stimulation for 60 minutes most cells displayed active caspase-3 and the whole cell population showed a higher similarity between the 7AAD and p65 signals (Figure 14 E). Depending on the similarity of nuclear 7AAD and p65 signals, cells can be separated into a group with p65 translocation into the nucleus and a group without p65 translocation to the nucleus (Figure 14 F). Summing up, these features allowed to describe p65 translocation as a hallmark of canonical NF- $\kappa$ B activation as well as caspase-3 activation as readout of apoptotic cell death at single cell and population levels.

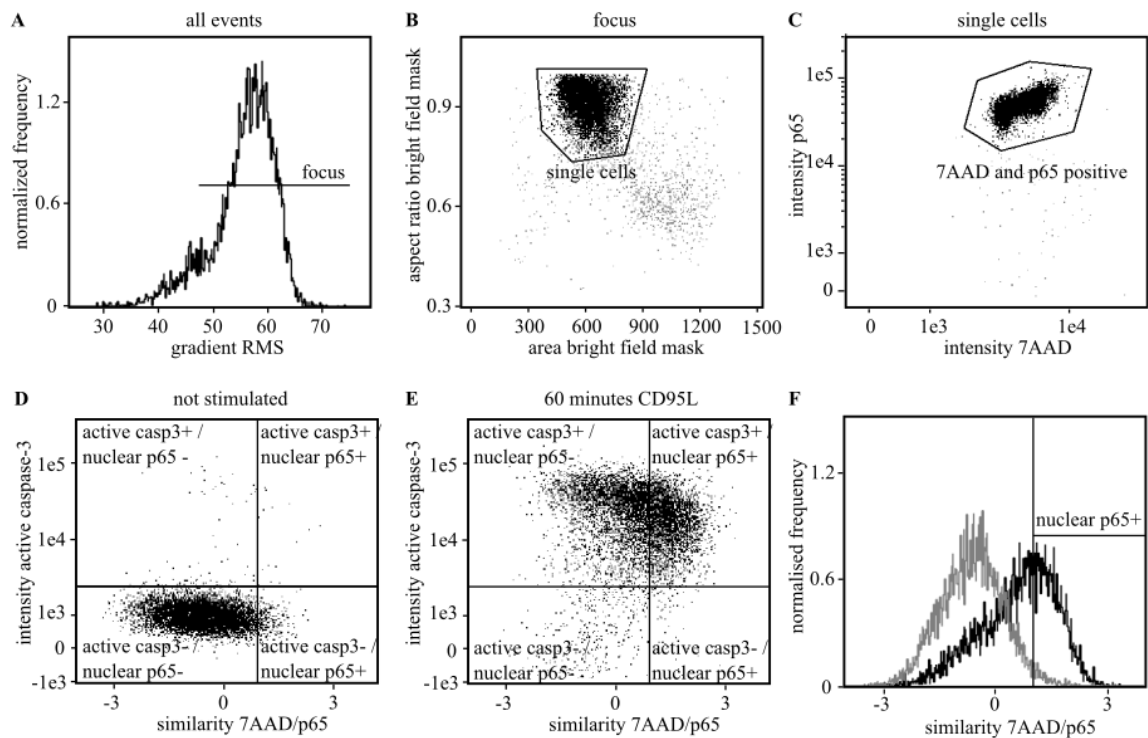


**Figure 14: Gating strategy for imaging flow cytometry analysis.** A) First, focused images of HeLa-CD95 cells were selected by using the feature gradient RMS. B) Secondly, single cells were selected by using the area and the aspect ratio feature on the bright field mask. C) Thirdly, cells that were stained for 7AAD and p65 were selected for further analysis. D+E) HeLa-CD95 cells were non-stimulated (D) or stimulated with 250 ng/ml CD95L (E). Dotplots for similarity of (7AAD/p65) and the intensity of active caspase-3 are shown. F) A histogram for the similarity between nuclear 7AAD and p65 signals are shown for non-stimulated cells (D, grey) or cells stimulated with 250 ng/ml CD95L (E, black).

It is well known, that activation of the executioner caspases-3 and -7 occurs during apoptosis, which is accompanied by morphological changes of the cells. To confirm the induction of apoptosis these morphological changes of dying apoptotic cells were analyzed. These changes can be monitored by using the contrast of the bright field image and the area of a mask that includes 50% of the nuclear 7AAD signal (Figure 15). Membrane blebbing during apoptosis increases the contrast while the nuclear fragmentation decreases the area of the highest 50% of the nuclear signal. Stimulation of HeLa-CD95 cells with 250 ng/ml for 180 minutes results in a shift from the “no apoptotic

morphology” gate into the “apoptotic morphology” gate (Figure 15). These features and the manual survey of cell images proves that apoptosis is induced.

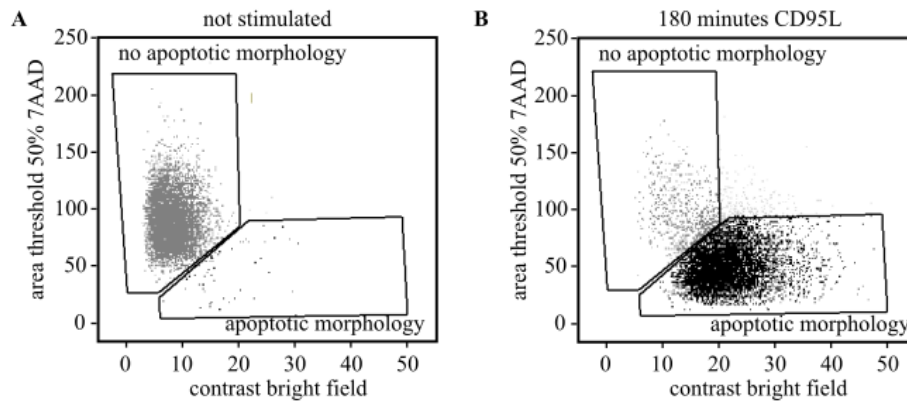


**Figure 15: Gating strategy for apoptotic and not apoptotic cell morphology.** A) Bright field images of not stimulated HeLa-CD95 cells were analyzed for morphological changes that occur during apoptotic cell death. Therefore, the features: contrast of the bright field and area of the threshold 50% mask of the nuclear 7AAD image, were analyzed representing the membrane blebbing and nuclear fragmentation of apoptotic cells, respectively. B) Cell were stimulated with 250 ng/ml CD95L for 180 minutes and analyzed as in A).

In order to determine the activation of NF- $\kappa$ B and the induction of apoptosis at single cell and population levels, time- and dose-dependent experiments were done in HeLa-CD95 cells stimulated with CD95L. By setting gates for caspase-3 activation, p65 translocation, and apoptotic morphology, the induction of apoptosis and the activation of the NF- $\kappa$ B pathway were quantified. Stimulation of HeLa-CD95 cells with 250 ng/ml resulted in a decrease of the cell population without active caspase-3 and without p65 in the nucleus (Figure 16 A). Already after 40 minutes of stimulation with 250 ng/ml CD95L, nearly all cells (90 %) were caspase-3 positive, while the morphological changes to apoptotic cells occurred at later time points (starting at 60 to 90 minutes, Figure 16 B). After 180 minutes of stimulation about 80% of the cells were morphologically apoptotic (Figure 16 B). This observation is in line with the mechanism of apoptotic cell death. The activation of executioner caspases like caspase-3 induces morphological changes in the cells and therefore had to occur ahead of these changes.

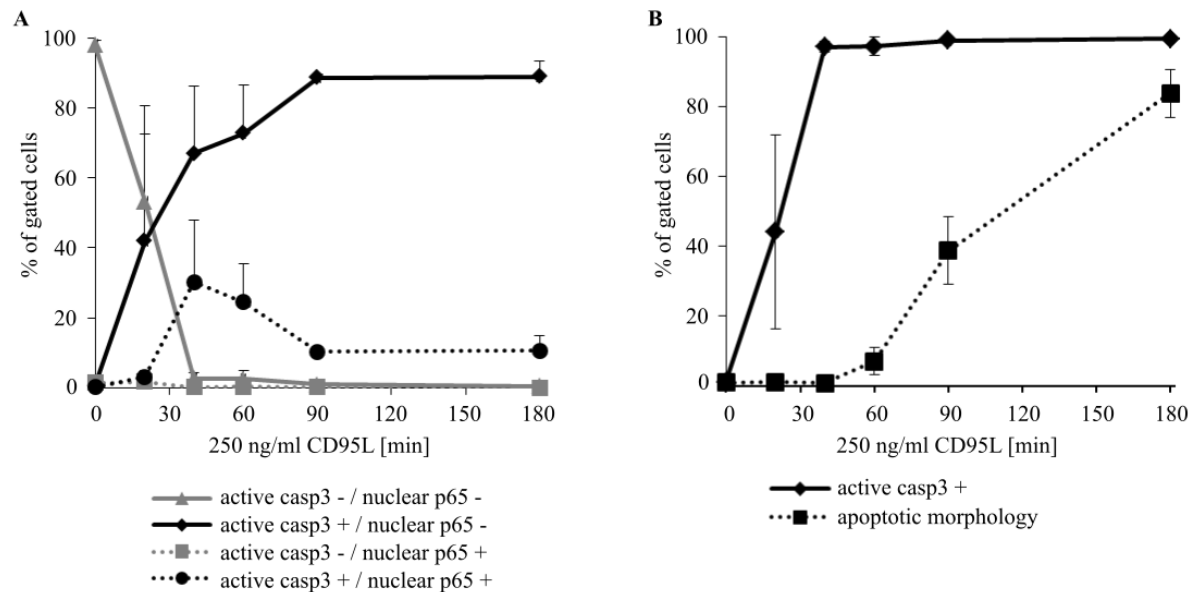


**Figure 16: CD95 stimulation promotes p65 translocation and caspase-3 activation in parallel.** A) HeLa-CD95 cells were stimulated with 250 ng/ml CD95L for up to 180 minutes. Cells were harvested and analyzed for caspase-3 cleavage and p65 translocation to the nucleus. B) Cells from A were analyzed for caspase-3 cleavage and apoptotic morphology. The means and SDs of three independent experiments are shown. Active casp-3 -: no active caspase-3, active casp-3 +: active caspase-3, nuclear p65 -: no p65 translocation into the nucleus, nuclear p65 +: p65 translocation into the nucleus.

Interestingly, CD95 stimulation resulted in a population of cells which displayed both, active caspase-3 and p65 translocation into the nucleus. The frequency of this population peaked at 30 % after 40 minutes stimulation with 250 ng/ml CD95L and vanished afterwards (Figure 16 A). For stimulation intervals longer than 90 minutes the detection of this population can be false positive because cells have apoptotic morphology with a fragmented nucleus and the nuclear fragmentation increases the similarity score. The population of cells with p65 translocation without caspase-3 activation stayed below 5% under these stimulation conditions (Figure 16 A). The main population of cells activated caspase-3 without p65 translocation to the nucleus after CD95L stimulation (Figure 16 A). With longer stimulation times the size of this population was increasing and after 90 minutes these population already comprised 90 % of the cells (Figure 16 A). Altogether, these results showed a

parallel induction of apoptosis and NF- $\kappa$ B pathway in a subset of cells while the apoptotic response was predominated at these stimulation doses.

To get further insights into the parallel activation of these pathways experiments with different concentrations of CD95L were performed. Stimulation of HeLa-CD95 cells with CD95L showed increasing caspase-3 activation upon stimulation with higher concentrations of CD95L from 50 to 1000 ng/ml (Figure 17). After stimulation with 500 ng/ml CD95L nearly all cells (<95 %) were gated as active caspase-3 positive. Moreover, the population of cells with parallel p65 translocation into the nucleus and caspase-3 activation was increasing up to 15 % with 250 to 500 ng/ml CD95L stimulation, but was lower (10 %) at stimulation with 1000 ng/ml CD95L (Figure 17). The amount of cells with p65 translocation and without activation of caspase-3 was below 5%, which was independent of CD95 stimulation (Figure 17). Summing up, higher concentrations of CD95L increased the induction of the apoptotic pathway. Very high doses of CD95 stimulation resulted in the detection of lower p65 translocation to the nucleus compared to lower doses that can be explained by reduced NF- $\kappa$ B activation or by accelerated NF- $\kappa$ B resulting in missing of the peak of p65 nuclear translocation.

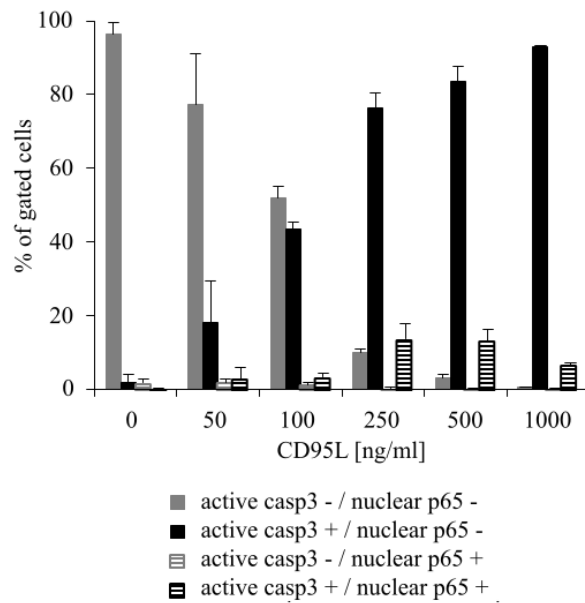


**Figure 17: Increasing doses of CD95 stimulation lead to the increased number of cells with caspase-3 activation. HeLa-CD95 cells were stimulated for 40 minutes with indicated concentrations of CD95L and analyzed with imaging flow cytometry for p65 translocation to the nucleus and caspase-3 activation. Means and SDs from three independent experiments are shown. active casp-3 -: no active caspase-3, active casp-3 +: active caspase-3, nuclear p65 -: no p65 translocation into the nucleus, nuclear p65 +: p65 translocation into the nucleus.**

Summing up, the imaging flow cytometry approach developed in this study allows following the activation of caspase-3, apoptosis and the NF- $\kappa$ B pathway on the single cell level. Using it for the analysis of CD95 signaling revealed that activation of caspase-3 and p65 occurred in parallel in at least a subpopulation of approximately 20 % of the cells. It was also shown that only a small number of cells showed p65 translocation without caspase-3 activation. Most cells (50 to 90 %) activate caspase-3 without p65 translocation, while activation of both pathways was detectable in less than 20 % of the cells. Dose-dependent analysis showed that with higher doses of CD95L stimulation for 40 minutes the number of cells with p65 translocation decreased while the number of cells inducing apoptosis is increased which can be explained by lower NF- $\kappa$ B activation or by missing the maximal NF- $\kappa$ B activation at higher stimulation doses at measured time interval.

### **3.2 NEMO and c-FLIP interact independently of CD95 stimulation**

The regulatory subunit of the IKK complex NEMO is an important regulator of the canonical NF- $\kappa$ B pathway (Golks et al., 2006; Koenig et al., 2014). It is well known that different c-FLIP isoforms are important for the activation of the NF- $\kappa$ B pathway *via* NEMO (Oztürk et al., 2012). In addition, a crystal structure of a complex consisting of NEMO and the viral c-FLIP homolog v-FLIP was published (Bagnéris et al., 2008) and the interaction of c-FLIP with other components of the IKK complex was shown in overexpression studies (Golks et al., 2006; Neumann et al., 2010).

To address the question, if c-FLIP-NEMO interaction is influenced by CD95 stimulation HeLa-CD95 cells stably overexpressing c-FLIP<sub>L</sub> and c-FLIP<sub>R</sub> (HeLa-FLIP<sub>R+L</sub>) were stimulated for 40 minutes with 250 ng/ml CD95L or left unstimulated and subjected to NEMO and c-FLIP immunoprecipitations (IPs, Figure 18 A, B). The two overexpressed c-FLIP isoforms c-FLIP<sub>L</sub> and c-FLIP<sub>R</sub> as well as the c-FLIP<sub>L</sub> cleavage product p43-FLIP were found in the NEMO IP (Figure 18 A). As expected, the c-FLIP<sub>L</sub> cleavage product p43-FLIP was only detectable after stimulation with CD95L (Figure 18 A). The cleavage product p22-FLIP was visible in lysates with and without stimulation with CD95L in accordance with previous publications (Golks et al., 2006). NEMO was found in the c-FLIP IP with and without stimulation with CD95L in these cells (Figure 18 B). Given these points, c-FLIP and NEMO interacted under c-FLIP-overexpressing conditions independent of CD95 stimulation. To verify the association of c-FLIP and NEMO under endogenous proteins levels, the IP experiments were repeated in HeLa-CD95 cells without c-FLIP overexpression. As expected, c-FLIP<sub>L</sub> was detectable in NEMO IP independent of CD95 stimulation (Figure 18 C). A signal at slightly higher molecular weight than 43 kDa was detectable in NEMO IP and could correspond to p43-FLIP even if it has a higher molecular weight than in the lysates (Figure 18 C). In addition, NEMO as well as c-FLIP<sub>L</sub>, c-FLIP<sub>R</sub> and p22-FLIP were detectable in the lysate and c-FLIP IPs (Figure 18 D). The signal of p43-FLIP is difficult to recognize because it is masked a little by the NEMO signal from prior detection but a weak signal of p43-FLIP was detectable in NEMO IP after



### **3.3 NEMO-derived peptides influence CD95-induced NF- $\kappa$ B activation**

From the finding that c-FLIP and NEMO interact (Figure 18) and that c-FLIP is an important regulator of CD95-induced NF- $\kappa$ B activation, the question arose if this interaction is important for NF- $\kappa$ B activation. In addition, a crystal structure of the Kaposi's sarcoma-associated herpesvirus v-FLIP (an viral c-FLIP homolog) and NEMO suggested a direct interaction of c-FLIP and NEMO (Bagn ris et al., 2008). To further analyze whether the c-FLIP-NEMO interaction is direct or indirect on base of the published structure a homology model of c-FLIP and NEMO was build. The homology model allowed a rational design of the peptides derived from the NEMO sequence being able to interact with c-FLIP and thereby possibly compete with the normal c-FLIP-NEMO interaction (homology model done by Nikita Ivanisenko, Institute of Cytology and Genetics, Novosibirsk, Russia). If the c-FLIP-NEMO interaction is indeed direct and important for CD95-induced NF- $\kappa$ B activation, a reduced NF- $\kappa$ B activation is suggested to occur in presence of this type of peptides.

As the rationally designed NEMO-derived peptides are charged and therefore hydrophilic, they would likely not be able to pass the hydrophobic lipid membrane of a cell. To enable the uptake into cells of the NEMO-derived peptides, the HIV tat sequence (tat), which is described as cell penetrating peptide, was fused with the NEMO-derived peptides (Jones and Sayers, 2012). The first tested peptide (tat-NEMO) consists of the tat sequence, the amino acid sequence of NEMO (aa227-245) that from *in silico* analysis was suggested to interact with c-FLIP (Figure 19 A). To check the cellular uptake of the designed peptide, the fluorescence dye FITC was fused to the tat-NEMO peptide as well (tat-Nemo-FITC, Figure 19 A). As a negative control, a peptide that is still able to enter cells with a tat sequence and the same fluorescence dye, but a scrambled sequence of the same amino acids of the NEMO sequence was used, termed thereafter scrambled peptide (tat-scr-Nemo-FITC, Figure 19 A). Hence, the two peptides have the same molecular weight and similar chemical properties. HeLa-CD95 cells were incubated with 25  $\mu$ M of the peptides and analyzed with imaging flow cytometry for ability to

enter cells. As expected, cells without peptide showed no signal in the FITC channel (Figure 19 B). Cells that were incubated with the peptide or its scrambled version showed signals in the FITC fluorescence channel (Figure 19 B, C, and D). The cell images showed the signal inside of the cells which illustrates that the peptides were able to enter the cells (Figure 19 B). The signal intensities were varying in individual cells, but were similar between the control peptide and the tat-Nemo-FITC peptide (Figure 19 C, D).

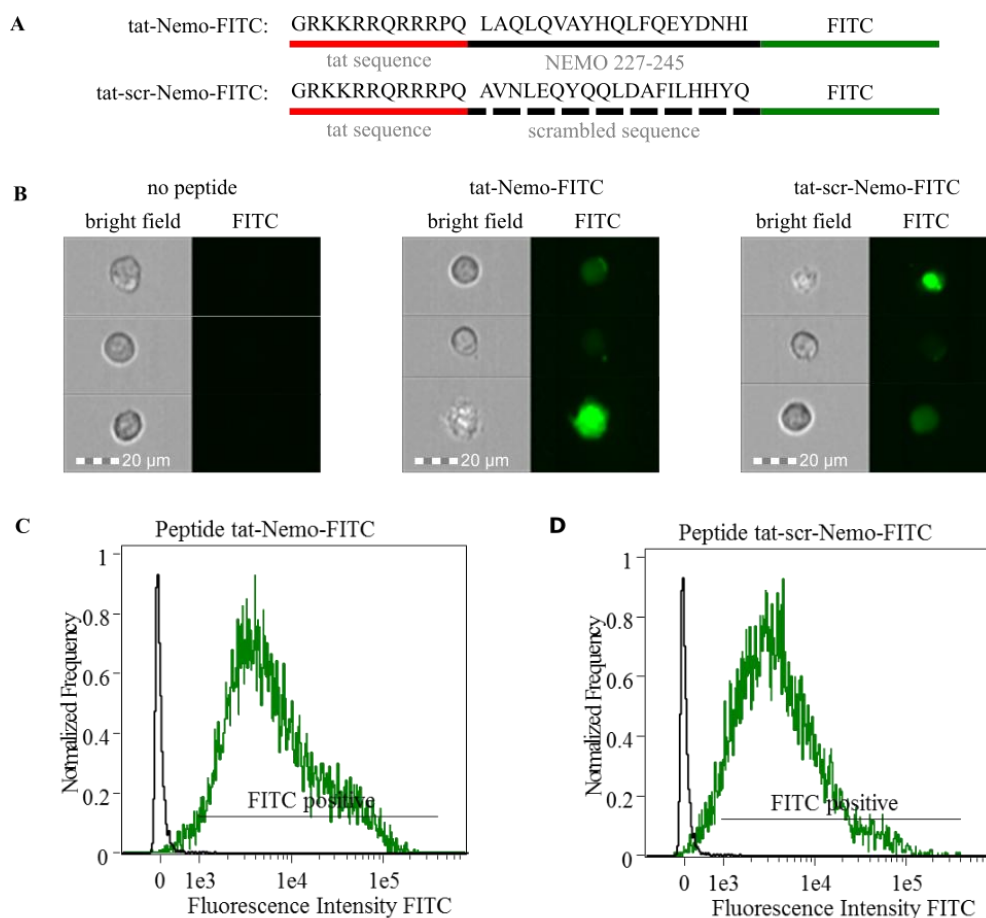


**Figure 19:** The tat-Nemo-FITC peptide is able to enter cells. A) Scheme of the structure and sequence of the NEMO-derived peptides. Tat-sequence is showed in red, FITC in green. B) HeLa-CD95 cells were incubated with 25  $\mu$ M of the peptides for one hour and analyzed with imaging flow cytometry. Bright field and FITC channels are shown. C) Fluorescence intensity for the FITC channel of 10,000 cells incubated with tat-NEMO-FITC and analyzed like in B. D) Fluorescent intensity of the FITC channel for tat-scr-Nemo-FITC peptide like C.

Since the peptides with tat-sequence were able to enter the cells but had no influence on CD95-induced NF- $\kappa$ B activation (data not shown) the question was raised whether the fluorescent dye FITC coupled to the peptides had blocked the interaction between the peptide and c-FLIP. Consequently, peptides with the same sequences but without fluorescent dye were used for further experiments (Figure 20 A). The effect of the peptides on CD95-induced NF- $\kappa$ B activation was tested in HeLa-CD95 cells. Cells were pre-incubated with 5 to 50  $\mu$ M of the peptides and stimulated with  $\alpha$ -APO-1 antibody (Figure 20 B). Increasing peptide concentrations resulted in a decrease of phospho-I $\kappa$ B $\alpha$  and total I $\kappa$ B $\alpha$  signal as detected *via* immunoblotting analysis (Figure 20 B). The decreased signal was most likely caused by increased phosphorylation and degradation of I $\kappa$ B $\alpha$ . However, the effect does not seem to be sequence specific because it was observed for the NEMO-derived peptide as well as for the scrambled peptide (Figure 20 B). Analysis of p65 translocation with imaging flow cytometry confirmed this effect (data not shown).



**Figure 20: Influence of the tat-Nemo peptide on CD95-induced NF- $\kappa$ B activation.** A) Scheme of the used peptides. Tat-sequence shown in red. B) HeLa-CD95 cells were incubated with indicated concentration of the peptides and stimulated with 1  $\mu$ g/ml  $\alpha$ -APO-1 for 30 minutes. Data from one out of three independent experiments is shown. Cells were lysed and lysates were analyzed with immunoblot analysis with the indicated antibodies. Actin acts as a loading control.

As the observed effect on NF- $\kappa$ B activation appeared to be not sequence specific the peptide structure was optimized. In the published NEMO-v-FLIP crystal structure NEMO forms dimers (Bagn ris et al., 2008) and the NEMO-peptide is also supposed to do so. The formation of dimers could be negatively influenced by the addition of the tat sequence to the N-terminus of the peptides. To check this hypothesis, a new protein was designed with the tat sequence at the C- instead of the N-terminal end of the peptide. The effect of these peptides on CD95-induced NF- $\kappa$ B activation were again not sequence specific as detected *via* immunoblotting analysis of I $\kappa$ B $\alpha$  phosphorylation and degradation as well as *via* imaging flow cytometry analysis of p65 translocation (data not shown).

The non-specific effects of the peptides on CD95-induced NF- $\kappa$ B activation could be caused by the tat-sequence that was present in both peptides. For this reason the cell penetrating part of the peptides was replaced by the R9 sequence, which is another small peptide known to mediate transfer through cell membranes (Figure 21 A) (Jones and Sayers, 2012). To further improve the dimerization ability three additional amino acids were added to the NEMO-derived part of the sequence. HeLa-CD95 cells were pre-incubated with the peptides and stimulated with CD95L. Analysis of I $\kappa$ B $\alpha$  phosphorylation and degradation after CD95 stimulation showed only minor differences between cells pre-incubated with the NEMO specific (Nemo-R9) and the scrambled control (scr-Nemo-R9) peptides (Figure 21 B). A pull-down assay with the peptides in c-FLIP overexpressing cells showed that the NEMO specific peptide was able to bind better to c-FLIP<sub>L</sub> and c-FLIP<sub>R</sub> than the scrambled control peptide (Figure 21 C). To get a better view on its effects on NF- $\kappa$ B activation, the p65 translocation to the nucleus was analyzed with imaging flow cytometry. Only little differences between the specific NEMO peptide and the scrambled control peptide with a slightly increased p65 translocation for the Nemo-R9 peptide were found (Figure 21 D). Notably, the Nemo-R9 peptide already showed a little slightly increased basal level of p65 translocation without stimulation followed by increase in nuclear p65 after stimulation (Figure 21 D). Additionally, the more downstream effects of NF- $\kappa$ B activation were studied. NF- $\kappa$ B activation results in IL-8 secretion (Lawrence, 2009). Analysis of IL-8 in the

supernatant of HeLa-CD95 cells, which were pre-incubated with peptides and the caspase inhibitor zVAD and stimulated for 24 h with 250 ng/ml CD95L, showed no significant difference in the IL-8 concentrations between the specific NEMO-derived and the scrambled control peptides (Figure 21 E). Summing up, these results show that the peptide with a R9 sequence is indeed able to bind c-FLIP, but does not influence CD95-induced NF- $\kappa$ B activity.

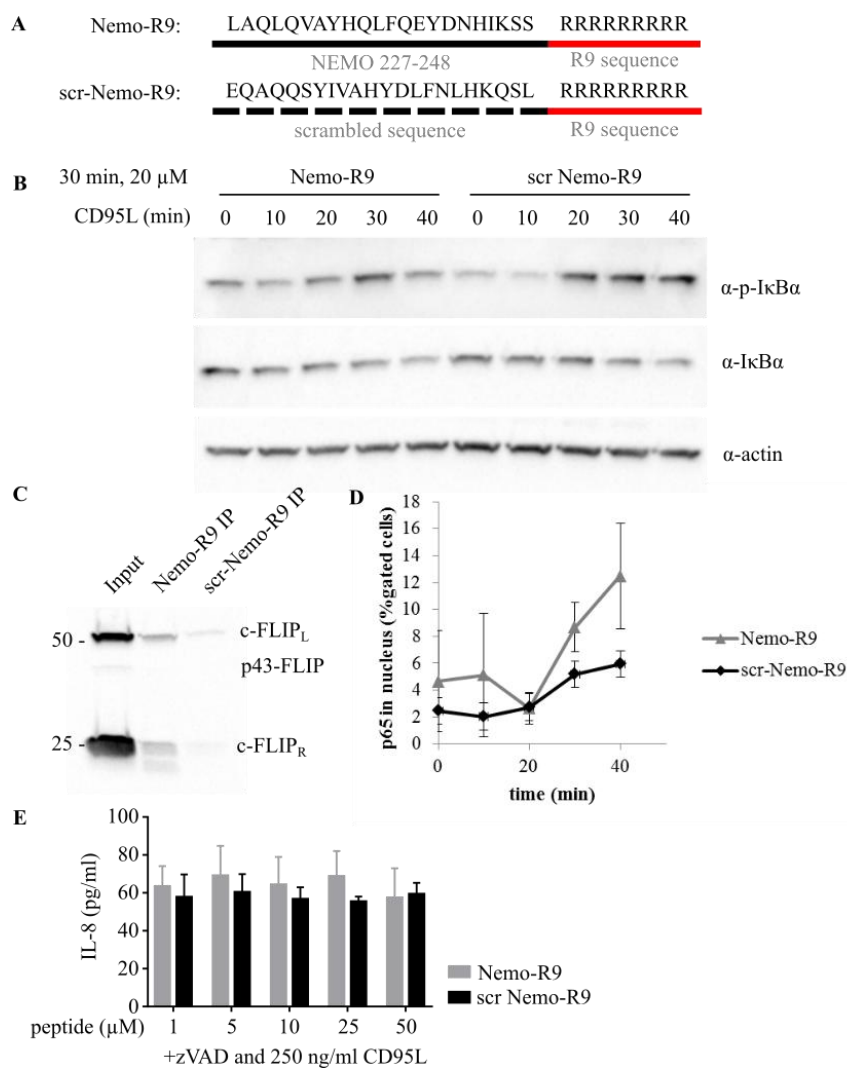


**Figure 21: Effect of the Nemo R9 peptide on NF- $\kappa$ B activation.** A) Scheme of the Nemo-R9 and scr-Nemo-R9 peptides. R9 sequence is shown in red. B) HeLa-CD95 cells were incubated with 20  $\mu$ M of Nemo-R9 or scr-Nemo-R9 for 30 minutes and stimulated with 250 ng/ml CD95L for indicated periods of time. Cells were lysates and analyzed with immunoblotting using the indicated antibodies. C) Peptides were immobilized to beads and incubated with HeLa FRL lysate. Pulldowns were analyzed with immunoblotting for c-FLIP. D) HeLa-CD95 cells were stimulated like in A and

analyzed with imaging flow cytometry for p65 translocation. Means and SD of two independent experiments are shown. E) HeLa-CD95 cells were incubated with indicated concentration of the peptides for 30 minutes followed by 50  $\mu$ M zVAD for 30 minutes and stimulated with 250 ng/ml CD95L for 24 hours. Supernatants were analyzed for IL-8 concentration with ELISA. Means and SD of two independent experiments are shown.

In addition to analyzing the effects of the NEMO-derived peptides containing the R9 sequence, the effects of peptides consisting only of R9 or the only the tat sequence were analyzed. Addition of these smaller peptides to HeLa-CD95 cells did not show effects on CD95-induced NF- $\kappa$ B activation (data not shown). To further understand the effect of cell penetrating part of the peptides, a NEMO-derived peptide without cell penetrating part as well as a scrambled control were tested (Figure 22 A). The scrambled sequence was checked for similarity to known sequences by BLAST search with a negative result. To analyze the effect of these peptides, HeLa-CD95 cells were pre-stimulated with the peptides followed by stimulation with 250 ng/ml CD95L for up to 60 minutes. Immunoblot analysis showed no differences in CD95-induced I $\kappa$ B $\alpha$  phosphorylation and degradation between the specific NEMO-derived peptide (FNIIP) and the scrambled control peptide (scrFNIIP, Figure 22 B). Phosphorylation of I $\kappa$ B $\alpha$  was strongest at 30 minutes for both peptides. The ability of the peptides to bind to c-FLIP was tested *via* pull-down assay by incubation with lysate from c-FLIP overexpressing cells. The NEMO specific FNIIP peptide was able to bind stronger to c-FLIP<sub>L</sub> and c-FLIP<sub>R</sub> than the scrambled control peptide (Figure 23 C). Summing up, these peptides without cell penetrating part were able to bind c-FLIP but had no effect on CD95-induced NF- $\kappa$ B activation.

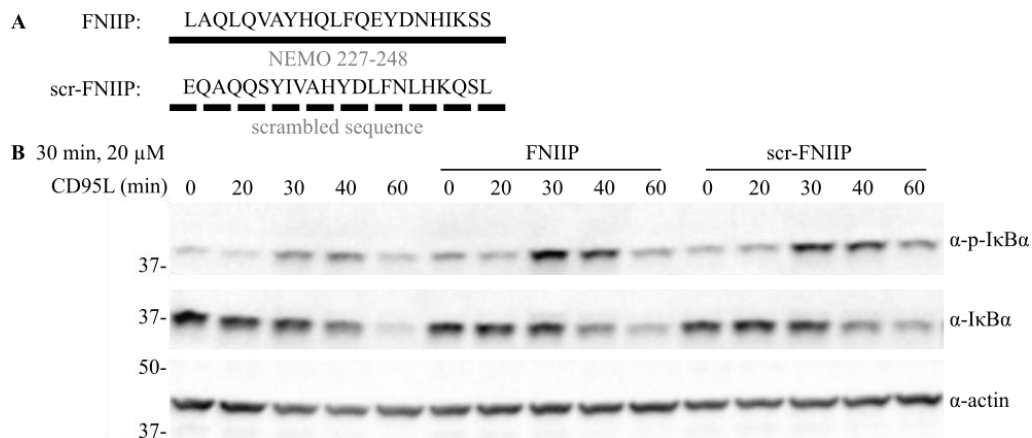


**Figure 22: Structure and effect of the FNIIIP peptide on CD95-induced NF- $\kappa$ B activation.** A) Scheme of the peptides FNIIIP and scr-FNIIIP. B) HeLa-CD95 cells were incubated with 20  $\mu$ M of FNIIIP or scr-FNIIIP peptides for 30 minutes and stimulated with 250 ng/ml CD95L for indicated periods of time period. Cells were lysed and analyzed with immunoblotting using the indicated antibodies. Actin was used as loading control. Representative results from one out of three independent experiments are shown.

To improve the binding of the peptides to c-FLIP, the sequence was further modified. The sequence modifications were calculated *in silico* in the c-FLIP-NEMO homology model based on the published v-FLIP NEMO crystal structure (*in silico* analysis and peptide optimization done by Nikita Ivanisenko, Institute of Cytology and Genetics, Novosibirsk, Russia). These modeling resulted in a peptide with a modified NEMO sequence with improved binding capacity to c-FLIP and the R9 sequence for cell entry (superFNIIIP). Additionally, a peptide with a modified sequence that should not be able to bind to c-FLIP (nosuperFNIIIP) was designed (Figure 23 A). For testing these peptides, HeLa-CD95 cells were pre-incubated with them and stimulated with CD95L for up to 60 minutes. No differences in I $\kappa$ B $\alpha$  phosphorylation and degradation after CD95L stimulation were monitored between incubation in presence of one of these peptides (Figure 23 B). Analysis of the peptide binding to c-FLIP was done *via* pull down assay in c-FLIP overexpressing cells. The superFNIIIP peptide was able to bind to c-FLIP<sub>L</sub> and c-FLIP<sub>R</sub> while nosuperFNIIIP showed no binding to c-FLIP (Figure 23 C).

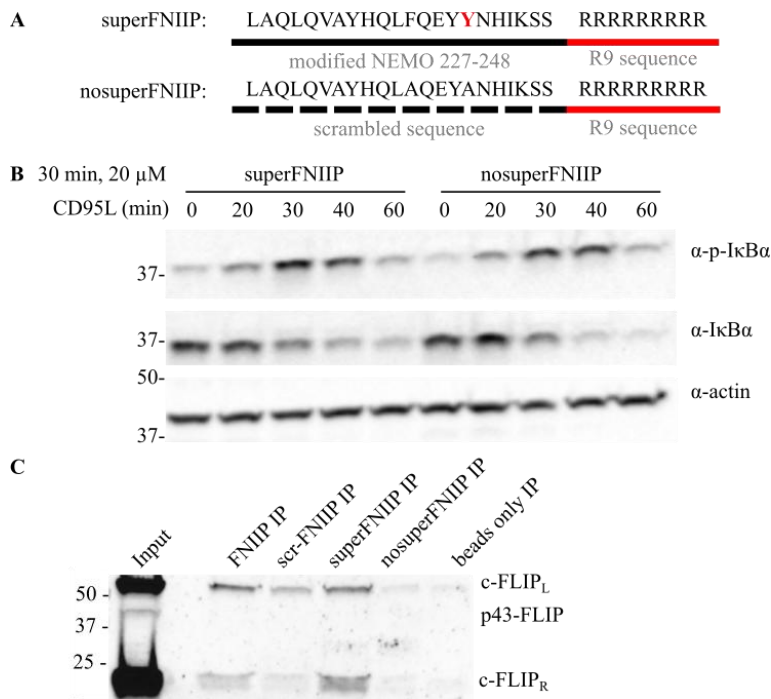


**Figure 23: Structure and effect of superFNIIP peptide on CD95-induced NF- $\kappa$ B activation.** A) Scheme of the peptides superFNIIP and nosuperFNIIP (different amino acid to FNIIP in red). R9-sequence is shown in red. B) HeLa-CD95 cells were incubated with 20  $\mu$ M of the peptides superFNIIP or nosuperFNIIP for 30 minutes and stimulated with 250 ng/ml CD95L for indicated time periods. Cells were lysed and subjected to immunoblotting analysis with the indicated antibodies. Actin was used as loading control. C) Peptides were bound to beads and incubated with lysates from HeLa FRL cells. Pull downs were analyzed with immunoblotting for c-FLIP.

To better compare the limited effects of the peptides on CD95-induced NF- $\kappa$ B activation, a quantitative analysis was performed. The effect of the peptides on NF- $\kappa$ B activation was monitored by analyzing IL-8 secretion after 24 hours of stimulation with 250 ng/ml CD95L. The peptides superFNIIP, nosuperFNIIP, FNIIP and scrFNIIP showed no significant differences in IL-8 secretion in HeLa-CD95 cells (Figure 24 A). Slightly increased IL-8 secretion was measured in the negative control peptides nosuperFNIIP and scrFNIIP compared to the peptides superFNIIP and FNIIP, respectively, but these differences were not significant. As c-FLIP<sub>L</sub> is the direct target of the peptides, the IL-8 secretion was analyzed in HeLa-CD95 cells stably overexpressing c-FLIP<sub>L</sub>. Treating the cells with 5, 10 or 25  $\mu$ M of FNIIP and scrFNIIP showed no significant differences in IL-8 secretion after CD95L stimulation (Figure 24 B). Use of the peptides superFNIIP and nosuperFNIIP that include a

cell penetrating R9 sequence showed decreased IL-8 secretion for the c-FLIP targeting peptide superFNIIP *versus* the scrambled control peptide nosuperFNIIP (Figure 24 B). This difference was significant at 10  $\mu$ M peptide but not at 5 or 25  $\mu$ M (Figure 24 B). No increasing effect with increasing FNIIP concentration was detectable (Figure 24 B).

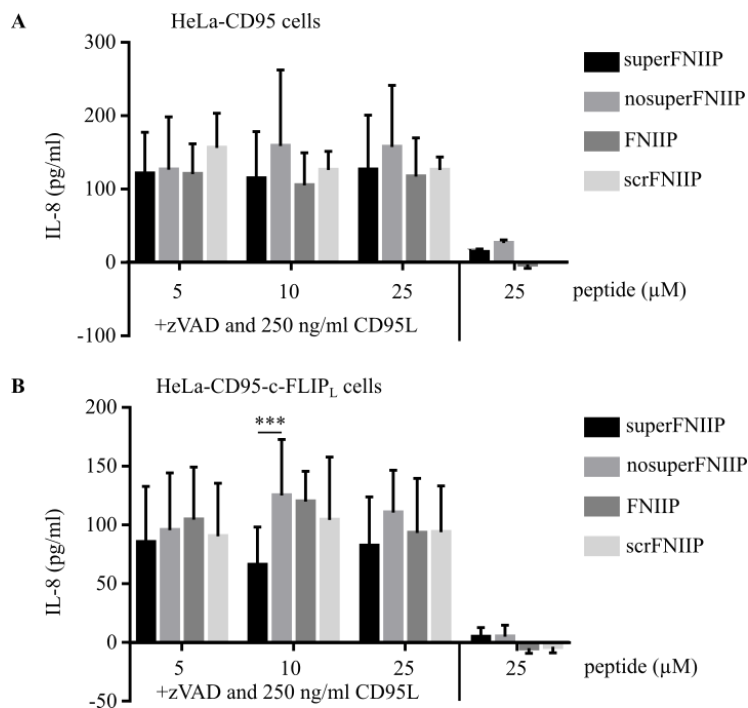


**Figure 24: Effects of NEMO-derived peptides on IL-8 secretion.** A) HeLa-CD95 cells were incubated with indicated concentration of the peptides for 30 minutes followed by 50  $\mu$ M zVAD for 30 minutes and stimulated with 250 ng/ml CD95L for 24 hours. Supernatants were analyzed with ELISA for IL-8 concentrations. B) HeLa-CD95 cells stably overexpressing c-FLIP<sub>L</sub> were treated and analyzed as in A. Means and SDs of three independent experiments is shown. Two-way ANOVA with Turkey's correction for multiple comparisons test was performed. All significant differences within the different stimulation concentrations are marked. \*\*\* $p < 0.001$ .

In summary, the analyzed peptides displayed only low NEMO-specific effects on CD95-induced NF- $\kappa$ B activation in HeLa-CD95 cells. The NEMO-derived peptides were able to bind stronger to c-FLIP than the scrambled control peptides. Analysis of IL-8 secretion in HeLa-CD95 cells

overexpressing c-FLIP<sub>L</sub> showed decreased NF-κB activation mediated *via* the improved peptide superFNIIP compared to its scrambled control peptide nosuperFNIIP.

### **3.4 Mass spectrometry analysis of c-FLIP and NEMO interacting proteins**

It is well known that c-FLIP is important for CD95-induced NF-κB activation and NEMO is a central regulator of the NF-κB pathway (Golks et al., 2006; Hayden and Ghosh, 2008). This study has shown that c-FLIP and NEMO interact and that NEMO-derived peptides can interact with c-FLIP<sub>L</sub>. To further understand the role of c-FLIP-NEMO interaction in CD95-induced NF-κB activation additional experiments were performed.

First, the known CD95-induced complexes were analyzed for the presence of both c-FLIP and NEMO. These complexes are the membrane bound CD95 DISC and a secondary high molecular weight complex called complex II that is not associated to the membrane and is able to induce CD95 signaling (Dickens et al., 2012b; Lavrik et al., 2008). Purification of these complexes with gel filtration followed by analysis with IPs was only partly successful because of low protein amounts in gel filtration analysis (data not shown). IPs of the CD95 DISC, followed by IPs for complex II, namely for caspase-8, c-FLIP and FADD, without prior gel filtration showed interaction of the known proteins at the DISC and complex II (data not shown). No NEMO, TRAF2 and RIP1 were found associated to the DISC or complex II.

In contrast to immunoblot analysis of complexes, mass spectrometry analysis is an unbiased approach that can uncover interaction partners without prior selection of expected proteins. To use this advantage in further specification of the c-FLIP-NEMO interaction and to find new interaction partners, IP experiments followed by mass spectrometry analysis were performed. Therefore,  $2 \cdot 10^7$

HeLa-CD95 cells were stimulated with 250 ng/ml CD95L for 40 minutes and lysed. Cell lysates were used for IPs with antibodies against NEMO and c-FLIP coupled to IP beads. The beads were washed and directly subjected to trypsinization for mass spectrometry. Mass spectrometry analysis was performed by Dr. Thilo Kähne at the Institute of Experimental Internal Medicine in Magdeburg.

In contrast to the analysis of c-FLIP and NEMO *via* IP and immunoblotting, no interaction of c-FLIP and NEMO was found using mass spectrometry analysis (Table 1, Figure 18). This surprising finding can be caused by masking effects of other proteins during mass spectrometry analysis. Furthermore, results from experiments that uncovered no c-FLIP peptides in c-FLIP IP and no NEMO peptides in the NEMO IP *via* mass spectrometry were excluded from further analysis. Peptides that were found in the control IP more than once were excluded from further analysis. Table 1 shows a list of proteins that were manually selected for further analysis. First, the effect of the protein UBC9, which is important for SUMOylation of proteins, was analyzed. Only a weak interaction of c-FLIP and NEMO with UBC9 was observed and no significant effects of UBC9 down regulation on CD95-induced NF- $\kappa$ B activation were detected (data not shown). Next, the effect of the protein BCL10 on CD95 signal transduction was analyzed as BCL10 is well known to influence NF- $\kappa$ B activation.

**Table 1: Results of mass spectrometry screening for new c-FLIP and NEMO interacting proteins. The protein identifier, its name and how often it was found in independent experiments in NEMO and c-FLIP IP with (+) or without (-) stimulation with CD95L is shown. Control IPs were done with protein A sepharose beads only. Green background: found always, red background: not found**

Identifier	Name (UniProt)	NEMO IP -	NEMO IP +	control IP +	FLIP IP -	FLIP IP +
O15519 (CFLAR_HUMAN)	CASP8 and FADD-like apoptosis regulator (c-FLIP)	0/4	0/3	0/5	3/3	3/3
Q9Y6K9 (NEMO_HUMAN)	NF-kappa-B essential modulator (NEMO)	4/4	3/3	1/5	0/3	0/3
O95999 (BCL10_HUMAN)	B-cell lymphoma/leukemia 10 (BCL10)	4/4	1/3	0/5	3/3	3/3
P63279 (UBC9_HUMAN)	SUMO-conjugating enzyme UBC9	3/4	2/3	0/5	3/3	2/3
P22061 (PIMT_HUMAN)	Protein-L-isoaspartate(D-aspartate) O-methyltransferase	2/4	2/3	0/5	0/3	2/3
Q9Y3F4 (STRAP_HUMAN)	Serine-threonine kinase receptor-associated protein	3/4	1/3	1/5	3/3	3/3
Q96HS1 (PGAM5_HUMAN)	Serine/threonine-protein phosphatase PGAM5, mitochondrial	4/4	2/3	0/5	3/3	3/3

### **3.5 BCL10 but not MALT1 influences CD95-induced NF-κB activation**

The CBM complex is an important regulator of B-cell receptor (BCR) and T-cell receptor (TCR) induced NF-κB activation and consists of the CARD11, BCL10 and MALT1 (Turvey et al., 2014). The protein BCL10, but not MALT1 and CARD11, was found in the mass spectrometry screen for new c-FLIP and NEMO interaction partners. From these facts the question if this complex is also important for CD95-induced NF-κB activation arose.

To answer this question, the interaction of BCL10 and MALT1 with the CD95 DISC, which is central for CD95 mediated signaling, was analyzed. HeLa-CD95 cells were stimulated with 250 ng/ml CD95L for 20, 40 and 60 minutes and DISC IPs were performed. No BCL10 was found in DISC IPs with  $\alpha$ -APO-1 antibodies (Figure 25 A). MALT1 was found associated to CD95 independent of stimulation with CD95L. In contrast to the known DISC proteins FADD, c-FLIP and caspase-8, that were only found in DISC IP after stimulation with CD95L (Figure 25 A). Next, c-FLIP IPs were performed in HeLa-CD95 cells without stimulation and upon 40 minutes of CD95 stimulation. As expected the cleavage of c-FLIP to p43-FLIP and an association of c-FLIP and FADD after stimulation was detected (Figure 25 B). MALT1 was found associated to c-FLIP with a decrease after stimulation (Figure 25 B). This could be explained by an association of MALT1 with c-FLIP<sub>L</sub> that is decreased upon c-FLIP<sub>L</sub> cleavage to p43-FLIP, the latter as above mentioned occurs upon CD95 stimulation. A little increase in BCL10 signals were detected after stimulation in the c-FLIP IP but a strong background signal in non-specific control IP (ctr-IP) shows non specificity of these signals (Figure 25 B). Next, NEMO IPs were performed. Surprisingly, neither MALT1 nor BCL10 were detected in NEMO IPs (Figure 25 C). Subsequently, MALT1 IPs were performed. As expected, BCL10 was found in MALT1 IP independent of CD95 stimulation (Figure 25 D). No FADD, c-FLIP and NEMO were detected in MALT1 IPs (Figure 25 D). BCL10 IPs were performed however no BCL10 was detected in BCL10 IPs (data not shown). As BCL10 was also not strongly associated to c-FLIP and NEMO in IP experiments no repeat with other BCL10 antibody for IP was performed. Summing up, these results indicate, that MALT1 is maybe interacting with CD95 and c-FLIP.

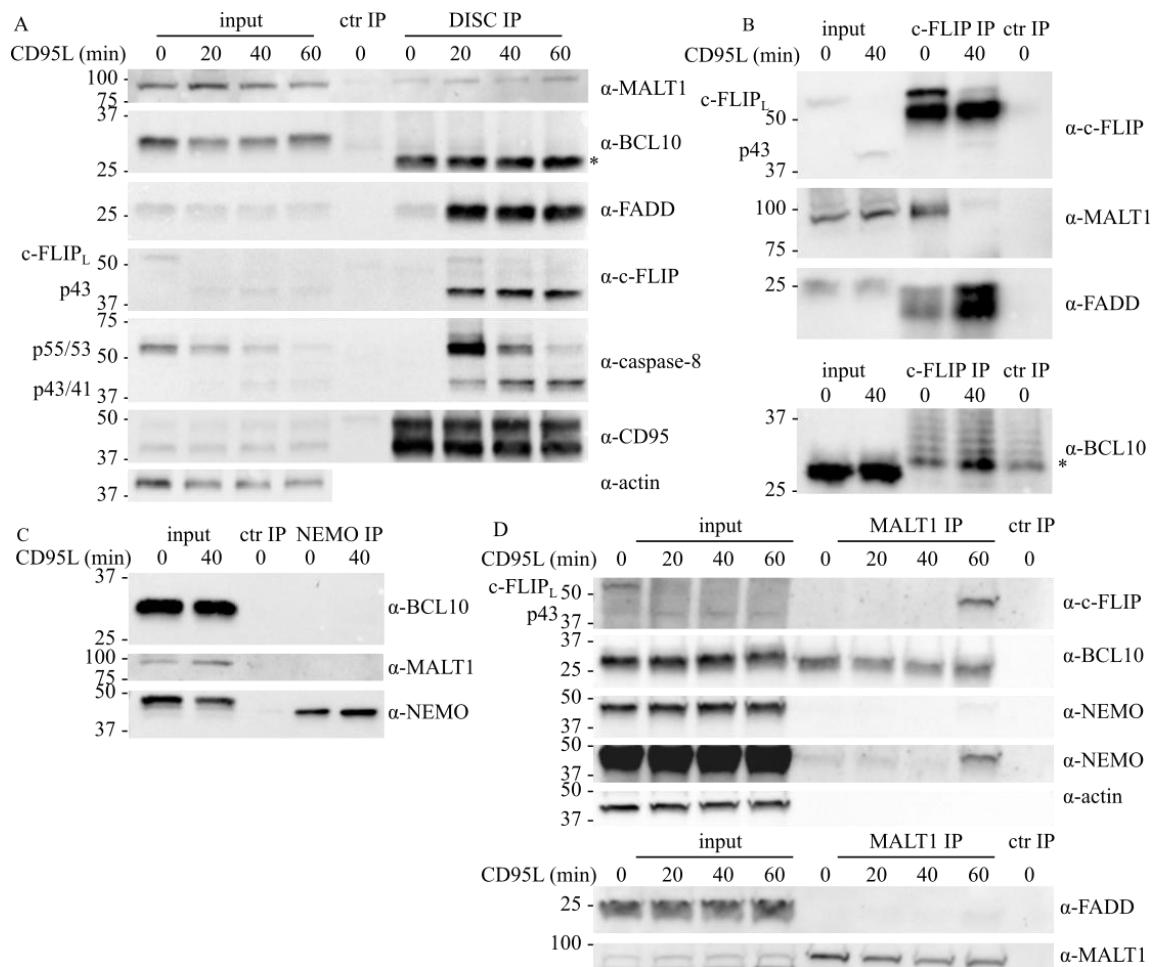


**Figure 25: Interaction of the CD95 DISC, c-FLIP and NEMO with the CBM complex. A-D) HeLa-CD95 cells were stimulated with 250 ng/ml CD95L for the indicated time intervals and subjected to indicated IPs. Lysates and IP eluates were analyzed with immunoblotting with indicated antibodies. A) DISC IPs with  $\alpha$ -APO-1 antibodies were performed. B) c-FLIP IPs were performed. C) NEMO IPs were performed. D) MALT1 IPs were performed and analyzed on two different gels. Actin acts as a loading control. Representative results from one out of at least three independent experiments are shown\* non-specific band, ctr-IP: beads only control IP**

To get further insights into the function of BCL10 and MALT1 in CD95 signaling, the effects of siRNA-mediated down regulation of these two proteins on CD95-induced NF- $\kappa$ B activation were analyzed. Immunoblot analysis of HeLa-CD95 cells with reduced BCL10 levels showed similar time-dependent pattern of I $\kappa$ B $\alpha$  phosphorylation and degradation after stimulation with CD95L for up to 40 minutes like in cells treated with non-targeted siRNA (Figure 26 A). The reduction of protein levels with siRNA was efficient for both proteins (Figure 26 A, B). Reduction in MALT1 protein levels

resulted in faster phosphorylation and degradation of I $\kappa$ B $\alpha$  after stimulation with CD95L for up to 60 minutes (Figure 26 B). The cleavage of c-FLIP to p43-FLIP was not affected by MALT1 knock down (Figure 26 B). Quantification of the I $\kappa$ B $\alpha$  phosphorylation from immunoblot analysis showed a faster I $\kappa$ B $\alpha$  phosphorylation in cell with MALT1 knock down (Figure 26 D).

To understand the effects on downstream NF- $\kappa$ B activation, the translocation of p65 to the nucleus was analyzed with imaging flow cytometry. Hence, HeLa-CD95 cells with knock down of BCL10 or MALT1 were stimulated with 250 ng/ml CD95L for 60 minutes. As expected, the observed effects are in accordance with results from immunoblotting. While no differences between I $\kappa$ B $\alpha$  phosphorylation in cells treated with scrambled control siRNA and BCL10 knock down were found *via* immunoblotting also no significant differences were found in p65 translocation between these two cell lines (Figure 26 B). As expected, the increased I $\kappa$ B $\alpha$  degradation in cells with MALT1 resulted in stronger p65 translocation after 60 minutes of stimulation with CD95L (Figure 26 B). Together these results indicate that MALT1 but not BCL10 is important for CD95-induced NF- $\kappa$ B activation.

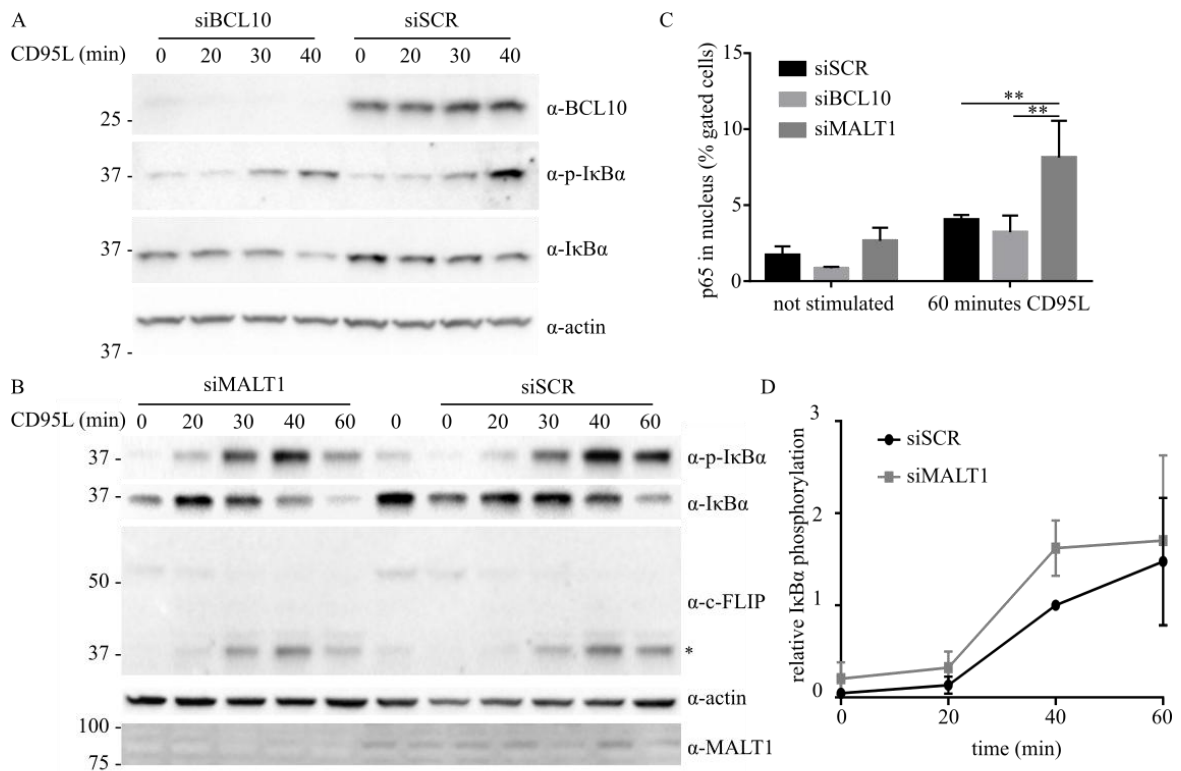


**Figure 26: MALT1 but not BCL10 influences CD95-induced NF-κB activation.** A) HeLa-CD95 cells were transfected with siRNA against BCL10 (siBCL10) or scrambled control siRNA and stimulated with 250 ng/ml CD95L for indicated times. Cells were lysed and lysates were analyzed with immunoblotting. B) MALT1 levels were reduced with siRNA (siMALT1) in HeLa-CD95 cells and cells were stimulated and analyzed like in A. C) HeLa-CD95 cells transfected with indicated siRNA, were stimulated with 250 ng/ml CD95L for 60 minutes and analyzed with imaging flow cytometry for p65 translocation to the nucleus. Means and SD from three independent experiments are shown. Two-way ANOVA with Turkey's correction for multiple comparisons was performed. D) Immunoblots from B were quantified and relative IκBα phosphorylation was calculated from three independent experiments. Band intensities of phospho- IκBα signals were divided by signal intensities from IκBα bands and normalized. Actin was used as a loading control. \*\*p < 0.01, \*non-specific band

Summing up the results, no interaction of BCL10 with the DISC, c-FLIP and NEMO was found while MALT1 was found to be associated to CD95 but not to NEMO. Low amounts of MALT1 were found to be bound to c-FLIP. Consequently, the reduction of BCL10 levels had no significant effects on CD95-induced NF-κB activation while the reduction of MALT1 protein level increased CD95-induced NF-κB activation. Further experiments should examine the effects of MALT1 inhibition on CD95 signaling and expression of NF-κB target cytokines.

### 3.6 NDP52 is a negative regulator of DR-induced NF- $\kappa$ B activation

Up to this point the results indicated that c-FLIP-NEMO interaction is taking place independent of CD95 stimulation and its detailed role on CD95-induced NF- $\kappa$ B activation has to be clarified, but it has to be considered that c-FLIP has been reported to play a role of an important mediator of CD95-induced NF- $\kappa$ B activation (Neumann et al., 2010; Oztürk et al., 2012). Identification of new c-FLIP interaction partners might help to understand the role of c-FLIP in CD95-induced NF- $\kappa$ B activation, hence, a yeast two hybrid (Y2H) screen was performed (Öztürk, 2014), which revealed a new binding partner of p22-FLIP and c-FLIP<sub>L</sub>, the autophagy receptor NDP52 (Calcoco2).

To verify this screening result showing the interaction of NDP52 and c-FLIP<sub>L</sub>, both were expressed in HeLa-CD95 cells followed by an IP for NDP52 (Figure 27 A). c-FLIP<sub>L</sub> was found in NDP52 IP after c-FLIP expression (Figure 27 A).

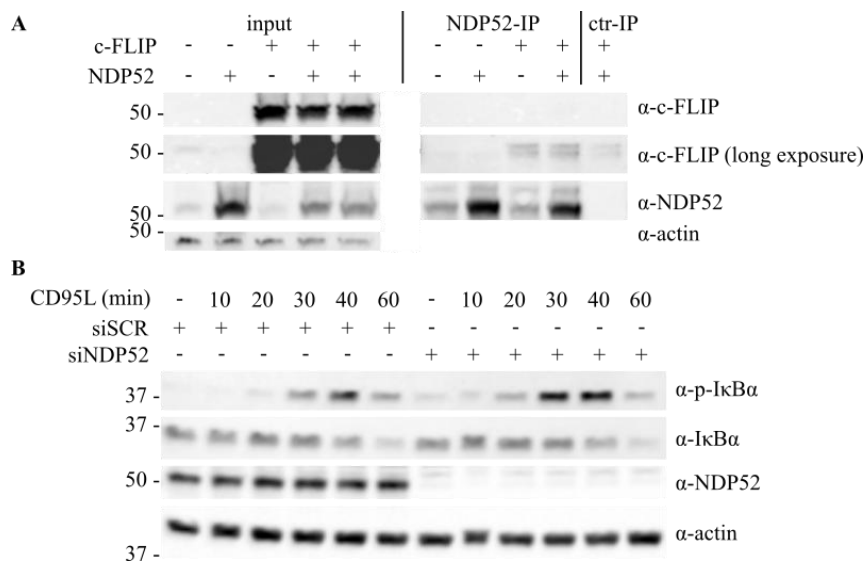


**Figure 27: NDP52 interacts with c-FLIP and reduces CD95-induced I $\kappa$ B $\alpha$  phosphorylation and degradation. A)** NDP52 and c-FLIP<sub>L</sub> were expressed in HeLa-CD95 cells. NDP52 IP was performed and analyzed with immunoblotting with the indicated antibodies. **B)** HeLa-CD95 with siRNA mediated NDP52 knock down or control siRNA were stimulated with 250 ng/ml CD95L for indicated time periods followed by immunoblot analysis of the samples using the indicated antibodies. Actin served as a loading control. ctr-IP control IP with beads only.

First studies on the effect of NDP52 overexpression and downregulation on CD95, TNFR and TCR stimulation describe a negative effect of NDP52 on NF- $\kappa$ B activation (Öztürk, 2014). To investigate the influence of NDP52 on CD95-induced NF- $\kappa$ B activation in detail, the effect of siRNA-mediated NDP52 knock down in HeLa-CD95 cells was analyzed. After stimulation with 250 ng/ml CD95L for 10 to 60 minutes NF- $\kappa$ B induction was detected earlier in cells with reduced NDP52 levels compared to non-targeted scrambled siRNA-transfected cells. This was revealed by immunoblotting analysis that showed a faster I $\kappa$ B $\alpha$  phosphorylation and degradation in cells with NDP52 downregulation (Figure 27 B).

Considering the accelerated degradation of I $\kappa$ B $\alpha$ , the NF- $\kappa$ B subunits p50 and p65 should translocate to the nucleus at earlier time points in cells with reduced NDP52-levels compared to non-targeted scrambled siRNA transfected cells. To check this hypothesis, HeLa-CD95 cells with and without NDP52 knock down were stimulated with 250 ng/ml CD95L and analyzed for p65 translocation with imaging flow cytometry. Indeed, measuring p65 translocation into the nucleus uncovered higher levels of p65 translocation into the nucleus after 40 minutes of CD95 stimulation in cells with siRNA-mediated knock down of NDP52 (siNDP52) compared to cells transfected with non-targeted scrambled siRNA (siSCR, Figure 28 A, B).

Further downstream, the NF- $\kappa$ B signaling pathway induces the secretion of different cytokines, *e.g.* IL-8 and IL-6 (Cullen and Martin, 2015; Cullen et al., 2013). For analysis of IL-8 secretion, HeLa-CD95 cells were stimulated with CD95L for 24 hours. Pre-treatment with 50  $\mu$ M of the caspase inhibitor zVAD for 30 minutes blocked cell death induction. After stimulation with 100 and 250 ng/ml CD95L for 24 h, respectively, IL-8 and IL-6 levels were measured in the cell culture supernatants with IL-8 and IL-6 ELISA (Figure 28 C, D). Cells with knock down of NDP52 had a significant higher concentration of IL-8 in the supernatant (Figure 28 C) after stimulation with CD95L compared to cells treated with control siRNA. Additionally, down regulation of NDP52 resulted in a significantly higher

fold increase of IL-6 in the supernatant after stimulation with 50 and 100 ng/ml CD95L compared to cells treated with control siRNA (Figure 28 D). In summary, these results indicate that NDP52 is a negative regulator of CD95-induced NF- $\kappa$ B activation and further support previous observations (Öztürk, 2014).

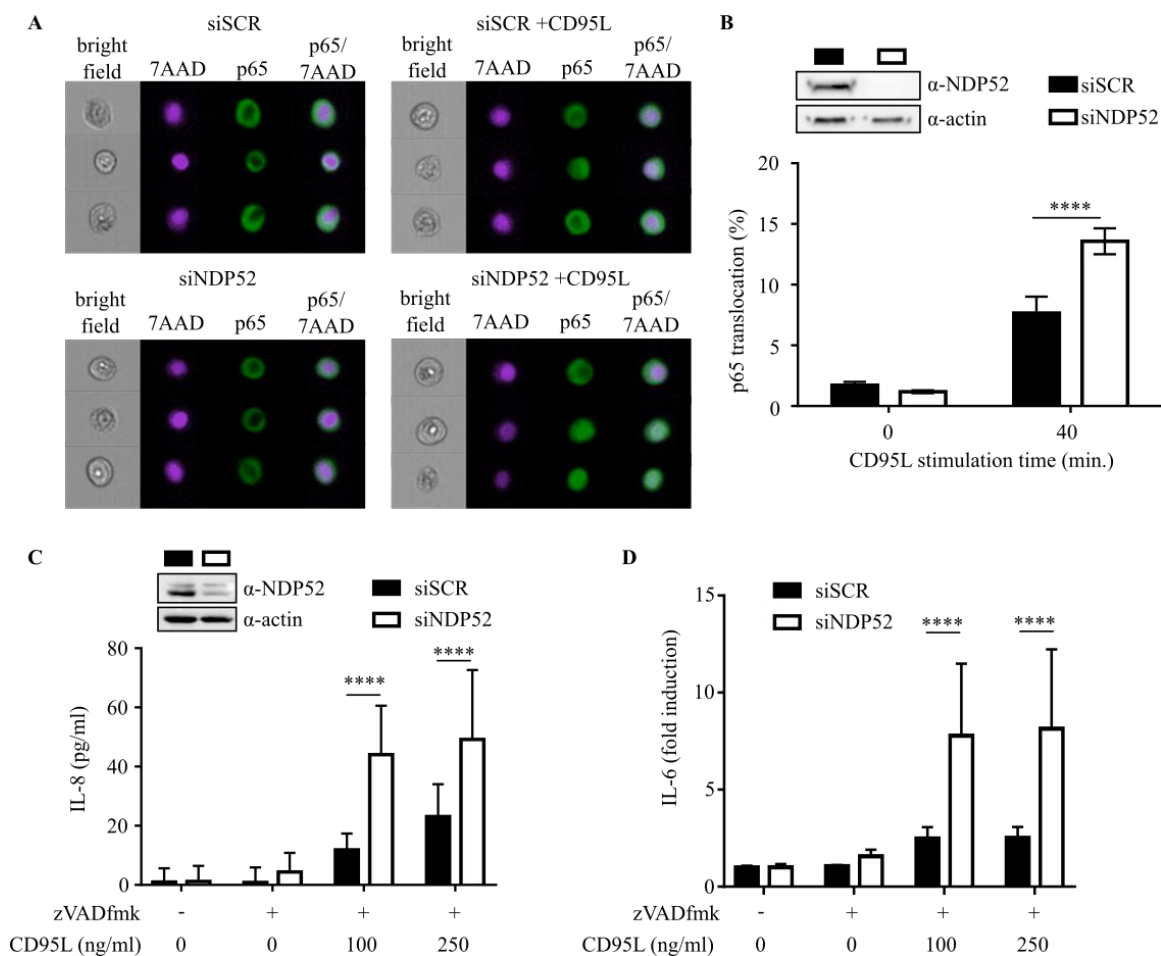


**Figure 28: NDP52 knock down increases CD95-induced NF- $\kappa$ B activation.** A) HeLa-CD95 cells with or without siRNA-mediated knock down of NDP52 were stimulated with 250 ng/ml CD95L for 40 minutes or left unstimulated, and analyzed with imaging flow cytometry for p65 translocation. Three representative pictures for each stimulation condition are shown. B) Quantification of p65 nuclear translocation from A. Means and standard deviations (SDs) of three independent experiments are shown. C) HeLa-CD95 cells were pre-treated with 50  $\mu$ M zVAD for 30 minutes and stimulated with indicated doses of CD95L for 24 h. IL-8 amounts were analyzed with ELISA. Means and SDs of four independent experiments are shown. D) HeLa-CD95 cells were treated as in C and IL-6 levels in supernatant were analyzed with ELISA. Mean and SD of relative IL-6 levels normalized for non-stimulated cells are shown for

**three independent experiments. Two-way ANOVA with Turkey's correction for multiple comparisons test was performed in B, C and D. \*\*\*\* p< 0.0001, min. minutes.**

As the results indicate that NDP52 negatively regulates CD95-induced NF- $\kappa$ B activity, the question arose, if NDP52 also influences NF- $\kappa$ B activation induced by other DRs. Analysis of HeLa-CD95 cells stimulated with 10 ng/ml TNF $\alpha$  for 10 to 60 minutes showed an increase of phosphorylation of I $\kappa$ B $\alpha$  after 10 minutes of CD95L stimulation in cells with siRNA mediated NDP52 knock down (siNDP52) while the maximum of I $\kappa$ B $\alpha$  phosphorylation in cells transfected with control siRNA was measured at 20 minutes. The differences in I $\kappa$ B $\alpha$  degradation between these cells were only less pronounced (Figure 29 A). To further verify these effects, downstream signaling was investigated after stimulation with TNF $\alpha$ . Analysis of the cell culture supernatant after stimulation of HeLa-CD95 cells with 50 and 100 ng/ml TNF $\alpha$  for 24 hours with ELISA showed significantly more IL-8 secretion after NDP52 knock down compared to cells transfected with scrambled control siRNA (Figure 29 B). Likewise, knock down of NDP52 increased the relative stimulation dependent secretion of IL-6 (Figure 29 C) compared to cells transfected with scrambled control siRNA. Thus, NDP52 acts as a negative regulator on TNF-R-induced NF- $\kappa$ B activation, which further supports previous observations (Öztürk, 2014).

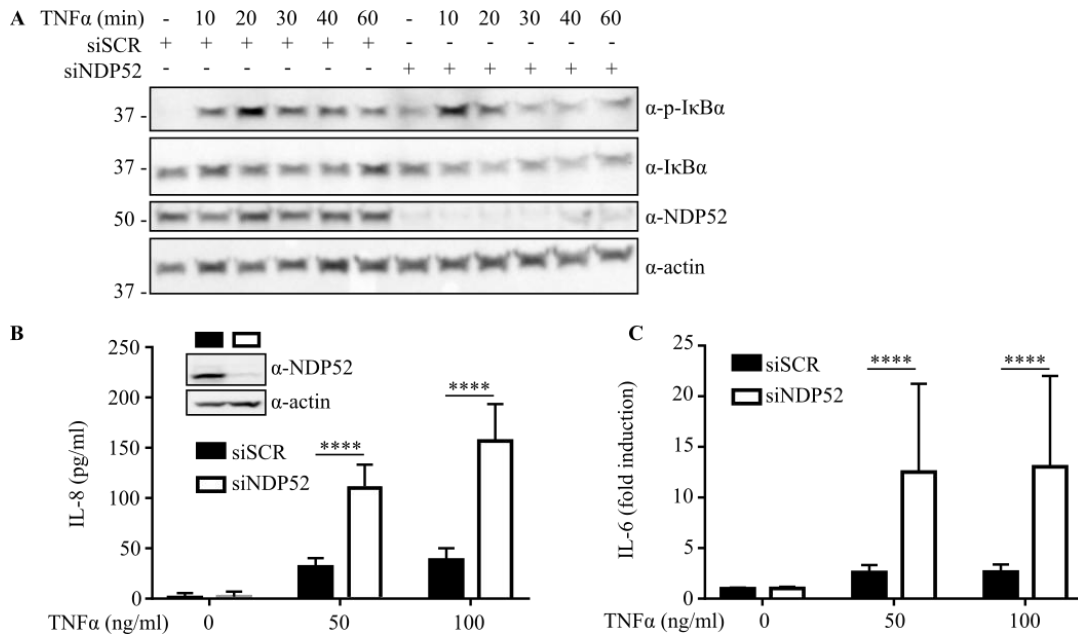


**Figure 29: NDP52 reduces TNF $\alpha$ -induced NF- $\kappa$ B activation.** A) HeLa-CD95 cells were transfected with scrambled control siRNA (siSCR) or siRNA directed against NDP52 (siNDP52), stimulated with 10 ng/ml TNF $\alpha$ , lysed, and analyzed by immunoblot with the indicated antibodies. Actin was used as a loading control. B) HeLa-CD95 cells were transfected with siSCR or siNDP52 and stimulated with 50 and 100 ng/ml TNF $\alpha$  for 24 h. IL-8 concentration in the supernatant was measured with ELISA. Means and SD's of four independent experiments are shown. C) HeLa-CD95 cells were treated as in B and IL-6 levels in supernatant were analyzed with IL-6 ELISA. Relative IL-6 levels normalized for non-stimulated cells are shown. Means and SDs of three independent experiments are shown. Two-way ANOVA with Turkey's correction for multiple comparisons test was performed in B and C. Actin served as a loading control. \*\*\*\*  $p < 0.0001$ .

Knocking down proteins with siRNA specifically reduces protein levels, but the siRNA might also have off-target effects and *e.g.* reduce the amount of other proteins. To confirm the results from experiments with siRNA against NDP52, IL-8 levels in HeLa cells with CRISPR/Cas9 induced NDP52 knock out (KO) (Lazarou et al., 2015) were analyzed after TNF $\alpha$  stimulation. Stimulation with 100 ng/ml TNF $\alpha$  for 24 hours resulted in higher IL-8 secretion in NDP52 KO than wild type (WT) conditions (Figure 30 A). These results validate the results from siRNA mediated knock down of NDP52. Another possibility to proof the specificity of the effect seen after siRNA-mediated knock down is the re-expression of proteins. Therefore, NDP52 was re-expressed in HeLa-CD95 cells with siRNA mediated NDP52 knock down. Stimulation of these cells with 100 ng/ml TNF $\alpha$  for 24 hours

resulted in a normalization of the IL-8 levels to the level of cells treated with non-targeted siRNA (Figure 30 B). Rather due to different transfection reagent the knock down efficiency was worse than before (Figure 29). Taken together, these results allow the conclusion that the experiments of siRNA-mediated knock down of NDP52 are indeed specific.

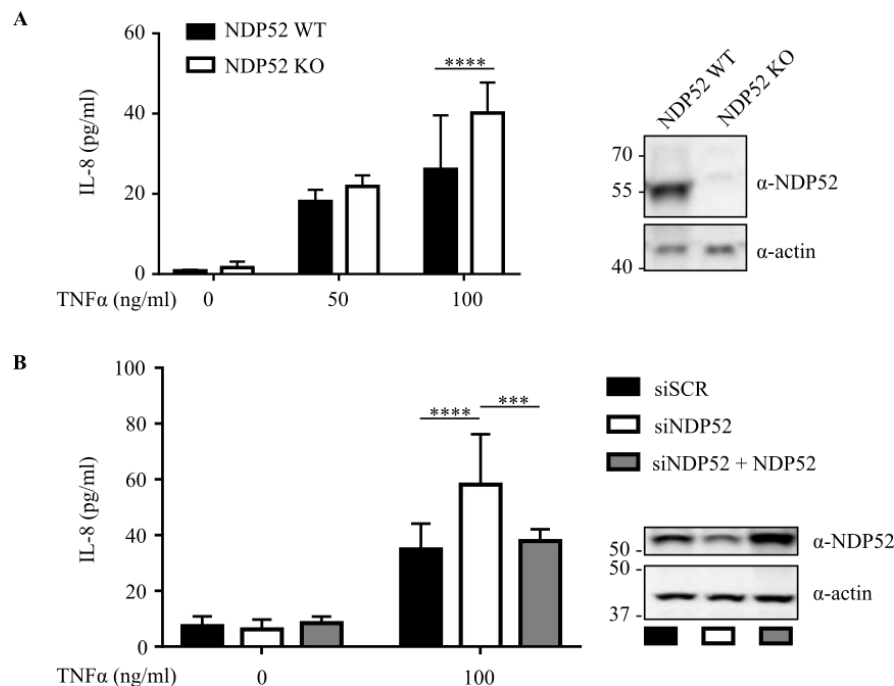


**Figure 30: NDP52 knock out increases TNF $\alpha$ -induced NF- $\kappa$ B activation.** A) HeLa cells with CRISPR/Cas9 mediated NDP52 knock out were stimulated with indicated amount of TNF $\alpha$  for 24 hours. Supernatant of the cells were analyzed with ELISA for IL-8 concentration. Cells were lysed and analyzed by immunoblotting with indicated antibodies. B) HeLa-CD95 cells were transfected with siSCR, siNDP52 or siNDP52 in combination with a plasmid for NDP52 overexpression. Cells were stimulated and analyzed like in A). Means and SDs of three independent experiments are shown in A and B. Two-way ANOVA with Turkey's correction for multiple comparisons test was performed. Actin served as a loading control. \*\*\*p < 0.001, \*\*\*\*p < 0.0001

To summarize these findings, it was shown that NDP52 knock down increased CD95-induced NF- $\kappa$ B activation. Namely, accelerated I $\kappa$ B $\alpha$  phosphorylation and degradation, a higher number of cells with p65 translocation to the nucleus and increased secretion of IL-6 and IL-8 were observed in cells with NDP52 knock down after CD95 stimulation compared to cell treated with non-targeted control siRNA. After stimulation with TNF $\alpha$  increased cytokine secretion was monitored in cells with

siRNA mediated NDP52 knock down and with CRISP/Cas9 mediated NDP52 knock out compared to control cells. The effect of siRNA mediated knock down on TNF $\alpha$ -induced IL-8 secretion was rescued by re-expression of NDP52. Hence, these results indicate a negative effect of NDP52 on DR-induced NF- $\kappa$ B activation and further support previous observations (Öztürk, 2014).

### **3.7 NDP52 interacts with NEMO and A20**

Similar effects of NDP52 on NF- $\kappa$ B activation in the CD95 and TNF-R pathways suggest a common mechanism (Öztürk, 2014). Because the primary and secondary complexes formed after stimulation of these two receptors are not identical, a more downstream mechanism is likely (Brenner et al., 2015; Lavrik and Krammer, 2012; Rangamani and Sirovich, 2007). NEMO is an important regulator of the canonical NF- $\kappa$ B activation and was found to be associated with c-FLIP (Figure 18). It is difficult to follow NEMO and NDP52 interactions in IP experiments because the specific protein signals of NEMO (50 kDa) and NDP52 (52 kDa) are often masked by the heavy chain of the IP antibody (approx. 50 kDa). To improve monitoring of the interactions between NEMO and NDP52, the IP antibodies were covalently coupled to beads and the precipitating protein complexes were eluted by acidic conditions without eluting the antibodies. Analysis of interactions in HeLa-CD95 cells showed an interaction of NDP52 and NEMO, which was independent of stimulation with CD95L (Figure 31 A). NEMO was found in complex with NDP52 as detected in NDP52 IPs and NDP52 was found in NEMO IP. The interaction of NEMO and NDP52 was not CD95 stimulation dependent, but was enhanced after stimulation to a small extent (Figure 31 A). To verify the interaction, NDP52 IPs were performed after stimulation with CD95L in a different cell line, the immortalized human T lymphocyte cell line “Jurkat”. The analysis confirmed the result seen in HeLa-CD95 cells and showed

an interaction between NEMO and NDP52 which was independent of CD95 stimulation in this cell line as well (Figure 31 B).

It is known that ubiquitination of NEMO is necessary for NF- $\kappa$ B activation (Emmerich et al., 2013; Harhaj and Dixit, 2011) and that NDP52 binds to ubiquitin (Xie et al., 2015). To analyze ubiquitination of proteins, so-called denaturing IPs are performed. For this, all protein complexes are denatured by heat and denaturing reagents before performing an IP. This approach allows to detect the PTMs of a protein without detecting PTMs of proteins that interact with the protein of interest under physiological conditions. Analysis of NEMO ubiquitination in HeLa-CD95 cells with denaturing IP after stimulation with CD95L showed an increase in NEMO poly-ubiquitination that peaked around 40 minutes of stimulation and was followed by a decrease in NEMO ubiquitination (Figure 31 C). NEMO ubiquitination is important for NF- $\kappa$ B activation (Adhikari et al., 2007; Sebban-Benin et al., 2007). These results indicate that NDP52 binds to NEMO and that NEMO is ubiquitinated after CD95L stimulation.

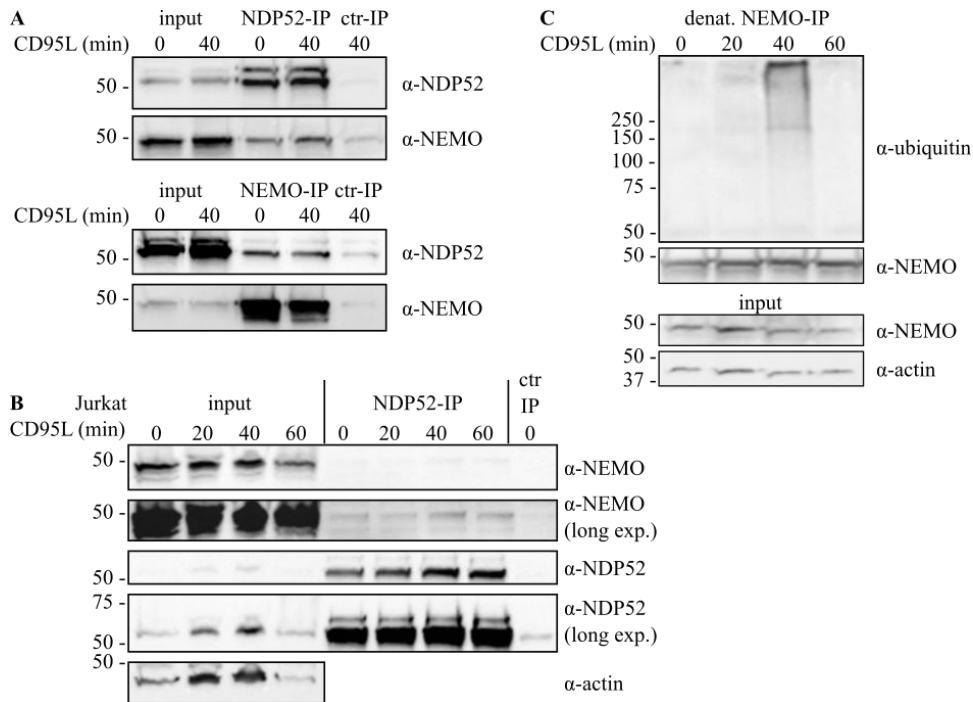


**Figure 31: NDP52 interacts with NEMO.** A) HeLa-CD95 cells were either stimulated with 250 ng/ml for 40 minutes or left unstimulated and IPs were carried out using anti-NDP52 or anti-NEMO antibodies or bead control (ctr-IP), respectively. Immunoblot was performed using the indicated antibodies. IP antibodies were coupled to beads to prevent the detection of the immunoglobulin chains on the immunoblot. B) Jurkat cells were stimulated with 250 ng/ml CD95L for indicated time periods and subjected to NDP52 IP like in A. C) HeLa-CD95 cells were stimulated with CD95L (250 ng/ml) for the indicated time periods and a NEMO-IP under denaturing conditions was performed. Actin served as a loading control. Representative blots from one out of at least three independent experiments are shown. ctr-IP: control IP with beads only.

The regulation of NEMO ubiquitination is an important step to control NF- $\kappa$ B signaling. Ubiquitin can be removed by DUBs (Harhaj and Dixit, 2011; Kovalenko et al., 2003; Wertz et al., 2004). The DUB A20 is important in removing K63-linked ubiquitin-chains from NEMO that act as a scaffold to recruit the TAB2/3-TAK1 complex, thereby activating the IKK complex (Adhikari et al., 2007; Brenner et al., 2015; Harhaj and Dixit, 2011). To check if A20 interacts with the NDP52-NEMO-complex, as suggested in the previous work (Öztürk, 2014), IPs with antibodies against A20 and NDP52 were performed in HeLa-CD95 and Jurkat cells stimulated with CD95L. In HeLa-CD95 and Jurkat cells A20 and NEMO were found in NDP52 IP (Figure 32 A, C). Stimulation with 250 ng/ml CD95L for 20, 40 and 60 minutes increased the amount of A20 found in NDP52 IPs (Figure 32 A, C).

To confirm this interaction, A20 IPs of lysates from the same cell lines were performed. NDP52 and NEMO were found associated to A20, which was slightly increased after CD95L stimulation (Figure 32 B, D). Taken together, A20 was found to be associated with NDP52-NEMO-complex independent of stimulation with a little increase after CD95 stimulation (Figure 32).

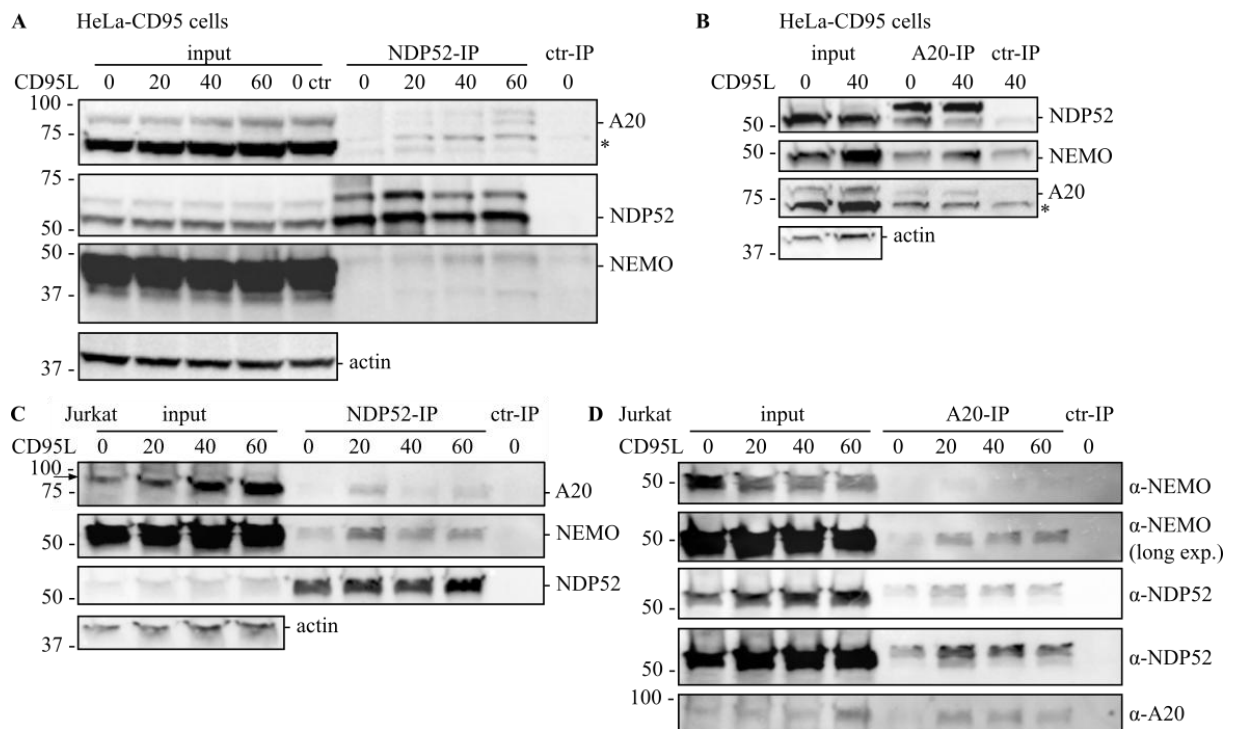


**Figure 32: NDP52 interacts with NEMO and A20.** A) HeLa-CD95 cells were stimulated with 250 ng/ml CD95L for indicated times or left unstimulated and IPs were carried out using anti-NDP52 antibody covalently coupled to the beads. Immunoblotting was performed using the indicated antibodies. B) HeLa-CD95 cells were treated like in A and IP with antibodies against A20 was performed. C) Jurkat cells were treated like in A. D) Jurkat cells were treated like in B). Shown results represent data from at least three independent experiments. Actin was used as a loading control. \*non-specific band, ctr-IP: beads only IP.

The observed ubiquitination of NEMO after CD95L stimulation and the association of NDP52 with A20 and NEMO lead to the hypothesis in this and previous studies (Öztürk, 2014) that NDP52 promotes A20-mediated deubiquitination of NEMO and thereby impairs NF- $\kappa$ B activation. To check this hypothesis, the effect of NDP52 over-expression on NEMO ubiquitination was analyzed. Hence, Flag-tagged NEMO, HA-tagged ubiquitin and NDP52 were co-expressed in HeLa-CD95 cells.

Denaturing Flag IP showed ubiquitination of NEMO, which was decreased in the presence of overexpressed NDP52 (Figure 33). This indicates that NDP52 may bridge the DUB A20 to deubiquitinate NEMO. Alternatively NDP52 might compete with A20 for binding to ubiquitinated NEMO or with other interaction partners of NEMO and thereby blocking NEMO ubiquitination.

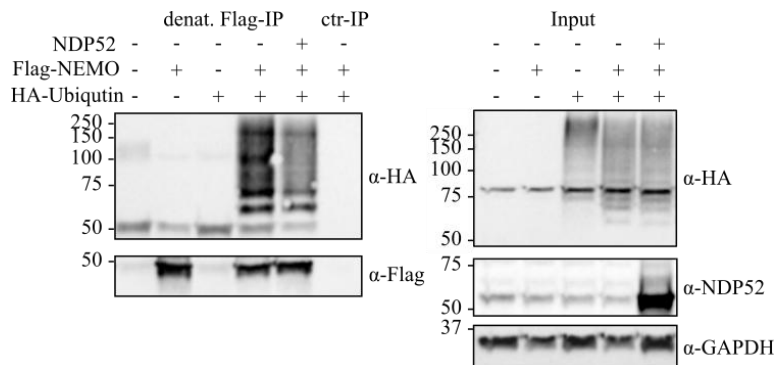


**Figure 33: NDP52 overexpression reduces NEMO ubiquitination.** HeLa-CD95 cells were transfected with NDP52, FLAG-tagged NEMO and HA-tagged ubiquitin. 24 h after transfection exogenous NEMO was immunoprecipitated using a FLAG antibody under denaturing conditions (1% SDS in the lysis buffer). IPs were subjected to immunoblotting analysis using the indicated antibodies. Representative data from one out of three independent experiments is shown. GAPDH was used as loading control.

The compelling data of this chapter show that NDP52, NEMO and A20 interact in HeLa-CD95 and Jurkat cells. The interactions were only marginally enhanced after CD95 stimulation. Analysis of NEMO ubiquitination unveiled increased ubiquitination after CD95 stimulation and a decreased ubiquitination after overexpression of NDP52.

## **4 Discussion**

### **4.1 Stimulation of CD95 induces NF- $\kappa$ B activity and caspase activation**

It is well understood that stimulation of the CD95 with CD95L results in activation of apoptotic caspases and the NF- $\kappa$ B pathway (Cullen et al., 2013; Krammer et al., 2007; Lavrik and Krammer, 2012). The present study tested the effect of three individual reagents for CD95 stimulation on CD95-induced NF- $\kappa$ B activation. As expected, stimulation with  $\alpha$ -APO-1 antibody, commercially available trimerized and purified CD95L as trimerized CD95L in the supernatant of stably transfected HEK293T cells resulted equally well in apoptosis induction and NF- $\kappa$ B activation (Neumann et al., 2010). These results indicate that the supernatant from HEK293T cells expressing trimerized CD95L is suitable for analysis of CD95-induced NF- $\kappa$ B activity. To completely rule out that no other parts of the supernatant are responsible for the observed NF- $\kappa$ B activation, HeLa-CD95 cells could be treated with supernatant from HEK293T cells not expressing CD95L or neutralizing antibodies could be used.

The simultaneous activation of apoptosis and NF- $\kappa$ B pathway is often measured by immunoblot analysis (Neumann et al., 2010). As a bulk population measurement, immunoblot analysis does not allow following signal transduction in single cells. It is important to understand signaling of single cells for effective cancer treatment, because it is necessary to kill every single cancer cell and not only the majority of cells (Ashkenazi, 2015). Importantly, NF- $\kappa$ B activation results in expression of anti-apoptotic proteins. To understand if apoptosis and the NF- $\kappa$ B pathway were activated in the same cell, analysis of single cells is needed. A new imaging flow cytometry protocol was established to follow activation of both pathways in parallel on the single cell level (Schmidt et al., 2015). Imaging flow cytometry combines flow cytometry with imaging and thereby allows taking images of a high number of single cells in a short period of time. The newly established protocol offers the possibility to follow the translocation of p65 to the nucleus as a marker for NF- $\kappa$ B activation and caspase-3 activation as

well as apoptotic morphological changes as markers for apoptosis induction (Schmidt et al., 2015). This measurement provides an insight into the activation of these two pathways without overexpression assays. Monitoring signaling events after CD95 stimulation showed that caspase-3 activation and p65 translocation occur in parallel in at least 20% of the cells while most of the cells activating caspase-3 without p65 translocation to the nucleus. As expected the activation of caspase-3 preceded the apoptotic morphological changes, namely shrinkage of the nucleus and membrane blebbing. With higher stimulation doses of CD95L higher cell death rates were observed, as described before (Fricker et al., 2010).

It was shown before that measuring p65 translocation with imaging flow cytometry as a marker for NF- $\kappa$ B activation correlates with well-known markers for NF- $\kappa$ B activation, *e.g.* phosphorylation and degradation of I $\kappa$ B $\alpha$  or p65 phosphorylation (Maguire et al., 2011, 2015). Another possibility to follow apoptosis induction and NF- $\kappa$ B activation on single cell level is the use of tagged proteins and probes in combination with confocal microscopy (Roux et al., 2015; Spencer and Sorger, 2011). Important advantages of imaging flow cytometry over confocal microscopy analysis of p65 translocation and apoptosis induction are that no fluorescence-tagged proteins have to be expressed in the cells and that higher number of cells can be analyzed in short time periods (Maguire et al., 2011). The disadvantages of imaging flow cytometry over confocal microscopic analysis are a lower image quality and the lacking possibility to follow a single cell over a time period as cells are fixed and discarded after measuring. As an illustration of this disadvantage, it is not possible to state that a cell with active caspase-3 and no p65 translocation to the nucleus has not had nuclear p65 at an earlier time point. Another feature of the quantitative single cell data derived from imaging flow cytometry measurement is that it can be used for fitting and calibration of biological *in silico* models.

The finding that NF- $\kappa$ B pathway is activated in apoptotic dying cells is in line with previous findings that CD95-induced NF- $\kappa$ B activation is important for the production and secretion of pro-

inflammatory proteins that act as “find me” and “eat me” signals for the attraction of immune cells to apoptotic dying cells (Cullen et al., 2013; Kreuz et al., 2004). This mechanism is important to clear apoptotic cells *in vivo*. Another feature of NF- $\kappa$ B activation is the increased expression of anti-apoptotic proteins. These proteins counteract apoptosis induction, *e.g.* expression of XIAP that blocks activity of caspases-3, -7 and -9 (Geserick et al., 2009; Turner et al., 2007). Increased expression of these anti-apoptotic proteins could counteract apoptosis induction and thereby influence the life/death decision in single cells. For TRAIL-R stimulation, single cell measurement allowed to model single cell decisions and to get new insights in mechanisms to kill TRAIL resistant cancer cells by combination of different drugs (Roux et al., 2015). Future studies should include the quantification of key anti-apoptotic proteins into a new imaging flow cytometry protocol and analyze their effects on CD95 signaling.

## **4.2 Interaction of c-FLIP and NEMO**

NEMO is the regulatory part of the IKK complex which is the central activator of canonical NF- $\kappa$ B activation. It was shown that NEMO interacts with the DISC protein c-FLIP under high expression conditions (Lawrence, 2009; Neumann et al., 2010). The results of the present study confirmed the interaction of c-FLIP and NEMO at endogenous protein levels. On the one hand, these findings are not in line with the finding from Baratchian and colleagues that c-FLIP and NEMO do not interact (Baratchian et al., 2016). On the other hand, IP experiments as performed in this study and by Baratchian and colleagues are designed to verify interactions and are not able to prove that no interaction takes place (Baratchian et al., 2016). In addition, the study by Baratchian and colleagues does not observe the interaction of p22-FLIP and NEMO that was shown before, but is not important for CD95-induced NF- $\kappa$ B activation (Golks et al., 2006). As the interaction of c-FLIP and NEMO was monitored independently of CD95 stimulation in the present study, the questions arose if this interaction is important for CD95-induced NF- $\kappa$ B activation or if further protein modification and recruitment of other proteins are important.

First, it was assumed that the c-FLIP-NEMO interaction is direct from the fact that c-FLIP and NEMO interaction was described before and the known crystal structure of the viral c-FLIP homologue v-FLIP with NEMO (Bagn ris et al., 2008). To further analyze this interaction, a homology model of c-FLIP and NEMO was build (done by Nikita Ivanisenko, Institute of Cytology and Genetics, Novosibirsk, Russia). From this model peptides derived from NEMO were designed that should be able to block the c-FLIP-NEMO interaction. These peptides were tested for their effects on CD95-induced NF- B activation. The peptides were not able to significantly inhibit NF- B activation under endogenous c-FLIP protein concentrations while they were able to block CD95-induced IL-8 secretion in cells overexpressing c-FLIP<sub>L</sub>. Further experiments with other NF- B activation readouts should be done to confirm these results. Moreover, it was shown that the peptides specifically interact with c-FLIP. This specific interaction and the effect of the peptides in cells with high c-FLIP expression indicate that the interaction of the NEMO-derived peptide with c-FLIP reduces CD95-induced NF- B activation. Future studies should test the effect of these peptides on c-FLIP-NEMO interaction in IP experiments to prove that the peptides are able to block this interaction and thereby to show that a direct c-FLIP-NEMO interaction induces the NF- B pathway after CD95 stimulation.

Interestingly, in a recent study the effect of similar peptides derived from the v-FLIP-NEMO structure on blocking v-FLIP-induced NF- B activation was tested in primary effusion lymphoma (PEL), a lymphogenic disorder associated with Kaposi's sarcoma-associated herpesvirus (KSHV) infection (Briggs et al., 2017). Briggs and colleagues have shown that the blockage of v-FLIP with peptides inhibited v-FLIP-induced NF- B activation and thereby the progression of viral infection and PEL. Briggs and colleagues have stabilized the alpha-helical structure of the peptides by cross linking and thereby enhanced its effects on v-FLIP-induced NF- B activation (Briggs et al., 2017). This approach of stabilizing NEMO-derived peptide by cross-linking should be used in future studies analyzing the effect of these peptides on c-FLIP-NEMO interaction and CD95-induced NF- B activation. Another interesting finding in the study of Briggs and colleagues is that the peptides were

able to act inside of the cells without addition of a cell penetrating part (Briggs et al., 2017). The fact that the peptides are possibly able to enter cells without a cell penetrating part and that the exact mechanism of cell penetration are not elucidated yet should be used to analyze the cellular import of new NEMO-derived peptides without cell penetrating part (Campbell et al., 2005; Jones and Sayers, 2012; Mueller et al., 2008). Given these ideas, new NEMO-derived peptides without cell penetrating part and with cross-linking should be tested for its effect on CD95-induced NF- $\kappa$ B activation and the c-FLIP-NEMO interaction.

In contrast to the direct c-FLIP-NEMO interaction hypothesis and our finding that c-FLIP and NEMO interact, Baratchian and colleagues have found no c-FLIP-NEMO interaction (Baratchian et al., 2016). Their study showed that the tested c-FLIP isoforms have different mechanism for NF- $\kappa$ B activation from v-FLIP. They found v-FLIP directly interacting with the central region of NEMO while they found no interaction of the c-FLIP isoforms c-FLIP<sub>L</sub>, c-FLIP<sub>S</sub> and the cleavage product p22-FLIP with NEMO. In addition, they have shown that the tested c-FLIP isoforms need the C-terminal part (aa 272–419) and the ubiquitin binding part of NEMO to activate the NF- $\kappa$ B pathway (Baratchian et al., 2016). Additionally, they demonstrated that the c-FLIP isoforms are depending on the kinase TAK1 for NF- $\kappa$ B activation. Moreover, their study showed that the cleavage product p22-FLIP and the short isoform c-FLIP<sub>S</sub> additionally recruit FADD and RIPK1 to NEMO while the long isoform c-FLIP<sub>L</sub> needs the activity of LUBAC to activate NEMO (Baratchian et al., 2016). In contrast to previous reports, they do not see different effects of c-FLIP<sub>L</sub> and non-cleavable c-FLIP<sub>L</sub> (not cleavable into p43-FLIP) on the induction of NF- $\kappa$ B activity (Baratchian et al., 2016; Koenig et al., 2014; Neumann et al., 2010). Different from previous studies, Baratchian and colleagues do not see an effect of p22-FLIP on NF- $\kappa$ B activation (Baratchian et al., 2016; Golks et al., 2006). All in all, the study by Baratchian and colleagues partly contradicts the results of this study and previous publications on c-FLIP-induced NF- $\kappa$ B activation while the finding that RIPK1 and FADD are important is in line with conclusions from TRAIL-R-induced NF- $\kappa$ B activation (Baratchian et al.,

2016; Henry and Martin, 2017). Future studies should further analyze the exact mechanism of CD95-induced NF- $\kappa$ B activity with a special focus on RIPK1 influence on CD95-induced NF- $\kappa$ B activation.

### **4.3 Effect of caspase inhibition on CD95-induced NF- $\kappa$ B activation**

It is well known that the pan caspase inhibitor zVAD blocks apoptosis induction (Poreba et al., 2013). Previous reports have shown that zVAD does not block CD95- or TRAIL-R-induced NF- $\kappa$ B activity (Cullen et al., 2013; Henry and Martin, 2017; Legembre et al., 2004; Neumann et al., 2010). In addition, it was shown before that the cleavage of c-FLIP<sub>L</sub> to p43-FLIP is a pre-requisite to activate the NF- $\kappa$ B pathway (Neumann et al., 2010). For the TRAIL-R that share a similar DISC to CD95 (Dickens et al., 2012a; Schleich et al., 2012), it was recently shown that procaspase-8 acts as a scaffold to bridge RIPK1 *via* FADD to a complex called FADDosome and thereby inducing NF- $\kappa$ B activation after TRAIL-R stimulation (Henry and Martin, 2017). Additionally, the publication by Henry and Martin showed that RIPK1 can be ubiquitinated and activate the IKK complex *via* the TAK1/TAB1/2/3 complex (Henry and Martin, 2017).

The present study confirmed that zVAD does not affect CD95-induced I $\kappa$ B $\alpha$  degradation while it blocks activation of executioner caspases. The shown ability of procaspase-8 to cleave c-FLIP to p43-FLIP at the CD95 DISC even in the presence of the caspase inhibitor zVAD is in line with previous findings for CD95 and TRAIL-R stimulation (Henry and Martin, 2017; Neumann et al., 2010). It was demonstrated before that p43-FLIP is needed for NF- $\kappa$ B activation and that TRAF2 is recruited to p43-FLIP (Kataoka and Tschopp, 2004; Neumann et al., 2010). In addition to these findings, it was shown before that c-FLIP<sub>L</sub> and procaspase-8 interact independently of DR stimulation and that the resulting c-FLIP cleavage product p43-FLIP is important to activate the ERK and the NF- $\kappa$ B pathway (Koenig et al., 2014). Equally important Koenig and colleagues showed that p43-FLIP interacts with TRAF2, Raf1 and RIPK1 and is needed for survival of T-cells (Koenig et al., 2014).

For TRAIL-R stimulation, Henry and Martin showed that reconstitution of caspase-8 KO cells with procaspase-8 restored IL-8 production after TRAIL stimulation while reconstitution of catalytic inactive procaspase-8 mutant (C360A) did not (Henry and Martin, 2017). In contrast to their statement that caspase-8 acts as a scaffold, these findings could also indicate that a rest of procaspases-8 activity (*e.g.* cleavage of c-FLIP<sub>L</sub> into p43-FLIP) that cannot be blocked by zVAD is needed for NF-κB activation. Additionally, they showed that reconstitution of caspase KO cells with procaspase-8 having a mutated FL motif in DED2 (F122G/L123G) that is not able to bind to the DISC did not rescue the TRAIL-R-induced IL-8 secretion. The shown effects can alternatively be explained by the possibility that procaspase-8 is able to cleave c-FLIP<sub>L</sub> to p43-FLIP at the DISC even with addition of the inhibitor zVAD while procaspase-8 with mutated FL motif is not able to recruit to the DISC and no NF-κB is activated. Under those circumstances no procaspase-8-c-FLIP heterodimers are formed at the DISC and hence no cleavage of c-FLIP<sub>L</sub> to p43-FLIP takes place. Future studies should analyze if NF-κB activation is induced *via* the same molecular mechanisms for CD95 and TRAIL-R signaling. Future experiments should address if procaspase-8 acts as a scaffold for RIPK1 recruitment also in CD95 signaling, which role the cleavage of c-FLIP<sub>L</sub> to p43-FLIP has in TRAIL- and CD95-induced NF-κB activation or if both functions are important in both pathways in parallel.

#### **4.4 MALT1 but not BCL10 influence CD95-induced NF-κB activation**

The identification of novel c-FLIP-NEMO interacting proteins would allow better understanding of their interaction mechanism and might get new insights in how this interaction influences CD95-induced NF-κB activation. Mass spectrometry analysis found BCL10 as an interacting protein of c-FLIP and NEMO. BCL10 is a core component of the well-known NF-κB activating CBM complex and thus a promising hit for finding new proteins that affect CD95-induced NF-κB activation (Turvey et al., 2014). While the CBM complex is important for TCR and BCR-induced NF-κB activation no reports on CD95-induced NF-κB activation are known so far (Turvey et al., 2014). A known interaction between the proteins of the CD95 DISC and the CBM complex is the interaction between

procaspase-8 and MALT1 that occur in absence of CD95 in lymphocytes (Figure 35). In line with the known interaction, it was shown that procaspase-8 has an important role in lymphocyte proliferation and procaspase-8 deficient T, B and NK cells have abolished activation of the NF- $\kappa$ B pathway after antigen, TLR or Fc-receptors (Su et al., 2005). The interaction between procaspases-8 and MALT1 is important for TCR-induced NF- $\kappa$ B activation and T-cell proliferation (Riley et al., 2015). A complex consisting of procaspase-8, c-FLIP, RIP1, TRAF2 and TRAF6, as well as the upstream NF- $\kappa$ B regulators PKC $\theta$  and the CBM complex that is formed in absence of CD95 needs procaspases-8 for recruitment of the CBM complex proteins (Misra et al., 2007). In addition, it was shown that procaspase-8 interacts with MALT1 and CBM complex in inflammasome activation and the interaction is important for alternate IL-1 $\beta$  activation (Gringhuis et al., 2012). On the molecular level, it was shown in lymphocytes that MALT1 interacts with procaspase-8 and activates it in a way that can cleave c-FLIP<sub>L</sub> but do not activate caspase-3 (Kawadler et al., 2008).

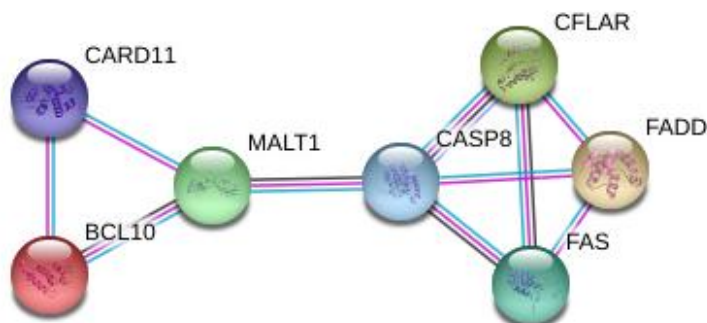


**Figure 34: Known interactions between the CBM complex and the CD95 DISC proteins CD95, caspase-8, FADD and c-FLIP.** Picture derived from the STRINGv10 database shows the known interactions of the human proteins CARD11, BCL10, MALT1, caspase-8 (CASP8), c-FLIP (CFLAR), FADD and CD95 (FAS). The proteins were manually selected to show possible interactions between the CBM-complex and the CD95 DISC. (Szklarczyk et al., 2015).

The interaction of BCL10 with NEMO and c-FLIP that was found by mass spectrometry analysis was not fully confirmed with IP experiments. Only very low amounts of BCL10 were found in the immunoblot analysis of the c-FLIP IP and surprisingly no BCL10 was found in NEMO IP. In line with

this, knock down of BCL10 did not show an effect on CD95-induced NF- $\kappa$ B activation. Knock down of MALT1, another protein of the CBM complex, showed increased NF- $\kappa$ B activation after CD95 stimulation, but MALT1 was not found associated to NEMO and only low amounts were found bound to c-FLIP. It has to be considered that the design of IP experiments does not allow proofing no interaction, because transient or weak interactions are may not be detectable. The contrast between the effects of BCL10 and MALT1 knock down suggest a role of MALT1 in CD95-induced NF- $\kappa$ B induction independent of the CBM complex. In addition, MALT1 was found connected to CD95 with and without its stimulation with CD95L. Possibly the MALT1-caspase-8 interaction influences CD95-induced NF- $\kappa$ B signaling or the DD-containing protein MALT1 interacts with CD95 *via* DD homotypic interactions and reduces total CD95 signaling by hindering DISC assembly (Riley et al., 2015). If the later is true, reduction of MALT1 protein levels would increase total CD95 signaling outcome and thereby also increase CD95-induced NF- $\kappa$ B activation.

Moreover, it is known that MALT1 paracaspase activity influences NF- $\kappa$ B activation on different levels of signal transduction independent of the CBM complex (Hailfinger et al., 2016). MALT1 cleaves HOIL1 and thereby reduces HOIP level in the LUBAC complex. This should result in reduced linear NEMO ubiquitination through the LUBAC complex, but an interaction of the CD95 DISC with LUBAC was not reported yet (Elton et al., 2016; Klein et al., 2015). Not in line with these findings was described that HOIP deficient hepatocytes have less I $\kappa$ B $\alpha$  phosphorylation after CD95 stimulation (Shimizu et al., 2017). The effect of MALT1 knock down on HOIP levels and the effect of the LUBAC complex on CD95-induced NF- $\kappa$ B activity should be examined in future studies. These studies should contain experiments in immune cells or cell lines derived from immune cells to analyze the effect of MALT1 on the interplay of antigen receptor-induced NF- $\kappa$ B activity and CD95-induced NF- $\kappa$ B activity.

Another feature of MALT1 paracaspase activity is the cleavage of negative NF- $\kappa$ B regulators like A20 (Turvey et al., 2014). On this level of signal transduction, lower MALT1 concentrations should result in higher levels of negative NF- $\kappa$ B regulators and thereby lower NF- $\kappa$ B activation. The increased NF- $\kappa$ B activation in MALT1 knock down cells after CD95 stimulation contradicts these effects. Perhaps the increased NF- $\kappa$ B activation in MALT1 knock down cell after CD95 stimulation on other levels of NF- $\kappa$ B signal transduction outweighs this feature (Hailfinger et al., 2016).

#### ***4.5 The autophagy receptor NDP52 suppresses CD95- and TNF-R-induced NF- $\kappa$ B activation***

The protein NDP52 is known to be an autophagy receptor that is also able to bind ubiquitin (Verlhac et al., 2015; Xie et al., 2015). NDP52 is important for the degradation of ubiquitin coated vesicles (Thurston et al., 2009). Surprisingly, it was found in a Y2H screen as an interacting protein of the DISC protein c-FLIP and its effects on DR-induced NF- $\kappa$ B activation were analyzed (Öztürk, 2014). The regulation of the NF- $\kappa$ B pathway is important for immune cell survival and the control of inflammation (Lawrence, 2009). Finding new regulators of DR-induced NF- $\kappa$ B activation helps to understand the life/death decision of cells and could support the finding of new therapies against diseases connected to deregulation of the NF- $\kappa$ B pathway.

The present study demonstrates that the autophagy receptor NDP52 acts as a negative regulator of DR-induced NF- $\kappa$ B activation, which further supports the findings by our group (Öztürk, 2014). It was shown that NDP52 knock down enhanced CD95-induced NF- $\kappa$ B activation. Namely, I $\kappa$ B $\alpha$  phosphorylation and degradation, p65 translocation to the nucleus and, IL-6 and IL-8 secretion as different hallmarks of NF- $\kappa$ B activation were enhanced after NDP52 knock down (Hayden and Ghosh, 2012). By the same token, TNF-R-induced IL-6 and IL-8 secretion was enhanced by NDP52 knock down and CRISPR/Cas9-induced NDP52 knock out. The effect of the knock down on TNF-R-induced NF- $\kappa$ B can be restored by re-expression of NDP52.

Summing up, we showed a new role of NDP52 as a negative regulator of DR-induced NF- $\kappa$ B activation. In line with these novel findings, it was reported that NDP52 can negatively regulate TLR-induced NF- $\kappa$ B activation (Inomata et al., 2012). Also in line with the negative regulatory effect of NDP52 on NF- $\kappa$ B activation, it was shown that the missense mutation V248A of NDP52 is associated with an increased risk for the inflammatory bowel disorder Crohn's disease (CD) (Ellinghaus et al., 2013). The same study has shown that the mutated version of NDP52 (V248A) has an increased stability after TLR3 stimulation (Ellinghaus et al., 2013). The shown negative regulation of NDP52 on DR-induced NF- $\kappa$ B activation suggests that this mutation decreases the ability of NDP52 to regulate NF- $\kappa$ B activity in the bowel. Further studies using mutated NDP52 should help to understand if this mutation is important for the ability of NDP52 to reduce NF- $\kappa$ B activity or if the reported effects in CD are caused by defects in the ability of NDP52 to induce autophagy. Further experiments should analyze the re-expression of NDP52 and mutated forms of NDP52 in NDP52 KO cells. The use of NEMO knock out cells or NF- $\kappa$ B inhibitors would show whether NDP52 acts on NF- $\kappa$ B activation upstream of the IKK complex. The additional use of autophagy inhibitors should help to clarify if autophagy influences the effects of NDP52 on DR-induced NF- $\kappa$ B activation.

#### ***4.6 NDP52 interacts with NEMO and A20 and can reduce NEMO ubiquitination***

As the effects of NDP52 knock down was found in CD95 and TNF-R pathways that have different signaling complexes, we analyzed NDP52 interaction with NEMO, the regulatory subunit of the IKK complex that is a central regulator of canonical NF- $\kappa$ B activation (Harhaj and Dixit, 2011; Vanden Berghe et al., 2015). In addition, an interaction of NEMO and NDP52 was already reported in Y2H screen on proteome scale (Wang et al., 2011) and was shown before in our group (Öztürk, 2014). The present study confirmed that NDP52 interacts with NEMO. Surprisingly, this interaction was not dependent on CD95 stimulation, which indicates that further modifications of these proteins are necessary for signal transduction and that other proteins are recruited to the complex.

It was shown before that NDP52 negatively regulates TLR-induced NF- $\kappa$ B activation, especially under A20 silencing conditions (Inomata et al., 2012). The activation of the NF- $\kappa$ B pathway is controlled by ubiquitination on different levels and A20 is a DUB that removes K63-linked ubiquitin chains from NEMO to limit NF- $\kappa$ B activation (Harhaj and Dixit, 2011; Sebban-Benin et al., 2007). In the present study, we show that NEMO is ubiquitinated and deubiquitinated after CD95 stimulation, which is also indicated by previous reports of our group (Öztürk, 2014). Further studies should analyze the type of ubiquitin linkage in the ubiquitin chains of NEMO induced by CD95 stimulation. As the DUB A20 is important in removing K63-linked ubiquitin-chains from NEMO that act as a scaffold to recruit the TAB2/3-TAK1 complex, thereby activating the IKK complex, we analyzed A20s interaction with NDP52 and NEMO (Adhikari et al., 2007; Brenner et al., 2015; Harhaj and Dixit, 2011). The present study has shown that A20 interacts with the NEMO-NDP52 complex and that this interaction is slightly enhanced by CD95 stimulation. Further experiments should address the mechanism of this interaction. Therefore use of mutated forms of NDP52, NEMO and A20 is necessary.

Another interesting feature of NDP52 is its ability to bind to ubiquitin that is also important for autophagic degradation of ubiquitin coated intracellular pathogens and vesicles (Thurston et al., 2009; Verlhac et al., 2015; Xie et al., 2015). By using biochemical analysis and crystal structures of ubiquitin and NDP52 it was shown before that NDP52 is able to bind to mono-ubiquitin and K48, K63, and linear ubiquitin chains *via* its second C-terminal zinc finger (Xie et al., 2015). In addition, it was described that expression of mutated NDP52 without its C-terminal domain (aa 1-394) can repress TRIF-induced NF- $\kappa$ B activation worse than full length NDP52 or NDP52 without its N-terminal SKICH domain (Inomata et al., 2012). Together these findings indicate that the ubiquitin binding function of NDP52 is important for its NF- $\kappa$ B repressing effects. Interestingly, the C-terminal part is missing in murine NDP52 and could give the answer why no effects of NDP52 KO in mice are described yet. The present study has analyzed the effect of NDP52 expression on the ubiquitination of

NEMO and has shown that NDP52 expression reduced NEMO ubiquitination. Equally important, it was shown that NDP52 interacts with A20 and NEMO. These results suggest that NDP52 bridges the DUB A20 to NEMO and thereby reduces NEMO ubiquitination and hence NF- $\kappa$ B activation (Figure 35). An alternative explanation of the observed effects could be that NDP52 interaction with NEMO blocks NEMO ubiquitination sites and thereby NDP52 overexpression reduces NEMO ubiquitination. Future studies should address the effects of the ubiquitin interaction of NDP52 on DR-induced NF- $\kappa$ B activity by using mutated NDP52 without its C-terminal zinc finger. In addition, the interaction with c-FLIP should be analyzed in detail due to the important role of c-FLIP in DR-induced signaling complexes.

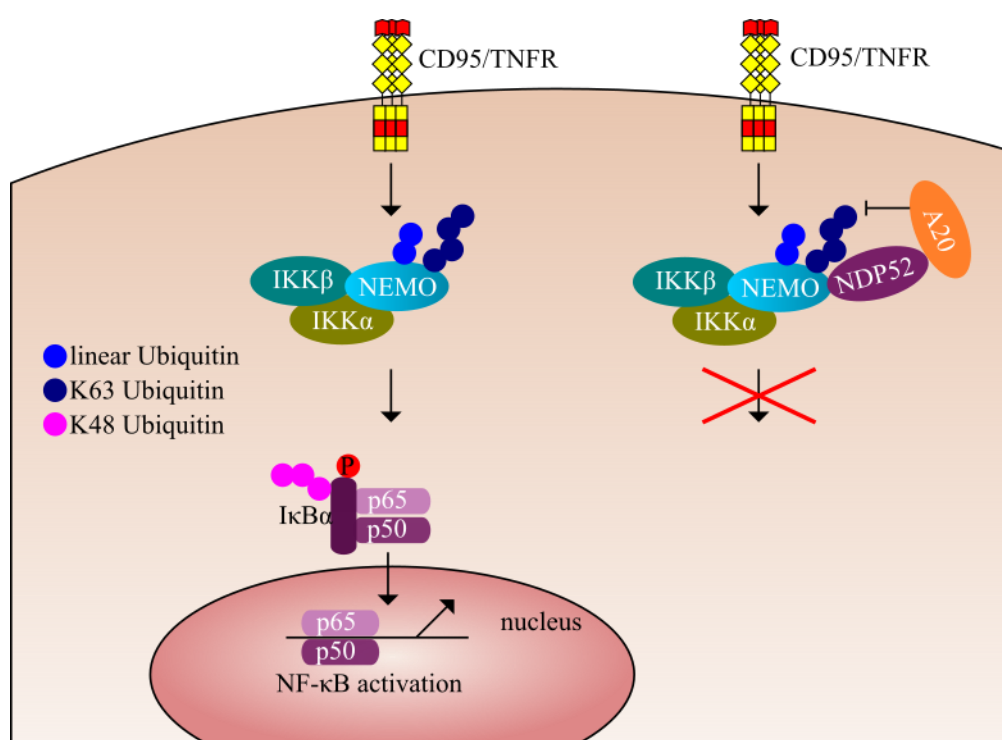


**Figure 35: Model of NDP52 effect on NEMO NF- $\kappa$ B activation.** Without NDP52, NEMO is ubiquitinated after DR stimulation and the active IKK complex phosphorylates I $\kappa$ B $\alpha$ . Thereby I $\kappa$ B $\alpha$  is ubiquitinated with K48 linked ubiquitin chains and proteasomally degraded. Its degradation allows p65 and p50 to translocate to the nucleus and start expression of NF- $\kappa$ B dependent genes. In the presence of NDP52, NDP52 bridges the DUB A20 to NEMO and thereby reduces NEMOs K63-linked ubiquitination resulting in decreased NF- $\kappa$ B activation.

## **4.7 Translational implications of this study**

The pro-apoptotic function of CD95 was discovered first and is important for immune cell homeostasis and tumor elimination (Itoh et al., 1991; Kischkel et al., 1995; Le Gallo et al., 2017). Deletions and mutations of the CD95 receptor and its ligand are described in many cancers and autoimmune disorders, *e.g.* autoimmune lymphoproliferative syndrome (ALPS) (Guégan and Legembre, 2018). While for a long time it was thought that mainly the pro-apoptotic function of CD95 signaling contributes to cancer progress, latest reports uncovered that also the pro-survival signaling, *e.g.* NF- $\kappa$ B activation, is important in cancer progress by promoting inflammation (Barnhart et al., 2004; Chen et al., 2010). Understanding the molecular mechanism of CD95 inducing the pro-inflammatory NF- $\kappa$ B pathway could help to identify under which conditions pro-survival signaling or cell death induction prevails. This knowledge could help to cure the mentioned diseases that are caused by dysfunction of CD95 signaling. In addition, it was shown that the blockage of CD95 results in a new form of cell death that cannot be blocked by the known cell death inhibitors (Hadji et al., 2014). This form of cell death preferably affects cancer cells, it is caused by blocked CD95 signaling and thus is called death induced by CD95 or CD95 ligand elimination (DICE) (Hadji et al., 2014). Probably, the blockage of CD95 induced pro-survival/ growth signaling (*e.g.* ERK, NF- $\kappa$ B) is important for DICE induction and gives rise to new anti-cancer therapies.

The present study has confirmed that the pro-apoptotic and the pro-survival NF- $\kappa$ B pathways are activated in parallel in single cells. In addition, the effect of the c-FLIP-NEMO interaction on CD95-induced NF- $\kappa$ B activity was analyzed. NEMO-derived peptides were designed and tested to reduce the c-FLIP-NEMO interaction. Possibly these peptides can be used to block CD95-induced NF- $\kappa$ B activation without influencing CD95-induced apoptosis and thereby giving raise to kill cancer cells that use increased CD95 activation as a survival mechanism. These peptides would reduce induction of the pro-inflammatory NF- $\kappa$ B signaling pathway without affecting CD95-induced apoptosis that is important for anti-tumor and anti-infectious response. Further improvement of the peptides including

cross-linking and modification of the cell penetrating part could increase their therapeutic potential. In general, small peptides up to 50 amino acids are used as drugs (Otvos and Wade, 2014). Their advantages of a high specificity, low toxicity and large variety come with the disadvantages of low stability, short half-life time and that they are often not orally available (Fosgerau and Hoffmann, 2015).

Finding new proteins that are important for CD95-induced NF- $\kappa$ B activation pathway provides new targets for the development of selective inhibitors. The present study reports NDP52 as a negative regulator of TNF-R- and CD95-induced NF- $\kappa$ B activation. The loss of DR-induced NF- $\kappa$ B suppression in the NDP52 V248A mutant could explain the association of this mutant with Crohn's disease (Ellinghaus et al., 2013). Further studies should analyze the exact molecular mechanism of the mutated forms of NDP52 and their role in DR-induced NF- $\kappa$ B activation.

## **List of abbreviations**

7AAD	7-aminoactinomycin D
A20	TNF- $\alpha$ interacting protein 3 (TNFAIP3)
ALPS	autoimmune lymphoproliferative syndrome
APAF1	apoptotic protease activating factor 1
BCL-2	B-cell lymphoma 2
BCL10	B-cell chronic lymphocytic leukemia/lymphoma 10
BCR	B-cell receptor
CARD	caspase activation and recruitment domain
CARD11	caspase recruitment domain family member 11(also known as CARMA1)
CD95	cluster of differentiation 95, known as FAS or Apo-1
c-FLIP	cellular FLICE-like inhibitory protein
cIAP1/2	cellular inhibitor of apoptosis 1/2
CYLD	cylindromatosis
DD	death domain
DED	death effector domain
DICE	death induced by CD95 or CD95 ligand elimination
DISC	death inducing signaling complex
DMSO	dimethylsulfoxid
DR	death receptor
DUB	deubiquitinase
FAS	also known as CD95
FADD	FAS associated protein with death domain
FCS	fetal calf/ bovine serum
ER	endoplasmatic reticulum
GIR	galectin 8 interacting region
HOIL-1	heme-oxidized ERP2 ubiquitin ligase
HOIP	HOIL-1 interacting protein
IP	immunoprecipitation
IAP	inhibitor of apoptosis proteins
IKK $\alpha$ / $\beta$ / $\gamma$	inhibitor of nuclear factor kappa-B kinase subunit alpha/ beta/ gamma
I $\kappa$ B	inhibitor of kappa B
LIR	LC3 interacting domain
LRSAM1	leucine rich repeat and sterile $\alpha$ motif containing 1
LUBAC	linear ubiquitin chain assembly complex
MALT1	mucosa associated lymphoid tissue lymphoma translocation 1
MLKL	mixed linkage kinase domain like pseudokinase
MW	molecular weight
NDP52	nuclear dot protein 52
NEMO	NF- $\kappa$ B essential modifier (also known as IKK $\gamma$ )
NF- $\kappa$ B	nuclear factor 'kappa-light-chain-enhancer' of activated B-cells
NIK	NF- $\kappa$ B-inducing kinase
OTU	ovarian tumor proteases
OTULIN	OTU domain containing deubiquitinase with linear linkage specificity
PBS	phosphate buffered saline
PCD	programmed cell death
PINK1	PTEN-induced putative kinase 1
RIPK1/RIP1	receptor interacting serine/threonine kinase 1
RIPK3/RIP3	receptor interacting serine/threonine kinase 3

SHARPIN	SHANK associated RH domain interactor
siRNA	small interfering RNA
TAK1	Transforming Growth Factor-Beta-Activated Kinase 1
TAB1/2/3	TAK1 binding protein 1/2/3
TBK1	tank binding kinase 1
tBid	truncated Bid
TL1A	TNF like protein 1A
TLR	toll-like receptor
TNF	tumor necrosis factor
TRAF2	TNF receptor-associated factor 2
TRAIL	TNF-related apoptosis inducing ligand
TRAIL-R	TRAIL receptor
TRADD	TNR-R type 1 associated DD protein
v-FLIP	viral FLICE-like inhibitory protein
XIAP	x-chromosome linked IAP
Y2H	yeast-to-hybrid
ZF	zinc finger
zVAD	carbobenzoxy-valyl-alanyl-aspartyl-[O-methyl]-fluoromethylketone (pan-caspase inhibitor)

## References

- Adhikari, A., Xu, M., and Chen, Z.J. (2007). Ubiquitin-mediated activation of TAK1 and IKK. *Oncogene* 26, 3214–3226.
- Asaoka, T., Kaunisto, A., and Eriksson, J.E. (2011). Regulation of Cell Death by c-FLIP Phosphorylation. In *Advances in TNF Family Research*, D. Wallach, A. Kovalenko, and M. Feldmann, eds. (New York, NY: Springer New York), pp. 625–630.
- Ashkenazi, A. (2015). Targeting the extrinsic apoptotic pathway in cancer: lessons learned and future directions. *J. Clin. Invest.* 125, 487–489.
- Bagn ris, C., Ageichik, A.V., Cronin, N., Wallace, B., Collins, M., Boshoff, C., Waksman, G., and Barrett, T. (2008). Crystal Structure of a vFlip-IKK $\gamma$  Complex: Insights into Viral Activation of the IKK Signalosome. *Mol. Cell* 30, 620–631.
- Baratchian, M., Davis, C.A., Shimizu, A., Escors, D., Bagn ris, C., Barrett, T., and Collins, M.K. (2016). Distinct Activation Mechanisms of NF- $\kappa$ B Regulator Inhibitor of NF- $\kappa$ B Kinase (IKK) by Isoforms of the Cell Death Regulator Cellular FLICE-like Inhibitory Protein (cFLIP). *J. Biol. Chem.* 291, 7608–7620.
- Barnhart, B.C., Legembre, P., Pietras, E., Bubici, C., Franzoso, G., and Peter, M.E. (2004). CD95 ligand induces motility and invasiveness of apoptosis-resistant tumor cells. *EMBO J.* 23, 3175–3185.
- Berchtold, L.A., Prause, M., St rling, J., and Mandrup-Poulsen, T. (2016). Cytokines and Pancreatic  $\beta$ -Cell Apoptosis. In *Advances in Clinical Chemistry*, (Elsevier), pp. 99–158.
- Berman, H.M. (2000). The Protein Data Bank. *Nucleic Acids Res.* 28, 235–242.
- Billen, L.P., Shamas-Din, A., and Andrews, D.W. (2008). Bid: a Bax-like BH3 protein. *Oncogene* 27 *Suppl 1*, S93-104.
- Brenner, D., Blaser, H., and Mak, T.W. (2015). Regulation of tumour necrosis factor signalling: live or let die. *Nat. Rev. Immunol.* 15, 362–374.
- Briggs, L.C., Chan, A.W.E., Davis, C.A., Whitelock, N., Hotiana, H.A., Baratchian, M., Bagn ris, C., Selwood, D.L., Collins, M.K., and Barrett, T.E. (2017). IKK $\gamma$ -Mimetic Peptides Block the

Resistance to Apoptosis Associated with Kaposi's Sarcoma-Associated Herpesvirus Infection. *J. Virol.* 91.

Busse, D. (2017). Construction and characterization of c-FLIP overexpressing cancer cell lines to analyze the effect of small molecules on death receptor signaling.

Campbell, G.R., Watkins, J.D., Esquieu, D., Pasquier, E., Loret, E.P., and Spector, S.A. (2005). The C Terminus of HIV-1 Tat Modulates the Extent of CD178-mediated Apoptosis of T Cells. *J. Biol. Chem.* 280, 38376–38382.

Chau, V., Tobias, J., Bachmair, A., Marriott, D., Ecker, D., Gonda, D., and Varshavsky, A. (1989). A multiubiquitin chain is confined to specific lysine in a targeted short-lived protein. *Science* 243, 1576–1583.

Chen, L., Park, S.-M., Tumanov, A.V., Hau, A., Sawada, K., Feig, C., Turner, J.R., Fu, Y.-X., Romero, I.L., Lengyel, E., et al. (2010). CD95 promotes tumour growth. *Nature* 465, 492–496.

Cildir, G., Low, K.C., and Tergaonkar, V. (2016). Noncanonical NF- $\kappa$ B Signaling in Health and Disease. *Trends Mol. Med.* 22, 414–429.

Corrocher, R., Tedesco, F., Rabusin, P., and De Sandre, G. (1975). Effect of human erythrocyte stromata on complement activation. *Br. J. Haematol.* 29, 235–241.

Creagh, E.M. (2014). Caspase crosstalk: integration of apoptotic and innate immune signalling pathways. *Trends Immunol.* 35, 631–640.

Cullen, S.P., and Martin, S.J. (2015). Fas and TRAIL 'death receptors' as initiators of inflammation: Implications for cancer. *Semin. Cell Dev. Biol.* 39, 26–34.

Cullen, S.P., Henry, C.M., Kearney, C.J., Logue, S.E., Feoktistova, M., Tynan, G.A., Lavelle, E.C., Leverkus, M., and Martin, S.J. (2013). Fas/CD95-induced chemokines can serve as "find-me" signals for apoptotic cells. *Mol. Cell* 49, 1034–1048.

Debatin, K.M., and Krammer, P.H. (1995). Resistance to APO-1 (CD95) induced apoptosis in T-ALL is determined by a BCL-2 independent anti-apoptotic program. *Leukemia* 9, 815–820.

Dickens, L.S., Boyd, R.S., Jukes-Jones, R., Hughes, M.A., Robinson, G.L., Fairall, L., Schwabe, J.W.R., Cain, K., and MacFarlane, M. (2012a). A Death Effector Domain Chain DISC Model Reveals a Crucial Role for Caspase-8 Chain Assembly in Mediating Apoptotic Cell Death. *Mol. Cell* *47*, 291–305.

Dickens, L.S., Powley, I.R., Hughes, M.A., and MacFarlane, M. (2012b). The ‘complexities’ of life and death: Death receptor signalling platforms. *Exp. Cell Res.* *318*, 1269–1277.

Du, C., Fang, M., Li, Y., Li, L., and Wang, X. (2000). Smac, a mitochondrial protein that promotes cytochrome c-dependent caspase activation by eliminating IAP inhibition. *Cell* *102*, 33–42.

Dubois, S.M., Alexia, C., Wu, Y., Leclair, H.M., Leveau, C., Schol, E., Fest, T., Tarte, K., Chen, Z.J., Gavard, J., et al. (2014). A catalytic-independent role for the LUBAC in NF- $\kappa$ B activation upon antigen receptor engagement and in lymphoma cells. *Blood* *123*, 2199–2203.

Duckett, C.S., Nava, V.E., Gedrich, R.W., Clem, R.J., Van Dongen, J.L., Gilfillan, M.C., Shiels, H., Hardwick, J.M., and Thompson, C.B. (1996). A conserved family of cellular genes related to the baculovirus iap gene and encoding apoptosis inhibitors. *EMBO J.* *15*, 2685–2694.

Eldridge, M.J., and Shenoy, A.R. (2015). Antimicrobial inflammasomes: unified signalling against diverse bacterial pathogens. *Curr. Opin. Microbiol.* *23*, 32–41.

Ellinghaus, D., Zhang, H., Zeissig, S., Lipinski, S., Till, A., Jiang, T., Stade, B., Bromberg, Y., Ellinghaus, E., Keller, A., et al. (2013). Association Between Variants of PRDM1 and NDP52 and Crohn’s Disease, Based on Exome Sequencing and Functional Studies. *Gastroenterology* *145*, 339–347.

Elmore, S. (2007). Apoptosis: A Review of Programmed Cell Death. *Toxicol. Pathol.* *35*, 495–516.

Elton, L., Carpentier, I., Staal, J., Driege, Y., Haegman, M., and Beyaert, R. (2016). MALT1 cleaves the E3 ubiquitin ligase HOIL-1 in activated T cells, generating a dominant negative inhibitor of LUBAC-induced NF- $\kappa$ B signaling. *FEBS J.* *283*, 403–412.

Emmerich, C.H., Ordureau, A., Strickson, S., Arthur, J.S.C., Pedrioli, P.G.A., Komander, D., and Cohen, P. (2013). Activation of the canonical IKK complex by K63/M1-linked hybrid ubiquitin chains. *Proc. Natl. Acad. Sci. U. S. A.* *110*, 15247–15252.

Espe, J. (2017). Analysen zur gezielten Modifikation des CD95 Signalwegs durch Small Molecules und Charakterisierung neu generierter c-FLIP überexprimierender Tumor-Zelllinien.

Fiil, B.K., Damgaard, R.B., Wagner, S.A., Keusekotten, K., Fritsch, M., Bekker-Jensen, S., Mailand, N., Choudhary, C., Komander, D., and Gyrd-Hansen, M. (2013). OTULIN restricts Met1-linked ubiquitination to control innate immune signaling. *Mol. Cell* 50, 818–830.

Fischer, H., Koenig, U., Eckhart, L., and Tschachler, E. (2002). Human caspase 12 has acquired deleterious mutations. *Biochem. Biophys. Res. Commun.* 293, 722–726.

Fosgerau, K., and Hoffmann, T. (2015). Peptide therapeutics: current status and future directions. *Drug Discov. Today* 20, 122–128.

Fricker, N., Beaudouin, J., Richter, P., Eils, R., Krammer, P.H., and Lavrik, I.N. (2010). Model-based dissection of CD95 signaling dynamics reveals both a pro- and antiapoptotic role of c-FLIPL. *J. Cell Biol.* 190, 377–389.

Fu, T.-M., Li, Y., Lu, A., Li, Z., Vajjhala, P.R., Cruz, A.C., Srivastava, D.B., DiMaio, F., Penczek, P.A., Siegel, R.M., et al. (2016). Cryo-EM Structure of Caspase-8 Tandem DED Filament Reveals Assembly and Regulation Mechanisms of the Death-Inducing Signaling Complex. *Mol. Cell* 64, 236–250.

Geserick, P., Hupe, M., Moulin, M., Wong, W.W.-L., Feoktistova, M., Kellert, B., Gollnick, H., Silke, J., and Leverkus, M. (2009). Cellular IAPs inhibit a cryptic CD95-induced cell death by limiting RIP1 kinase recruitment. *J. Cell Biol.* 187, 1037–1054.

Gilmore, T.D. (2006). Introduction to NF-kappaB: players, pathways, perspectives. *Oncogene* 25, 6680–6684.

Goldstein, G., Scheid, M., Hammerling, U., Schlesinger, D.H., Niall, H.D., and Boyse, E.A. (1975). Isolation of a polypeptide that has lymphocyte-differentiating properties and is probably represented universally in living cells. *Proc. Natl. Acad. Sci. U. S. A.* 72, 11–15.

Golks, A., Brenner, D., Fritsch, C., Krammer, P.H., and Lavrik, I.N. (2005). c-FLIPR, a new regulator of death receptor-induced apoptosis. *J. Biol. Chem.* 280, 14507–14513.

Golks, A., Brenner, D., Krammer, P.H., and Lavrik, I.N. (2006). The c-FLIP-NH2 terminus (p22-FLIP) induces NF-kappaB activation. *J. Exp. Med.* 203, 1295–1305.

Gringhuis, S.I., Kaptein, T.M., Wevers, B.A., Theelen, B., van der Vlist, M., Boekhout, T., and Geijtenbeek, T.B.H. (2012). Dectin-1 is an extracellular pathogen sensor for the induction and processing of IL-1 $\beta$  via a noncanonical caspase-8 inflammasome. *Nat. Immunol.* 13, 246–254.

Guégan, J.-P., and Legembre, P. (2017). Non-apoptotic functions of Fas/CD95 in the immune response. *FEBS J.*

Guégan, J.-P., and Legembre, P. (2018). Nonapoptotic functions of Fas/CD95 in the immune response. *FEBS J.* 285, 809–827.

Guicciardi, M.E., and Gores, G.J. (2009). Life and death by death receptors. *FASEB J.* 23, 1625–1637.

Guo, W., Dong, A., Pan, X., Lin, X., Lin, Y., He, M., Zhu, B., Jin, L., and Yao, R. (2016). Role of caspase-10 in the death of acute leukemia cells. *Oncol. Lett.* 12, 1623–1629.

Gupta, I., Singh, K., Varshney, N.K., and Khan, S. (2018). Delineating Crosstalk Mechanisms of the Ubiquitin Proteasome System That Regulate Apoptosis. *Front. Cell Dev. Biol.* 6, 11.

Haas, T.L., Emmerich, C.H., Gerlach, B., Schmukle, A.C., Cordier, S.M., Rieser, E., Feltham, R., Vince, J., Warnken, U., Wenger, T., et al. (2009). Recruitment of the linear ubiquitin chain assembly complex stabilizes the TNF-R1 signaling complex and is required for TNF-mediated gene induction. *Mol. Cell* 36, 831–844.

Hadji, A., Ceppi, P., Murmann, A.E., Brockway, S., Pattanayak, A., Bhinder, B., Hau, A., De Chant, S., Parimi, V., Kolesza, P., et al. (2014). Death induced by CD95 or CD95 ligand elimination. *Cell Rep.* 7, 208–222.

Hailfinger, S., Schmitt, A., and Schulze-Osthoff, K. (2016). The paracaspase MALT1 dampens NF- $\kappa$ B signalling by cleaving the LUBAC subunit HOIL-1. *FEBS J.* 283, 400–402.

Harhaj, E.W., and Dixit, V.M. (2011). Deubiquitinases in the regulation of NF- $\kappa$ B signaling. *Cell Res.* 21, 22–39.

Hauenstein, A.V., Xu, G., Kabaleeswaran, V., and Wu, H. (2017). Evidence for M1-Linked Polyubiquitin-Mediated Conformational Change in NEMO. *J. Mol. Biol.* *429*, 3793–3800.

Hayden, M.S., and Ghosh, S. (2008). Shared principles in NF-kappaB signaling. *Cell* *132*, 344–362.

Hayden, M.S., and Ghosh, S. (2012). NF- $\kappa$ B, the first quarter-century: remarkable progress and outstanding questions. *Genes Dev.* *26*, 203–234.

Heller, M., Edelstein, P., and Mayer, M. (1975). Membrane-bound enzymes. III. Protease activity in leucocytes in relation to erythrocyte membranes. *Biochim. Biophys. Acta* *413*, 472–482.

Henry, C.M., and Martin, S.J. (2017). Caspase-8 Acts in a Non-enzymatic Role as a Scaffold for Assembly of a Pro-inflammatory “FADDosome” Complex upon TRAIL Stimulation. *Mol. Cell* *65*, 715-729.e5.

Hershko, A., Heller, H., Elias, S., and Ciechanover, A. (1983). Components of ubiquitin-protein ligase system. Resolution, affinity purification, and role in protein breakdown. *J. Biol. Chem.* *258*, 8206–8214.

Horn, S., Hughes, M.A., Schilling, R., Sticht, C., Tenev, T., Ploesser, M., Meier, P., Sprick, M.R., MacFarlane, M., and Leverkus, M. (2017). Caspase-10 Negatively Regulates Caspase-8-Mediated Cell Death, Switching the Response to CD95L in Favor of NF- $\kappa$ B Activation and Cell Survival. *Cell Rep.* *19*, 785–797.

Huett, A., Heath, R.J., Begun, J., Sassi, S.O., Baxt, L.A., Vyas, J.M., Goldberg, M.B., and Xavier, R.J. (2012). The LRR and RING domain protein LRSAM1 is an E3 ligase crucial for ubiquitin-dependent autophagy of intracellular *Salmonella Typhimurium*. *Cell Host Microbe* *12*, 778–790.

Hughes, M.A., Powley, I.R., Jukes-Jones, R., Horn, S., Feoktistova, M., Fairall, L., Schwabe, J.W.R., Leverkus, M., Cain, K., and MacFarlane, M. (2016). Co-operative and Hierarchical Binding of c-FLIP and Caspase-8: A Unified Model Defines How c-FLIP Isoforms Differentially Control Cell Fate. *Mol. Cell* *61*, 834–849.

Husnjak, K., and Dikic, I. (2012). Ubiquitin-Binding Proteins: Decoders of Ubiquitin-Mediated Cellular Functions. *Annu. Rev. Biochem.* *81*, 291–322.

Ikeda, F., Deribe, Y.L., Skånland, S.S., Stieglitz, B., Grabbe, C., Franz-Wachtel, M., van Wijk, S.J.L., Goswami, P., Nagy, V., Terzic, J., et al. (2011). SHARPIN forms a linear ubiquitin ligase complex regulating NF- $\kappa$ B activity and apoptosis. *Nature* 471, 637–641.

Imamura, R., Konaka, K., Matsumoto, N., Hasegawa, M., Fukui, M., Mukaida, N., Kinoshita, T., and Suda, T. (2004). Fas Ligand Induces Cell-autonomous NF- $\kappa$ B Activation and Interleukin-8 Production by a Mechanism Distinct from That of Tumor Necrosis Factor- $\alpha$ . *J. Biol. Chem.* 279, 46415–46423.

Inomata, M., Niida, S., Shibata, K., and Into, T. (2012). Regulation of Toll-like receptor signaling by NDP52-mediated selective autophagy is normally inactivated by A20. *Cell. Mol. Life Sci. CMLS* 69, 963–979.

Irmeler, M., Thome, M., Hahne, M., Schneider, P., Hofmann, K., Steiner, V., Bodmer, J.-L., Schröter, M., Burns, K., Mattmann, C., et al. (1997). Inhibition of death receptor signals by cellular FLIP. *Nature* 388, 190–195.

Itoh, N., Yonehara, S., Ishii, A., Yonehara, M., Mizushima, S., Sameshima, M., Hase, A., Seto, Y., and Nagata, S. (1991). The polypeptide encoded by the cDNA for human cell surface antigen Fas can mediate apoptosis. *Cell* 66, 233–243.

Jacobs, M.D., and Harrison, S.C. (1998). Structure of an IkappaBalpha/NF-kappaB complex. *Cell* 95, 749–758.

Jones, A.T., and Sayers, E.J. (2012). Cell entry of cell penetrating peptides: tales of tails wagging dogs. *J. Controlled Release* 161, 582–591.

Jönsson, G., Paulie, S., and Grandien, A. (2003). cIAP-2 block apoptotic events in bladder cancer cells. *Anticancer Res.* 23, 3311–3316.

Karl, I., Jossberger-Werner, M., Schmidt, N., Horn, S., Goebeler, M., Leverkus, M., Wajant, H., and Giner, T. (2014). TRAF2 inhibits TRAIL- and CD95L-induced apoptosis and necroptosis. *Cell Death Dis.* 5, e1444.

Kataoka, T., and Tschopp, J. (2004). N-Terminal Fragment of c-FLIP(L) Processed by Caspase 8 Specifically Interacts with TRAF2 and Induces Activation of the NF- $\kappa$ B Signaling Pathway. *Mol. Cell. Biol.* 24, 2627–2636.

Kawadler, H., Gantz, M.A., Riley, J.L., and Yang, X. (2008). The paracaspase MALT1 controls caspase-8 activation during lymphocyte proliferation. *Mol. Cell* *31*, 415–421.

Kerr, J.F., Wyllie, A.H., and Currie, A.R. (1972). Apoptosis: a basic biological phenomenon with wide-ranging implications in tissue kinetics. *Br. J. Cancer* *26*, 239–257.

Keusekotten, K., Elliott, P.R., Glockner, L., Fiil, B.K., Damgaard, R.B., Kulathu, Y., Wauer, T., Hospenthal, M.K., Gyrd-Hansen, M., Krappmann, D., et al. (2013). OTULIN antagonizes LUBAC signaling by specifically hydrolyzing Met1-linked polyubiquitin. *Cell* *153*, 1312–1326.

Khoury, G.A., Baliban, R.C., and Floudas, C.A. (2011). Proteome-wide post-translational modification statistics: frequency analysis and curation of the swiss-prot database. *Sci. Rep.* *1*.

Kim, B.-W., Beom Hong, S., Hoe Kim, J., Hoon Kwon, D., and Kyu Song, H. (2013). Structural basis for recognition of autophagic receptor NDP52 by the sugar receptor galectin-8. *Nat. Commun.* *4*, 1613.

Kischkel, F.C., Hellbardt, S., Behrmann, I., Germer, M., Pawlita, M., Krammer, P.H., and Peter, M.E. (1995). Cytotoxicity-dependent APO-1 (Fas/CD95)-associated proteins form a death-inducing signaling complex (DISC) with the receptor. *EMBO J.* *14*, 5579–5588.

Klein, T., Fung, S.-Y., Renner, F., Blank, M.A., Dufour, A., Kang, S., Bolger-Munro, M., Scurll, J.M., Priatel, J.J., Schweigler, P., et al. (2015). The paracaspase MALT1 cleaves HOIL1 reducing linear ubiquitination by LUBAC to dampen lymphocyte NF- $\kappa$ B signalling. *Nat. Commun.* *6*, 8777.

Koenig, A., Buskiewicz, I.A., Fortner, K.A., Russell, J.Q., Asaoka, T., He, Y.-W., Hakem, R., Eriksson, J.E., and Budd, R.C. (2014). The c-FLIPL Cleavage Product p43FLIP Promotes Activation of Extracellular Signal-regulated Kinase (ERK), Nuclear Factor B (NF- $\kappa$ B), and Caspase-8 and T Cell Survival. *J. Biol. Chem.* *289*, 1183–1191.

Koenig, U., Eckhart, L., and Tschachler, E. (2001). Evidence that caspase-13 is not a human but a bovine gene. *Biochem. Biophys. Res. Commun.* *285*, 1150–1154.

Komander, D., Clague, M.J., and Urbé, S. (2009). Breaking the chains: structure and function of the deubiquitinases. *Nat. Rev. Mol. Cell Biol.* *10*, 550–563.

Korioth, F., Gieffers, C., Maul, G.G., and Frey, J. (1995). Molecular characterization of NDP52, a novel protein of the nuclear domain 10, which is redistributed upon virus infection and interferon treatment. *J. Cell Biol.* *130*, 1–13.

Korsmeyer, S.J., Wei, M.C., Saito, M., Weiler, S., Oh, K.J., and Schlesinger, P.H. (2000). Pro-apoptotic cascade activates BID, which oligomerizes BAK or BAX into pores that result in the release of cytochrome c. *Cell Death Differ.* *7*, 1166–1173.

Kovalenko, A., Chable-Bessia, C., Cantarella, G., Israël, A., Wallach, D., and Courtois, G. (2003). The tumour suppressor CYLD negatively regulates NF-kappaB signalling by deubiquitination. *Nature* *424*, 801–805.

Krammer, P.H., Arnold, R., and Lavrik, I.N. (2007). Life and death in peripheral T cells. *Nat. Rev. Immunol.* *7*, 532–542.

Kreuz, S., Siegmund, D., Rumpf, J.-J., Samel, D., Leverkus, M., Janssen, O., Häcker, G., Dittrich-Breiholz, O., Kracht, M., Scheurich, P., et al. (2004). NFκB activation by Fas is mediated through FADD, caspase-8, and RIP and is inhibited by FLIP. *J. Cell Biol.* *166*, 369–380.

Kroemer, G., Mariño, G., and Levine, B. (2010). Autophagy and the integrated stress response. *Mol. Cell* *40*, 280–293.

Lavrik, I.N. (2014). Systems biology of death receptor networks: live and let die. *Cell Death Dis.* *5*, e1259.

Lavrik, I.N., and Krammer, P.H. (2009). Life and Death Decisions in the CD95 System: Main Pro- and Anti-Apoptotic Modulators. *Acta Naturae* *1*, 80–83.

Lavrik, I.N., and Krammer, P.H. (2012). Regulation of CD95/Fas signaling at the DISC. *Cell Death Differ.* *19*, 36–41.

Lavrik, I., Golks, A., and Krammer, P.H. (2005). Death receptor signaling. *J. Cell Sci.* *118*, 265–267.

Lavrik, I.N., Mock, T., Golks, A., Hoffmann, J.C., Baumann, S., and Krammer, P.H. (2008). CD95 Stimulation Results in the Formation of a Novel Death Effector Domain Protein-containing Complex. *J. Biol. Chem.* *283*, 26401–26408.

Lawrence, T. (2009). The Nuclear Factor NF- $\kappa$ B Pathway in Inflammation. *Cold Spring Harb. Perspect. Biol.* 1, a001651–a001651.

Lazarou, M., Sliter, D.A., Kane, L.A., Sarraf, S.A., Wang, C., Burman, J.L., Sideris, D.P., Fogel, A.I., and Youle, R.J. (2015). The ubiquitin kinase PINK1 recruits autophagy receptors to induce mitophagy. *Nature* 524, 309–314.

Le Gallo, M., Poissonnier, A., Blanco, P., and Legembre, P. (2017). CD95/Fas, Non-Apoptotic Signaling Pathways, and Kinases. *Front. Immunol.* 8, 1216.

Legembre, P., Barnhart, B.C., Zheng, L., Vijayan, S., Straus, S.E., Puck, J., Dale, J.K., Lenardo, M., and Peter, M.E. (2004). Induction of apoptosis and activation of NF- $\kappa$ B by CD95 require different signalling thresholds. *EMBO Rep.* 5, 1084–1089.

Levine, B., Mizushima, N., and Virgin, H.W. (2011). Autophagy in immunity and inflammation. *Nature* 469, 323–335.

Lork, M., Verhelst, K., and Beyaert, R. (2017). CYLD, A20 and OTULIN deubiquitinases in NF- $\kappa$ B signaling and cell death: so similar, yet so different. *Cell Death Differ.* 24, 1172–1183.

Maguire, O., Collins, C., O’Loughlin, K., Miecznikowski, J., and Minderman, H. (2011). Quantifying nuclear p65 as a parameter for NF- $\kappa$ B activation: Correlation between ImageStream cytometry, microscopy, and Western blot. *Cytometry A* 79A, 461–469.

Maguire, O., O’Loughlin, K., and Minderman, H. (2015). Simultaneous assessment of NF- $\kappa$ B/p65 phosphorylation and nuclear localization using imaging flow cytometry. *J. Immunol. Methods* 423, 3–11.

Maubach, G., and Naumann, M. (2017). NEMO Links Nuclear Factor- $\kappa$ B to Human Diseases. *Trends Mol. Med.* 23, 1138–1155.

McClurg, U.L., and Robson, C.N. (2015). Deubiquitinating enzymes as oncotargets. *Oncotarget* 6.

Meininger, I., and Krappmann, D. (2016). Lymphocyte signaling and activation by the CARMA1-BCL10-MALT1 signalosome. *Biol. Chem.* 397.

Micheau, O., and Tschopp, J. (2003). Induction of TNF receptor I-mediated apoptosis via two sequential signaling complexes. *Cell* 114, 181–190.

Misra, R.S., Russell, J.Q., Koenig, A., Hinshaw-Makepeace, J.A., Wen, R., Wang, D., Huo, H., Littman, D.R., Ferch, U., Ruland, J., et al. (2007). Caspase-8 and c-FLIPL Associate in Lipid Rafts with NF- $\kappa$ B Adaptors during T Cell Activation. *J. Biol. Chem.* 282, 19365–19374.

Mohr, A., Deedigan, L., Jencz, S., Mehrabadi, Y., Houlden, L., Albarenque, S.-M., and Zwacka, R.M. (2018). Caspase-10: a molecular switch from cell-autonomous apoptosis to communal cell death in response to chemotherapeutic drug treatment. *Cell Death Differ.* 25, 340–352.

Mostowy, S., Sancho-Shimizu, V., Hamon, M.A., Simeone, R., Brosch, R., Johansen, T., and Cossart, P. (2011). p62 and NDP52 proteins target intracytosolic *Shigella* and *Listeria* to different autophagy pathways. *J. Biol. Chem.* 286, 26987–26995.

Mueller, J., Kretschmar, I., Volkmer, R., and Boisguerin, P. (2008). Comparison of Cellular Uptake Using 22 CPPs in 4 Different Cell Lines. *Bioconjug. Chem.* 19, 2363–2374.

Mühlethaler-Mottet, A., Flahaut, M., Bourlout, K.B., Nardou, K., Coulon, A., Liberman, J., Thome, M., and Gross, N. (2011). Individual caspase-10 isoforms play distinct and opposing roles in the initiation of death receptor-mediated tumour cell apoptosis. *Cell Death Dis.* 2, e125.

Muzio, M., Stockwell, B.R., Stennicke, H.R., Salvesen, G.S., and Dixit, V.M. (1998). An induced proximity model for caspase-8 activation. *J. Biol. Chem.* 273, 2926–2930.

Neumann, L., Pforr, C., Beaudouin, J., Pappa, A., Fricker, N., Krammer, P.H., Lavrik, I.N., and Eils, R. (2010). Dynamics within the CD95 death-inducing signaling complex decide life and death of cells. *Mol. Syst. Biol.* 6.

Niu, J., Shi, Y., Iwai, K., and Wu, Z.-H. (2011). LUBAC regulates NF- $\kappa$ B activation upon genotoxic stress by promoting linear ubiquitination of NEMO: NEMO linear ubiquitination upon genotoxic stress. *EMBO J.* 30, 3741–3753.

Otvos, L., and Wade, J.D. (2014). Current challenges in peptide-based drug discovery. *Front. Chem.* 2, 62.

Öztürk, S. (2014). Regulation of NF- $\kappa$ B activation by Calcoco2. Ruprecht-Karls-Universität Heidelberg.

Oztürk, S., Schleich, K., and Lavrik, I.N. (2012). Cellular FLICE-like inhibitory proteins (c-FLIPs): fine-tuners of life and death decisions. *Exp. Cell Res.* *318*, 1324–1331.

Peter, M.E., Hadji, A., Murmann, A.E., Brockway, S., Putzbach, W., Pattanayak, A., and Ceppi, P. (2015). The role of CD95 and CD95 ligand in cancer. *Cell Death Differ.* *22*, 549–559.

Poreba, M., Strózyk, A., Salvesen, G.S., and Drag, M. (2013). Caspase substrates and inhibitors. *Cold Spring Harb. Perspect. Biol.* *5*, a008680.

Poukkula, M., Kaunisto, A., Hietakangas, V., Denessiouk, K., Katajamäki, T., Johnson, M.S., Sistonen, L., and Eriksson, J.E. (2005). Rapid Turnover of c-FLIPshort Is Determined by Its Unique C-terminal Tail. *J. Biol. Chem.* *280*, 27345–27355.

Qiao, Q., Yang, C., Zheng, C., Fontán, L., David, L., Yu, X., Bracken, C., Rosen, M., Melnick, A., Egelman, E.H., et al. (2013). Structural Architecture of the CARMA1/Bcl10/MALT1 Signalosome: Nucleation-Induced Filamentous Assembly. *Mol. Cell* *51*, 766–779.

Rahighi, S., Ikeda, F., Kawasaki, M., Akutsu, M., Suzuki, N., Kato, R., Kensche, T., Uejima, T., Bloor, S., Komander, D., et al. (2009). Specific recognition of linear ubiquitin chains by NEMO is important for NF- $\kappa$ B activation. *Cell* *136*, 1098–1109.

Randow, F., and Youle, R.J. (2014). Self and nonself: how autophagy targets mitochondria and bacteria. *Cell Host Microbe* *15*, 403–411.

Rangamani, P., and Sirovich, L. (2007). Survival and apoptotic pathways initiated by TNF- $\alpha$ : Modeling and predictions. *Biotechnol. Bioeng.* *97*, 1216–1229.

Riley, J.S., Malik, A., Holohan, C., and Longley, D.B. (2015). DED or alive: assembly and regulation of the death effector domain complexes. *Cell Death Dis.* *6*, e1866.

Rivkin, E., Almeida, S.M., Ceccarelli, D.F., Juang, Y.-C., MacLean, T.A., Srikumar, T., Huang, H., Dunham, W.H., Fukumura, R., Xie, G., et al. (2013). The linear ubiquitin-specific deubiquitinase gumbly regulates angiogenesis. *Nature* *498*, 318–324.

Roux, J., Hafner, M., Bandara, S., Sims, J.J., Hudson, H., Chai, D., and Sorger, P.K. (2015). Fractional killing arises from cell-to-cell variability in overcoming a caspase activity threshold. *Mol. Syst. Biol.* *11*, 803.

Salvesen, G.S., and Ashkenazi, A. (2011). SnapShot: Caspases. *Cell* *147*, 476-476.e1.

Scaffidi, C. (1998). Two CD95 (APO-1/Fas) signaling pathways. *EMBO J.* *17*, 1675–1687.

Schleich, K., Warnken, U., Fricker, N., Öztürk, S., Richter, P., Kammerer, K., Schnölzer, M., Krammer, P.H., and Lavrik, I.N. (2012). Stoichiometry of the CD95 Death-Inducing Signaling Complex: Experimental and Modeling Evidence for a Death Effector Domain Chain Model. *Mol. Cell* *47*, 306–319.

Schleich, K., Buchbinder, J.H., Pietkiewicz, S., Kähne, T., Warnken, U., Öztürk, S., Schnölzer, M., Naumann, M., Krammer, P.H., and Lavrik, I.N. (2016). Molecular architecture of the DED chains at the DISC: regulation of procaspase-8 activation by short DED proteins c-FLIP and procaspase-8 prodomain. *Cell Death Differ.*

Schmidt, J.H., Pietkiewicz, S., Naumann, M., and Lavrik, I.N. (2015). Quantification of CD95-induced apoptosis and NF- $\kappa$ B activation at the single cell level. *J. Immunol. Methods* *423*, 12–17.

Sebban-Benin, H., Pescatore, A., Fusco, F., Pascuale, V., Gautheron, J., Yamaoka, S., Moncla, A., Ursini, M.V., and Courtois, G. (2007). Identification of TRAF6-dependent NEMO polyubiquitination sites through analysis of a new NEMO mutation causing incontinentia pigmenti. *Hum. Mol. Genet.* *16*, 2805–2815.

Shimizu, Y., Peltzer, N., Sevko, A., Lafont, E., Sarr, A., Draberova, H., and Walczak, H. (2017). The Linear ubiquitin chain assembly complex acts as a liver tumor suppressor and inhibits hepatocyte apoptosis and hepatitis: Shimizu et al. *Hepatology* *65*, 1963–1978.

Spencer, S.L., and Sorger, P.K. (2011). Measuring and Modeling Apoptosis in Single Cells. *Cell* *144*, 926–939.

Su, H., Bidère, N., Zheng, L., Cubre, A., Sakai, K., Dale, J., Salmena, L., Hakem, R., Straus, S., and Lenardo, M. (2005). Requirement for caspase-8 in NF-kappaB activation by antigen receptor. *Science* *307*, 1465–1468.

Szklarczyk, D., Franceschini, A., Wyder, S., Forslund, K., Heller, D., Huerta-Cepas, J., Simonovic, M., Roth, A., Santos, A., Tsafou, K.P., et al. (2015). STRING v10: protein-protein interaction networks, integrated over the tree of life. *Nucleic Acids Res.* *43*, D447-452.

Thome, M., Schneider, P., Hofmann, K., Fickenscher, H., Meinel, E., Neipel, F., Mattmann, C., Burns, K., Bodmer, J.-L., Schröter, M., et al. (1997). Viral FLICE-inhibitory proteins (FLIPs) prevent apoptosis induced by death receptors. *Nature* *386*, 517–521.

Thurston, T.L.M., Ryzhakov, G., Bloor, S., von Muhlinen, N., and Randow, F. (2009). The TBK1 adaptor and autophagy receptor NDP52 restricts the proliferation of ubiquitin-coated bacteria. *Nat. Immunol.* *10*, 1215–1221.

Thurston, T.L.M., Wandel, M.P., von Muhlinen, N., Foeglein, Á., and Randow, F. (2012). Galectin 8 targets damaged vesicles for autophagy to defend cells against bacterial invasion. *Nature* *482*, 414–418.

Tokunaga, F., and Iwai, K. (2012). Linear ubiquitination: a novel NF- $\kappa$ B regulatory mechanism for inflammatory and immune responses by the LUBAC ubiquitin ligase complex. *Endocr. J.* *59*, 641–652.

Tokunaga, F., Sakata, S., Saeki, Y., Satomi, Y., Kirisako, T., Kamei, K., Nakagawa, T., Kato, M., Murata, S., Yamaoka, S., et al. (2009). Involvement of linear polyubiquitylation of NEMO in NF- $\kappa$ B activation. *Nat. Cell Biol.* *11*, 123–132.

Tolani, B., Matta, H., Gopalakrishnan, R., Punj, V., and Chaudhary, P.M. (2014). NEMO is essential for Kaposi's sarcoma-associated herpesvirus-encoded vFLIP K13-induced gene expression and protection against death receptor-induced cell death, and its N-terminal 251 residues are sufficient for this process. *J. Virol.* *88*, 6345–6354.

Trauth, B.C., Klas, C., Peters, A.M., Matzku, S., Möller, P., Falk, W., Debatin, K.M., and Krammer, P.H. (1989). Monoclonal antibody-mediated tumor regression by induction of apoptosis. *Science* *245*, 301–305.

Tsukada, M., and Ohsumi, Y. (1993). Isolation and characterization of autophagy-defective mutants of *Saccharomyces cerevisiae*. *FEBS Lett.* *333*, 169–174.

Turner, D.J., Alaish, S.M., Zou, T., Rao, J.N., Wang, J.-Y., and Strauch, E.D. (2007). Bile salts induce resistance to apoptosis through NF-kappaB-mediated XIAP expression. *Ann. Surg.* *245*, 415–425.

Turvey, S.E., Durandy, A., Fischer, A., Fung, S.-Y., Geha, R.S., Gewies, A., Giese, T., Greil, J., Keller, B., McKinnon, M.L., et al. (2014). The CARD11-BCL10-MALT1 (CBM) signalosome complex: Stepping into the limelight of human primary immunodeficiency. *J. Allergy Clin. Immunol.* *134*, 276–284.

Vanden Berghe, T., Kaiser, W.J., Bertrand, M.J., and Vandenabeele, P. (2015). Molecular crosstalk between apoptosis, necroptosis, and survival signaling. *Mol. Cell. Oncol.* *2*, e975093.

Vandenabeele, P., Galluzzi, L., Vanden Berghe, T., and Kroemer, G. (2010). Molecular mechanisms of necroptosis: an ordered cellular explosion. *Nat. Rev. Mol. Cell Biol.* *11*, 700–714.

Verlhac, P., Viret, C., and Faure, M. (2015). Dual function of CALCOCO2/NDP52 during xenophagy. *Autophagy* *11*, 965–966.

Wajant, H. (2003). Death receptors. *Essays Biochem.* *39*, 53–71.

Walczak, H., Iwai, K., and Dikic, I. (2012). Generation and physiological roles of linear ubiquitin chains. *BMC Biol.* *10*, 23.

Walczak, H., Kazuhire, I., and Dikic, I. (2013). Death Receptor-Ligand Systems in Cancer, Cell Death, and Inflammation. *Cold Spring Harb. Perspect. Biol.* *5*, a008698–a008698.

Wang, D., You, Y., Lin, P.-C., Xue, L., Morris, S.W., Zeng, H., Wen, R., and Lin, X. (2007). Bcl10 plays a critical role in NF-kappaB activation induced by G protein-coupled receptors. *Proc. Natl. Acad. Sci. U. S. A.* *104*, 145–150.

Wang, J., Huo, K., Ma, L., Tang, L., Li, D., Huang, X., Yuan, Y., Li, C., Wang, W., Guan, W., et al. (2011). Toward an understanding of the protein interaction network of the human liver. *Mol. Syst. Biol.* *7*, 536.

Wertz, I.E., O'Rourke, K.M., Zhou, H., Eby, M., Aravind, L., Seshagiri, S., Wu, P., Wiesmann, C., Baker, R., Boone, D.L., et al. (2004). De-ubiquitination and ubiquitin ligase domains of A20 downregulate NF-kappaB signalling. *Nature* *430*, 694–699.

van Wijk, S.J.L., Fricke, F., Herhaus, L., Gupta, J., Hötte, K., Pampaloni, F., Grumati, P., Kaulich, M., Sou, Y., Komatsu, M., et al. (2017). Linear ubiquitination of cytosolic Salmonella Typhimurium activates NF- $\kappa$ B and restricts bacterial proliferation. *Nat. Microbiol.* *2*, 17066.

Xie, X., Li, F., Wang, Y., Wang, Y., Lin, Z., Cheng, X., Liu, J., Chen, C., and Pan, L. (2015). Molecular basis of ubiquitin recognition by the autophagy receptor CALCOCO2. *Autophagy* *11*, 1775–1789.

Yang, J.K., Wang, L., Zheng, L., Wan, F., Ahmed, M., Lenardo, M.J., and Wu, H. (2005). Crystal Structure of MC159 Reveals Molecular Mechanism of DISC Assembly and FLIP Inhibition. *Mol. Cell* *20*, 939–949.

Yang, Y., Schmitz, R., Mitala, J., Whiting, A., Xiao, W., Ceribelli, M., Wright, G.W., Zhao, H., Yang, Y., Xu, W., et al. (2014). Essential role of the linear ubiquitin chain assembly complex in lymphoma revealed by rare germline polymorphisms. *Cancer Discov.* *4*, 480–493.

Ye, Y., and Rape, M. (2009). Building ubiquitin chains: E2 enzymes at work. *Nat. Rev. Mol. Cell Biol.* *10*, 755–764.

Zhang, Q., Lenardo, M.J., and Baltimore, D. (2017). 30 Years of NF- $\kappa$ B: A Blossoming of Relevance to Human Pathobiology. *Cell* *168*, 37–57.

Zinngrebe, J., Montinaro, A., Peltzer, N., and Walczak, H. (2014). Ubiquitin in the immune system. *EMBO Rep.* *15*, 28–45.

## ***Curriculum vitae***

## ***Publications***

Pischel D, **Buchbinder JH**, Sundmacher K, Lavrik IN, Flassig RJ. A guide to automated apoptosis detection: How to make sense of imaging flow cytometry data. *PLoS One*. 2018 May 16;13(5):e0197208

Lim MCC, Maubach G, Sokolova O, Feige MH, Diezko R, **Buchbinder J**, Backert S, Schlüter D, Lavrik IN, Naumann M. Pathogen-induced ubiquitin-editing enzyme A20 bifunctionally shuts off NF- $\kappa$ B and caspase-8-dependent apoptotic cell death. *Cell Death Differ*. 2017 Jun 2.

Pietkiewicz S, Wolfe C, **Buchbinder JH** and Lavrik IN. Measuring Procaspase-8 and -10 Processing upon Apoptosis Induction. *Bio-protocol* 7(1): e2081.

Just S, Nishanth G, **Buchbinder JH**, Wang X, Naumann M, Lavrik I, Schlüter D. A20 Curtails Primary but Augments Secondary CD8<sup>+</sup> T Cell Responses in Intracellular Bacterial Infection. *Sci Rep*. 2016 Dec 22;6:39796.

Schleich K, **Buchbinder JH**, Pietkiewicz S, Kähne T, Warnken U, Öztürk S, Schnölzer M, Naumann M, Krammer PH, Lavrik IN. 2015. Molecular architecture of the DED chains at the DISC: regulation of procaspase-8 activation by short DED proteins c-FLIP and procaspase-8 prodomain. *Cell Death Differ*. 2016 Apr;23(4):681-94.

Pietkiewicz S, **Schmidt JH**, Lavrik IN. 2015. Quantification of apoptosis and necroptosis at the single cell level by a combination of Imaging Flow Cytometry with classical Annexin V/propidium iodide staining. *J Immunol Methods*. 2015 Aug;423:99-103

**Schmidt JH**, Pietkiewicz S, Naumann M, Lavrik IN. 2015. Quantification of CD95- induced apoptosis and NF- $\kappa$ B activation at the single cell level. *J Immunol Methods*. 2015 Aug;423:12-7

## ***Declaration***

Jörn Buchbinder, Brunnerstr. 2, 39112 Magdeburg

### **Erklärung**

Hiermit erkläre ich, dass die von mir eingereichte Dissertation zu dem Thema

### **Regulation of CD95-induced NF- $\kappa$ B activation**

Selbstständig verfasst, nicht schon als Dissertation verwendet habe und die benutzten Hilfsmittel und Quellen vollständig angegeben wurden.

Weiterhin erkläre ich, dass ich weder diese noch eine Arbeit zu Erlangung des akademischen Grades doctor rerum naturalium (Dr. rer. nat.) an anderen Einrichtungen eingereicht habe.

Magdeburg, den 19.06.2018